32

A Solid Shell Element

TABLE OF CONTENTS

		Page
§32.1.	**Introduction**	32–3
§32.2.	**Geometric Description**	32–3
	§32.2.1. The Flattened Brick	32–4
	§32.2.2. Natural Coordinates	32–6
	§32.2.3. Coordinate Transformations	32–6
	§32.2.4. Warped to Flat Geometric Transformation	32–8
	§32.2.5. Warping Check	32–8
	§32.2.6. Volume Computation	32–9
§32.3.	**SS8 Element Description**	32–11
	§32.3.1. Global Displacements	32–12
	§32.3.2. Local Displacements	32–12
	§32.3.3. Flattening	32–12
§32.4.	**SS8 Stiffness Matrix**	32–13
	§32.4.1. Behavioral Assumptions	32–13
	§32.4.2. Top Level Implementation	32–15
	§32.4.3. Calculation Steps	32–15
§32.5.	**Constitutive Properties**	32–18
	§32.5.1. Laminate Fabrication	32–18
	§32.5.2. Wall Fabrication Assumptions	32–18
	§32.5.3. MBT Constitutive Equations	32–19
	§32.5.4. MBT Thickness Integration	32–20
	§32.5.5. Implementation of MBT Integration	32–21
	§32.5.6. Transverse Shear Constitutive Equations	32–23
§32.6.	**Membrane, Bending and Thickness (MBT) Stiffness**	32–24
	§32.6.1. Four-Noded Quadrilateral Geometry	32–24
	§32.6.2. Quadrilateral Invariant Relations	32–25
	§32.6.3. The Assumed Strains	32–27
	§32.6.4. The Fitted Strain Field	32–28
	§32.6.5. Extending the Quadrilateral Strains to SS8	32–29
	§32.6.6. Membrane Strain Implementation	32–29
	§32.6.7. Thickness Interpolation	32–31
	§32.6.8. Strain Field Consistency Checks	32–32
	§32.6.9. The Thickness Strain	32–33
	§32.6.10. Thickness Strain Implementation	32–34
	§32.6.11. MBT Strain Implementation	32–35
	§32.6.12. The MBT Stiffness Matrix	32–37
§32.7.	**Transverse Shear Stiffness**	32–38
	§32.7.1. Assumptions and Requirements	32–38
	§32.7.2. Comment on the Foregoing Assumptions	32–38
	§32.7.3. Strain Computation	32–39
	§32.7.4. Transverse Shear Strain Implementation	32–41

§32.7.5. Shear Stiffness Matrix Implementation 32–41
§32.7.6. RBM Cleanup 32–43
§32.8. **A Special Geometry** 32–45
§32.8.1. Stiffness of an Isotropic Rectangular-Prismatic Element 32–45
§32.8.2. Torsion Response of Individual Element 32–48
§32.9. **Numerical Tests** 32–50
§32.9.1. Patch Tests 32–50
§32.9.2. Invariance 32–50
§32.9.3. Two-Ply Rectangular Plate 32–50
§32.9.4. Inplane Distortion Sensitivity 32–50
§32.9.5. Homogeneous and Laminated Pinched Ring 32–52
§32.9.6. Pinched Cylindrical Shell 32–53
§32.9.7. Scordelis-Lo Roof 32–54
§32.9.8. Pinched Hemisphere 32–55
§32.9.9. Pretwisted Beam 32–56
§32.10. **Conclusions** 32–57
§32.10.1. General Strengths 32–57
§32.10.2. Special Strengths 32–57
§32.10.3. Weaknesses and Question Marks 32–57
§32.11. **Acknowledgements** 32–57
§32.12. **References** 32–58

§32.1. Introduction

Solid-shell elements form a class of finite element models intermediate between thin shell and conventional solid elements. They have the same node and freedom configuration of solid elements but account for shell-like behavior in the thickness direction. They are useful for modeling shell-like portions of a 3D structure without the need to connect solid element nodes to shell nodes. See Figure 1(a).

This report presents in detail the derivation and computer implementation of an 8-node solid shell element called SS8. Most of the derivation follows the Assumed Natural Strain (ANS) method introduced by Park and Stanley [21] for doubly curved thin-shell elements and by Bathe and Dvorkin [2] for Mindlin-Reissner plates.

The derivation of solid-shell elements is more complicated than that of standard solid elements since they are prone to the following problems:

1. Shear and membrane locking. These have been adressed with the hybrid strain formulation [1,13,20], hybrid stress [24], and the Assumed and Enhanced Natural Strain formulations [7,8,14,19,23].
2. Trapezoidal locking caused by deviation of midplane planform from rectangular shape [8,16,17].
3. Thickness locking due to Poisson's ratio coupling of the inplane and transverse normal stresses [1,7,14,19,22,20,25,26].

As noted, the formulation that follows uses primarily the *Assumed Natural Strain* (ANS) method with adjustments to make the element kinematics work correctly for laminate wall constructions such as that depicted in Figure 1(b). This is done by assuming a uniform thickness stress instead of a uniform strain, which results in modified thickness-integrated constitutive equations.

A *Mathematica* implementation of the SS8 element is also presented in this report. This implementation was used for rapid prototyping and experimentation. This was perticularly useful for some element components, such as the inplane strains, which were frequently updated during the course of the project. A Fortran 77 implementation is presented in a separate document [11].

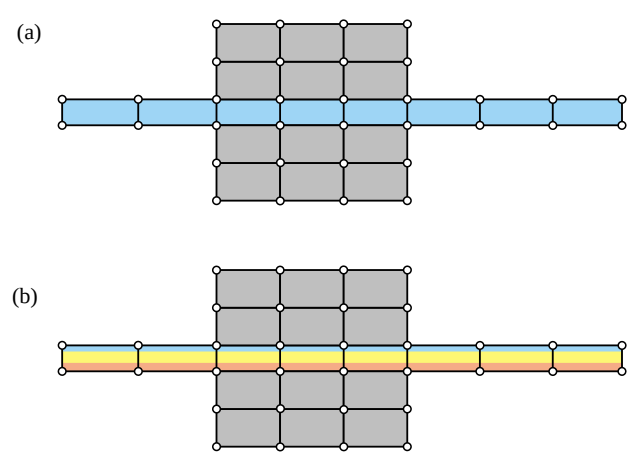

Figure 1. Solid shell elements (in color) connected to standard solid brick elements (in gray). Figure (b) shows a laminate wall configuration.

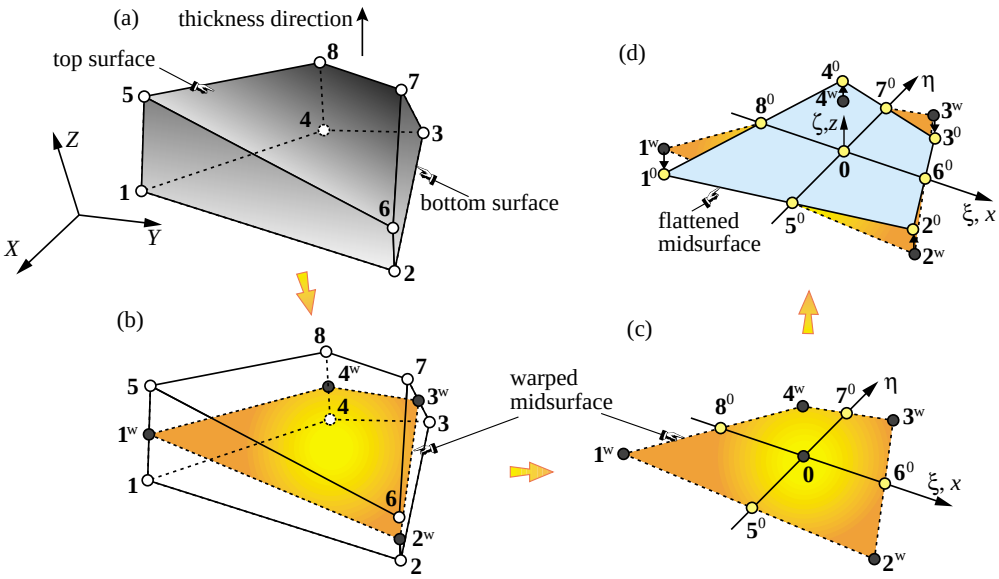

Figure 2. Initial steps in morphing a conventional 8-node brick (hexahedron) into the SS8 solid shell element: (a) the source brick, (b) the warped midsurface, (c) isolated warped midsurface and medians, (d) the flattened midsurface.

§32.2. Geometric Description

The point of departure is the well known 8-node brick (hexahedron) element shown in Figure 2(a). The element is referred to a global Cartesian system $\{X, Y, Z\}$. The local node numbers are 1 through 8, arranged as illustrated in that figure. This *hexahedron numbering* is used to define preferred directions, as explained next. The coordinates of these 8 nodes may be grouped in a table:

$$\begin{bmatrix} X_1 & X_2 & X_3 & X_4 & X_5 & X_6 & X_7 & X_8 \\ Y_1 & Y_2 & Y_3 & Y_4 & Y_5 & Y_6 & Y_7 & Y_8 \\ Z_1 & Z_2 & Z_3 & Z_4 & Z_5 & Z_6 & Z_7 & Z_8 \end{bmatrix} \tag{32.1}$$

Anticipating the transition to a thick shell element, one of the brick dimensions is identified as the *shell thickness direction* also called *wall direction*. This has edges going from nodes 1,2,3,4 to 5,6,7,8, respectively. Segments 1-5, 2-6, 3-7, and 4-8 are called the *thickness edges*. Face 1-2-3-4 defines the *bottom surface* and face 5-6-7-8 the *top surface*. Surfaces extending along the other two directions are called *inplane surfaces*. Directions contained in an inplane surface are called *inplane directions*.

The four thickness edge midpoints are denoted by 1^w, 2^w, 3^w and 4^w, where superscript w stands for "warped." See Figure 2(b). These four points are the corners of a quadrilateral known as the *warped midsurface*. It is qualified as warped since the four corners do not generally lie in a plane. Figure 2(c) shows the isolated warped midsurface. The midpoints between its corners are called 5^w, 6^w, 7^w and 8^w. The segments 5^w-7^w and 8^w-6^w that join the midpoints are called the *midsurface medians*. No matter how warped the surface is, the midsurface medians cross at a point 0 and hence define a plane.

§32.2.1. The Flattened Brick

The plane defined by the midsurface medians is called the *midsurface plane*. Using this fact, the local Cartesian axes are defined as follows:

x along median 6^0-8^0

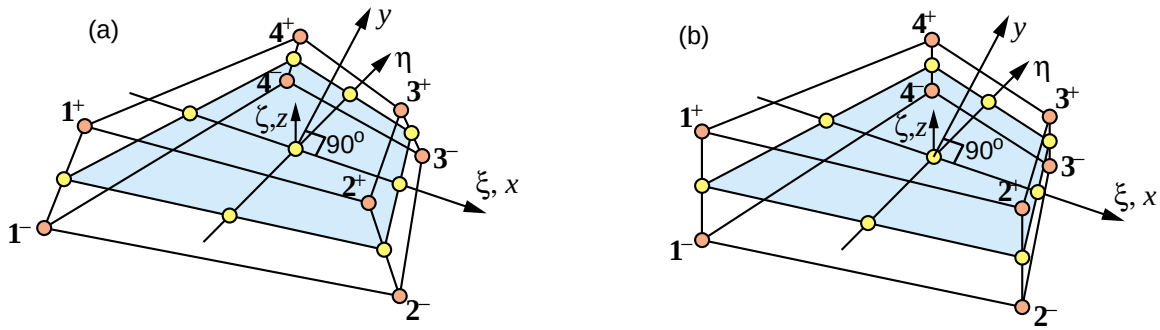

Figure 3. The flattened brick geometry: (a) thickness tapered (TT) element, (b) thickness-prismatic (TP) element

z normal to the midsurface plane at the intersection of the medians

y normal to x and z and hence located in the midsurface plane, forming a right-handed system.

Points 1^w through 4^w are projected on that plane to locations labeled 1^0, 2^0, 3^0 and 4^0, respectively. Since the projection is along the z direction this is done by equating their $\{x, y\}$ coordinates:

$$\begin{bmatrix} x_1^0 & x_2^0 & x_3^0 & x_4^0 \\ y_1^0 & y_2^0 & y_3^0 & y_4^0 \end{bmatrix} = \begin{bmatrix} x_1^w & x_2^w & x_3^w & x_4^w \\ y_1^w & y_2^w & y_3^w & y_4^w \end{bmatrix} \tag{32.2}$$

Points 1^0 through 4^0 are the corners of a flat quadrilateral, shown in Figure 2(d). Other points in the original brick are moved by the appropriate amount along z to get a *flattened brick*, as shown in Figure 3. This is the geometry on which the solid-shell element development will be based. Nodes 1 through 8 of the original brick map to 1^- through 4^+ of the flattened brick. The local coordinates of these eight nodes can be expressed as in array form as

$$\begin{bmatrix} x_1^- & x_2^- & x_3^- & x_4^- & x_1^+ & x_2^+ & x_3^+ & x_4^+ \\ y_1^- & y_2^- & y_3^- & y_4^- & y_1^+ & y_2^+ & y_3^+ & y_4^+ \\ z_1^- & z_2^- & z_3^- & z_4^- & z_1^+ & z_2^+ & z_3^+ & z_4^+ \end{bmatrix}$$
$$= \begin{bmatrix} x_1^0 - \frac{1}{2}s_{x1}h_1 & x_2^0 - \frac{1}{2}s_{x2}h_2 & x_3^0 - \frac{1}{2}s_{x3}h_3 & x_4^0 - \frac{1}{2}s_{x4}h_4 & x_1^0 + \frac{1}{2}s_{x1}h_1 & x_2^0 + \frac{1}{2}s_{x2}h_2 & x_3^0 + \frac{1}{2}s_{x3}h_3 & x_4^0 + \frac{1}{2}s_{x4}h_4 \\ y_1^0 - \frac{1}{2}s_{y1}h_1 & y_2^0 - \frac{1}{2}s_{y2}h_2 & y_3^0 - \frac{1}{2}s_{y3}h_3 & y_4^0 - \frac{1}{2}s_{y4}h_4 & y_1^0 + \frac{1}{2}s_{y1}h_1 & y_2^0 + \frac{1}{2}s_{y2}h_2 & y_3^0 + \frac{1}{2}s_{y3}h_3 & y_4^0 + \frac{1}{2}s_{y4}h_4 \\ -\frac{1}{2}h_1 & -\frac{1}{2}h_2 & -\frac{1}{2}h_3 & -\frac{1}{2}h_4 & \frac{1}{2}h_1 & \frac{1}{2}h_2 & \frac{1}{2}h_3 & \frac{1}{2}h_4 \end{bmatrix} \tag{32.3}$$

Here $h_n = z_n^+ - z_n^-$ $(n = 1, 2, 3, 4)$ are the corner thicknesses, as depicted in Figure 4, and $\{s_{xn}, s_{yn}\}$ are the $\{x, y\}$ slopes of the nth thickness edge with respect to the midsurface normal z.

If $h_1 = h_2 = h_2 = h_4 = h$ the flattened brick is said to be of *constant thickness*. It is of *variable thickness* otherwise. If $s_{x1} = s_{y1} = s_{x2} = s_{y2} = s_{x3} = s_{y3} = s_{x4} = s_{y4} = 0$ the flattened brick is said to be *thickness prismatic* or TP for short. In this case $x_n^- = x_n^+$, $n = 1, 2, 3, 4$. This situation happens in modeling thick flat plates. If at least one slope is nonzero, the flattened brick is said to be *thickness tapered* or TT for short. This occurs in modeling curved thick shells. Figures 3 and 4 illustrate these geometric concepts.

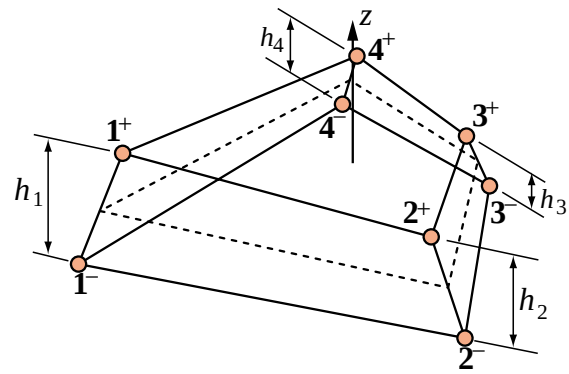

Figure 4. Corner thicknesses in a flattened brick.

The distinction between TP and TT geometries and constant versus variable thickness is important in the evaluation of the solid shell element. The element will pass the patch test under certain geometric constraints but only approximately otherwise.

§32.2.2. Natural Coordinates

On first impression it appears as if two sets of natural hexahedron coordinates need to be defined, one for the actual (warped) brick, and the other for the flattened brick. After some thought, however, one realizes the the same set: $\{\xi, \eta, \zeta\}$ can be used for both geometries. It is only necessary to state for which of the two configurations that set is being used. The relation between the two geometries is mathematically stated in §2.4.

Coordinates ξ and η are directed along the midsurface medians 6^w-8^w (same as 6^0-8^0) and 5^w-7^w (same as 5^0-7^0), respectively, while ζ parametrizes the thickness direction. Equations $\zeta = -1$, $\zeta = 0$ and $\zeta = 1$ characterize the points of the bottom surface, midsurface and top surfaces, respectively, in both warped and flattened geometries.

§32.2.3. Coordinate Transformations

The relation between local and global coordinates is

$$\mathbf{x} = \begin{bmatrix} x \\ y \\ z \end{bmatrix} = \begin{bmatrix} T_{d11} & T_{d12} & T_{d12} \\ T_{d21} & T_{d22} & T_{d23} \\ T_{d31} & T_{d32} & T_{d33} \end{bmatrix} \begin{bmatrix} X - X_0 \\ Y - Y_0 \\ Z - Z_0 \end{bmatrix} = \mathbf{T}_d(\mathbf{X} - \mathbf{X}_0) \tag{32.4}$$

where matrix $\mathbf{T}_d$ stores the direction cosines of $\{x, y, z\}$ with respect to $\{X, Y, Z\}$, and

$$X_0 = \tfrac{1}{4}(X_1^w + X_2^w + X_3^w + X_4^w), \quad Y_0 = \tfrac{1}{4}(Y_1^w + Y_2^w + Y_3^w + Y_4^w), \quad Z_0 = \tfrac{1}{4}(Z_1^w + Z_2^w + Z_3^w + Z_4^w), \tag{32.5}$$

are the global coordinates of the median intersection point, labeled as 0 in Figure 2.

Inserting the coordinates of the original brick into (32.4) produces the local coordinates of its 8 corners, which are arranged as the 3×8 array

$$\begin{bmatrix} x_1 & x_2 & x_3 & x_4 & x_5 & x_6 & x_7 & x_8 \\ y_1 & y_2 & y_3 & y_4 & y_5 & y_6 & y_7 & y_8 \\ z_1 & z_2 & z_3 & z_4 & z_5 & z_6 & z_7 & z_8 \end{bmatrix} \tag{32.6}$$

```
SS8LocalSystem[XYZcoor_]:= Module[{
  XYZ,XYZ1,XYZ2,XYZ3,XYZ4,XYZ5,XYZ6,XYZ7,XYZ8,XYZ0,
  XYZ1w,XYZ2w,XYZ3w,XYZ4w,XYZ50,XYZ60,XYZ70,XYZ80,
  dx1,dx2,dx3,dy1,dy2,dy3,dz1,dz2,dz3,xlr,ylr,zlr,
  x1,x2,x3,x4,x5,x6,x7,x8,y1,y2,y3,y4,y5,y6,y7,y8,
  z1,z2,z3,z4,z5,z6,z7,z8,xw,yw,hw,x,y,z,dx,dy,dz,
  x10,x20,x30,x40,y10,y20,y30,y40,xyz,xyzwh,A0},
  {XYZ1,XYZ2,XYZ3,XYZ4,XYZ5,XYZ6,XYZ7,XYZ8}=XYZcoor;
   XYZ1w=(XYZ5+XYZ1)/2; XYZ2w=(XYZ6+XYZ2)/2;
   XYZ3w=(XYZ7+XYZ3)/2; XYZ4w=(XYZ8+XYZ4)/2;
   XYZ50=(XYZ1w+XYZ2w)/2;  XYZ60=(XYZ2w+XYZ3w)/2;
   XYZ70=(XYZ3w+XYZ4w)/2;  XYZ80=(XYZ4w+XYZ1w)/2;
   XYZ0=(XYZ1w+XYZ2w+XYZ3w+XYZ4w)/4;
   XYZ=Transpose[XYZcoor]-XYZ0;
   {dx1,dx2,dx3}=XYZ60-XYZ80; {dy1,dy2,dy3}=XYZ70-XYZ50;
   xlr=Sqrt[ dx1^2+dx2^2+dx3^2 ];
   If [xlr<=0, Print["SS8LocalSystem: midnodes 6-8 coincide"];
       Return[Null]];
   dx1=dx1/xlr; dx2=dx2/xlr; dx3=dx3/xlr;
   dz1=dx2*dy3-dx3*dy2; dz2=dx3*dy1-dx1*dy3;
   dz3=dx1*dy2-dx2*dy1; zlr=Sqrt[dz1^2+dz2^2+dz3^2];
   If [zlr<=0, Print["SS8LocalSystem: colinear medians"];
       Return[Null]];
   dz1=dz1/zlr; dz2=dz2/zlr; dz3=dz3/zlr;
   dy1=dz2*dx3-dz3*dx2; dy2=dz3*dx1-dz1*dx3;
   dy3=dz1*dx2-dz2*dx1; ylr=Sqrt[dy1^2+dy2^2+dy3^2];
   dx={dx1,dx2,dx3}; dy={dy1,dy2,dy3}; dz={dz1,dz2,dz3};
   {dx,dy,dz}=Simplify[{dx,dy,dz}]; Td={dx,dy,dz};
   xyz=Td.XYZ; {x,y,z}=xyz;
   {x1,x2,x3,x4,x5,x6,x7,x8}=x;
   {y1,y2,y3,y4,y5,y6,y7,y8}=y;
   {z1,z2,z3,z4,z5,z6,z7,z8}=z;
   xw={x5+x1,x6+x2,x7+x3,x8+x4}/2;
   yw={y5+y1,y6+y2,y7+y3,y8+y4}/2;
   zw={z5+z1,z6+z2,z7+z3,z8+z4}/2;
   hw={z5-z1,z6-z2,z7-z3,z8-z4}; xyzwh={xw,yw,zw,hw};
   {x10,x20,x30,x40}=xw; {y10,y20,y30,y40}=yw;
   A0=(1/2)*((x30-x10)*(y40-y20)-(x40-x20)*(y30-y10));
   Return[{xyz,xyzwh,Td,A0}]];
```

Figure 5. *Mathematica* module for the SS8 element localization.

Array (32.6) should not be confused with the first one in (32.3) since brick flattening has not been done yet. Next one derives the x, y coordinates of the warped midsurface nodes and the corner thicknesses. The elements is flattened by subtracting out the z_n^w coordinates. The operation is:

$$\begin{bmatrix} x_1^w & x_2^w & x_3^w & x_4^w \\ y_1^w & y_2^w & y_3^w & y_4^w \\ z_1^w & z_2^w & z_3^w & z_4^w \\ h_1 & h_2 & h_3 & h_4 \end{bmatrix} = \begin{bmatrix} \frac{1}{2}(x_5+x_1) & \frac{1}{2}(x_6+x_2) & \frac{1}{2}(x_7+x_3) & \frac{1}{2}(x_8+x_4) \\ \frac{1}{2}(y_5+y_1) & \frac{1}{2}(y_6+y_2) & \frac{1}{2}(y_7+y_3) & \frac{1}{2}(y_8+y_4) \\ \frac{1}{2}(z_5+z_1) & \frac{1}{2}(z_6+z_2) & \frac{1}{2}(z_7+z_3) & \frac{1}{2}(z_8+z_4) \\ z_5-z_1 & z_6-z_2 & z_7-z_3 & z_8-z_4 \end{bmatrix} \begin{bmatrix} x_1^0 & x_2^0 & x_3^0 & x_4^0 \\ y_1^0 & y_2^0 & y_3^0 & y_4^0 \\ 0 & 0 & 0 & 0 \\ h_1 & h_2 & h_3 & h_4 \end{bmatrix} \tag{32.7}$$

These element localization operations are implemented in the *Mathematica* module `SS8LocalSystem` listed in Figure 5. The module is referenced as

```
{xyz,xyzwh,Td,A0} = SS8LocalSystem[XYZcoor]
```
(32.8)

The only argument is

`XYZcoor` The global coordinates of the 8 corner nodes of the original brick, arranged as `{{X1,Y1,Z1},{X2,Y2,Z2}, ... {X8,Y8,Z8}}`.

The module returns a list containing four items:

`xyz` The local coordinates of the 8 corner nodes of the original brick, arranged as
`{{x1,x2,...x8},{y1,y2,...y8},{z1,z2,...z8}}`
Note: to get the node by node arrangement
`xyzcoor={{x1,y1,z1},{x2,y2,z2}, ... {x8,y8,z8}}`
transpose this array: `xyzcoor=Transpose[xyz]`.

`xyzwh` The local coordinates of the warped midsurface corners and the corner thicknesses of the flattened element, arranged as
`{{x1w,x2w,x3w,x4w},{y1w,y2w,y3w,y4w},{z1w,z2w,z3w,z4w},{h1,h2,h3,h4}}`
Note that `x10=x1w`, `x20=x2w`, etc., so the flat midsurface coordinates are immediately available from the first two rows.

`Td` The 3×3 direction cosine matrix $\mathbf{T}_d$ defined in (32.4).

`A0` The signed area of the flat midsurface. A negative or zero area would flag an input error.

If an error is detected during processing, the module returns `Null`.

§32.2.4. Warped to Flat Geometric Transformation

For further use in the transformation of flat to actual (warped) geometry of Section 3, the "flattening" coordinate transformations are recorded here. The warped geometry is described by the isoparametric transformations

$$\begin{bmatrix} x^w \\ y^w \\ z^w \end{bmatrix} = \begin{bmatrix} x_1 & x_2 & x_3 & x_4 & x_5 & x_6 & x_7 & x_8 \\ y_1 & y_2 & y_3 & y_4 & y_5 & y_6 & y_7 & y_8 \\ z_1 & z_2 & z_3 & z_4 & z_5 & z_6 & z_7 & z_8 \end{bmatrix} \begin{bmatrix} N_1 \\ N_2 \\ \vdots \\ N_8 \end{bmatrix} \tag{32.9}$$

where N_i are the trilinear shape functions

$$\begin{aligned} N_1 &= \tfrac{1}{8}(1-\xi)(1-\eta)(1-\zeta), & N_2 &= \tfrac{1}{8}(1+\xi)(1-\eta)(1-\zeta), \\ N_3 &= \tfrac{1}{8}(1+\xi)(1+\eta)(1-\zeta), & N_4 &= \tfrac{1}{8}(1-\xi)(1+\eta)(1-\zeta), \\ N_5 &= \tfrac{1}{8}(1-\xi)(1-\eta)(1+\zeta), & N_6 &= \tfrac{1}{8}(1+\xi)(1-\eta)(1+\zeta), \\ N_7 &= \tfrac{1}{8}(1+\xi)(1+\eta)(1+\zeta), & N_8 &= \tfrac{1}{8}(1-\xi)(1+\eta)(1+\zeta). \end{aligned} \tag{32.10}$$

The flattening transformation can be mathematically stated as

$$\begin{bmatrix} x^0 \\ y^0 \\ z^0 \end{bmatrix} = \begin{bmatrix} x^w \\ y^w \\ z^w \end{bmatrix} - \begin{bmatrix} 0 \\ 0 \\ z_1^w N_1^Q + z_2^w N_2^Q + z_3^w N_3^Q + z_4^w N_4^Q \end{bmatrix} \tag{32.11}$$

Here $z_1^w = \frac{1}{2}(z_5 + z_1)$, $z_2^w = \frac{1}{2}(z_6 + z_2)$, $z_3^w = \frac{1}{2}(z_7 + z_3)$ and $z_4^w = \frac{1}{2}(z_8 + z_3)$, whereas $N_1^Q = \frac{1}{4}(1-\xi)(1-\eta)$, $N_2^Q = \frac{1}{4}(1+\xi)(1-\eta)$, $N_3^Q = \frac{1}{4}(1+\xi)(1+\eta)$, $N_4^Q = \frac{1}{4}(1-\xi)(1+\eta)$ are the bilinear shape functions of the flat midsurface, which is a quadrilateral.[1]

[1] Since the coordinate directions are not treated equally, the flattened element is no longer isoparametric.

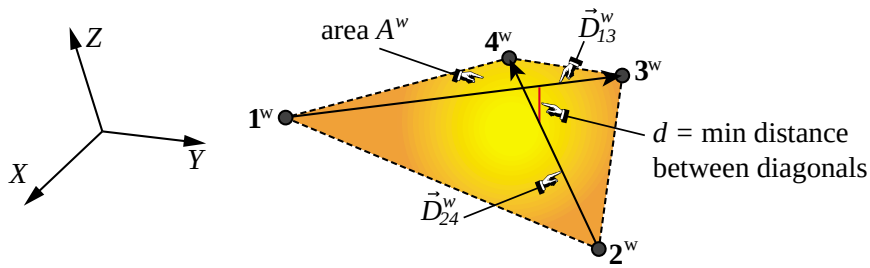

Figure 6. Ingredients for computing a warping measure Ψ: minimum distance d between diagonals, and area A^w of warped midsurface.

§32.2.5. Warping Check

The derivation of the solid shell stiffness matrix is carried out on the flattened (unwarped) brick geometry, and globalized to the actual geometry. If the element is warped, certain tests, notably patch tests for constant strain states, are only approximately satisfied. Poor results can be expected if the element is excessively warped. Consequently it is convenient to have a "deviation from flatness" measure to be checked during model preprocessing.

Several warping measures for shell elements have been proposed over the years. Here we shall use a minor variation of the oldest one, invented at Boeing by 1965 for the SAMECS code, which has the advantages of easy physical interpretation. The geometric ingredients are shown in Figure 6. Denote by d the shortest distance between the diagonals $\vec{D}^w_{13}$ and $\vec{D}^w_{24}$ of the warped midsurface, and A^w the area of the midsurface. The dimensionless warping measure is defined as

$$\Psi = \frac{d}{\sqrt{2|A^w|}}, \quad \text{where} \quad |A^w| = \left|\vec{D}^w_{13} \times \vec{D}^w_{24}\right| \tag{32.12}$$

(Boeing's measure is $d/\sqrt{A^w}$; the factor change makes (32.12) identical to $\frac{1}{4}(|z^w_1| + |z^w_2| + |z^w_3| + |z^w_4|)/\sqrt{A}$ for slightly warped elements.) Using the abbreviations $X_{ij} = X_i - Y_j$, $Y_{ij} = Y_i - Y_j$, $Z_{ij} = Z_i - Z_j$, the expression of Ψ in terms of the global node coordinates can be shown to be

$$\Psi = \frac{|X_{21}p + Y_{21}q + Z_{21}r|}{(p^2 + q^2 + r^2)^{3/4}}, \tag{32.13}$$

in which $p = Y_{41}Z_{32} - Z_{41}Y_{32}$, $q = Z_{41}X_{32} - X_{41}Z_{32}$ and $r = X_{41}Y_{32} - Y_{41}X_{32}$. In the numerator of (32.13) $\{X_{21}, Y_{21}, Z_{21}\}$ may be actually replaced by $\{X_{ji}, Y_{ji}, Z_{ji}\}$ where $j = 2, 3, 4, 1$ is the cyclic permutation of $i = 1, 2, 3, 4$.

If $\Psi = 0$ the original brick is flat in the sense that its midsurface is flat. If $\Psi > \Psi_{max}$ warping is excessive and the preprocessing should be aborted. If $\Psi_{warn} < \Psi < \Psi_{max}$ an error warning should be given. Boeing manuals recommend $\Psi_{max} = 0.075$ and $\Psi_{warn} = \frac{1}{4}\Psi_{max}$.[2]

A *Mathematica* implementation of the computation of Ψ is shown in Figure 7. Module `SS8Warping` receives the original brick coordinates `XYZcoor` ordered `{{X1,Y1,Z1},{X2,Y2,Z2}, ... {X8,Y8,Z8}}`, and returns `Psi`.

[2] For the SS8 element a much lower treshold, say $\Psi_{max} = 0.01$, is recommended until its ability to handle warped configurations is further ascertained.

```
SS8Warping[XYZcoor_]:=Module[
 {X1,Y1,Z1,X2,Y2,Z2,X3,Y3,Z3,X4,Y4,Z4,
  X5,Y5,Z5,X6,Y6,Z6,X7,Y7,Z7,X8,Y8,Z8,
  X1w,Y1w,Z1w,X2w,Y2w,Z2w,X3w,Y3w,Z3w,X4w,Y4w,Z4w,
  p,q,r,Psi},
 {{X1,Y1,Z1},{X2,Y2,Z2},{X3,Y3,Z3},{X4,Y4,Z4},
  {X5,Y5,Z5},{X6,Y6,Z6},{X7,Y7,Z7},{X8,Y8,Z8}}=XYZcoor;
  {X1w,Y1w,Z1w}=({X1,Y1,Z1}+{X5,Y5,Z5})/2;
  {X2w,Y2w,Z2w}=({X2,Y2,Z2}+{X6,Y6,Z6})/2;
  {X3w,Y3w,Z3w}=({X3,Y3,Z3}+{X7,Y7,Z7})/2;
  {X4w,Y4w,Z4w}=({X4,Y4,Z4}+{X8,Y8,Z8})/2;
  p=(Y3w-Y1w)*(Z4w-Z2w)-(Z3w-Z1w)*(Y4w-Y2w);
  q=(Z3w-Z1w)*(X4w-X2w)-(X3w-X1w)*(Z4w-Z2w);
  r=(X3w-X1w)*(Y4w-Y2w)-(Y3w-Y1w)*(X4w-X2w);
  Psi=Abs[((X2w-X1w)*p+(Y2w-Y1w)*q+(Z2w-Z1w)*r)]/
          (p^2+q^2+r^2)^(3/4)/Sqrt[2];
  Return[Psi]];
```

Figure 7. *Mathematica* module to compute the warping measure Ψ.

§32.2.6. Volume Computation

The computation of the signed volume of the original or flattened brick is useful for several tasks. For example, preprocessing checks for positive volume, as well as mass and gravity load computations.

Consider an arbitrary 8-node brick with corner coordinates (32.2). and natural coordinates $\{\xi, \eta, \zeta\}$. The entries of the 3×3 Jacobian $\mathbf{J}$ of $\{X, Y, Z\}$ with respect to $\{\xi, \eta, \zeta\}$ are given by

$$\mathbf{J} = \frac{\partial(X, Y, Z)}{\partial(\xi, \eta, \zeta)} = \begin{bmatrix} \partial X/\partial\xi & \partial Y/\partial\xi & \partial Z/\partial\xi \\ \partial X/\partial\eta & \partial Y/\partial\eta & \partial Z/\partial\eta \\ \partial X/\partial\zeta & \partial Y/\partial\zeta & \partial Z/\partial\zeta \end{bmatrix} = \begin{bmatrix} J_{X\xi} & J_{Y\xi} & J_{Z\xi} \\ J_{X\eta} & J_{Y\eta} & J_{Z\eta} \\ J_{X\zeta} & J_{Y\zeta} & J_{Z\zeta} \end{bmatrix},$$

$$\begin{aligned} J_{X\xi} &= \sum_{i=1}^{8} \frac{\partial N_i}{\partial\xi} X_i, \quad J_{X\eta} = \sum_{i=1}^{8} \frac{\partial N_i}{\partial\eta} X_i, \quad J_{X\zeta} = \sum_{i=1}^{8} \frac{\partial N_i}{\partial\zeta} X_i, \\ J_{Y\xi} &= \sum_{i=1}^{8} \frac{\partial N_i}{\partial\xi} Y_i, \quad J_{Y\eta} = \sum_{i=1}^{8} \frac{\partial N_i}{\partial\eta} Y_i, \quad J_{Y\zeta} = \sum_{i=1}^{8} \frac{\partial N_i}{\partial\zeta} Y_i, \\ J_{Z\xi} &= \sum_{i=1}^{8} \frac{\partial N_i}{\partial\xi} Z_i, \quad J_{Z\eta} = \sum_{i=1}^{8} \frac{\partial N_i}{\partial\eta} Z_i, \quad J_{Z\zeta} = \sum_{i=1}^{8} \frac{\partial N_i}{\partial\tilde{\zeta}} Z_i, \end{aligned} \tag{32.14}$$

in which $N_i(\xi, \eta, \zeta)$, are the isoparametric shape functions (32.10). The brick volume is given by

$$V = \int_{-1}^{1}\int_{-1}^{1}\int_{-1}^{1} J\, d\xi\, d\eta\, d\zeta, \quad \text{in which} \quad J = \det(\mathbf{J}). \tag{32.15}$$

This integral is evaluated by a product Gauss quadrature rule. It can be shown that[3] a $2 \times 2 \times 2$ rule exactly integrates (32.15) because the variation of each natural coordinate: ξ, η and ζ in J is at most quadratic. Consequently only the $1 \times 1 \times 1$ and $2 \times 2 \times 2$ rules need to be considered.

A *Mathematica* implementation of the computation of V is listed in Figure 8. Module `SS8Volume` is referenced as

```
vol = SS8Volume[XYZcoor,n]
```
(32.16)

[3] Some finite element books still erroneously state that a 1-point Gauss rule gives the exact volume of the 8-node brick. That statement is correct in two dimensions for 4-node quadrilateral elements, but not in 3D.

```
SS8Volume[XYZcoor_,n_]:=Module[
 {X1,Y1,Z1,X2,Y2,Z2,X3,Y3,Z3,X4,Y4,Z4,
  X5,Y5,Z5,X6,Y6,Z6,X7,Y7,Z7,X8,Y8,Z8,
  J11,J12,J13,J21,J22,J23,J31,J32,J33,
  dNhex,Xhex,Yhex,Zhex,g=Sqrt[1/3],gtab,vol=0},
 {{X1,Y1,Z1},{X2,Y2,Z2},{X3,Y3,Z3},{X4,Y4,Z4},
  {X5,Y5,Z5},{X6,Y6,Z6},{X7,Y7,Z7},{X8,Y8,Z8}}=XYZcoor;
  If [n!=1&&n!=2, Print["SS8Volume: n not 1 or 2"];
      Return[Null]];
  dNhex[{ξ_,η_,ζ_}]:=
    {{-(1-η)*(1-ζ), (1-η)*(1-ζ), (1+η)*(1-ζ),-(1+η)*(1-ζ),
      -(1-η)*(1+ζ), (1-η)*(1+ζ), (1+η)*(1+ζ),-(1+η)*(1+ζ)},
     {-(1-ξ)*(1-ζ),-(1+ξ)*(1-ζ), (1+ξ)*(1-ζ), (1-ξ)*(1-ζ),
      -(1-ξ)*(1+ζ),-(1+ξ)*(1+ζ), (1+ξ)*(1+ζ), (1-ξ)*(1+ζ)},
     {-(1-ξ)*(1-η),-(1+ξ)*(1-η),-(1+ξ)*(1+η),-(1-ξ)*(1+η),
       (1-ξ)*(1-η), (1+ξ)*(1-η), (1+ξ)*(1+η), (1-ξ)*(1+η)}}/8;
  Xhex={X1,X2,X3,X4,X5,X6,X7,X8};
  Yhex={Y1,Y2,Y3,Y4,Y5,Y6,Y7,Y8};
  Zhex={Z1,Z2,Z3,Z4,Z5,Z6,Z7,Z8};
  If [n==1,{dNξ,dNη,dNζ}=dNhex[{0,0,0}];
            J11=dNξ.Xhex; J21=dNη.Xhex; J31=dNζ.Xhex;
            J12=dNξ.Yhex; J22=dNη.Yhex; J32=dNζ.Yhex;
            J13=dNξ.Zhex; J23=dNη.Zhex; J33=dNζ.Zhex;
      vol=Simplify[J11*J22*J33+J21*J32*J13+J31*J12*J23-
                   J31*J22*J13-J11*J32*J23-J21*J12*J33]*8;
      Return[vol]];
  gtab={{-g,-g,-g},{ g,-g,-g},{ g, g,-g},{-g, g,-g},
        {-g,-g, g},{ g,-g, g},{ g, g, g},{-g, g, g}};
  For [i=1,i<=8,i++, {dNξ,dNη,dNζ}=dNhex[gtab[[i]] ];
       J11=dNξ.Xhex; J21=dNη.Xhex; J31=dNζ.Xhex;
       J12=dNξ.Yhex; J22=dNη.Yhex; J32=dNζ.Yhex;
       J13=dNξ.Zhex; J23=dNη.Zhex; J33=dNζ.Zhex;
       vol+=Simplify[J11*J22*J33+J21*J32*J13+J31*J12*J23-
                     J31*J22*J13-J11*J32*J23-J21*J12*J33]];
  Return[Simplify[vol]]];
```

Figure 8. *Mathematica* module to compute brick volume.

The arguments are

`XYZcoor` The Cartesian coordinates of the 8 corner nodes of the brick. For the original brick use the global coordinates arranged as
`{{X1,Y1,Z1},{X2,Y2,Z2}, ... {X8,Y8,Z8}}`.
Same result should be obtained using the local coordinates arranged as
`{{x1,y1,z1},{x2,y2,z2}, ... {x8,y8,z8}}`.
For the volume of the flattened brick[4] use
`{{x1,y1,-h1/2},{x2,y2,-h2/2}, ... {x8,y8,h4/2}}`.

`n` Gauss rule integration index. Use `n=1` or `n=2` to specify the $1 \times 1 \times 1$ or the $2 \times 2 \times 2$ rules, respectively.

The module returns the volume `vol=`V as function value. A negative volume would flag an input error.

§32.3. SS8 Element Description

The SS8 solid-shell element has eight nodes numbered 1 through 8, which are located at the corners of the actual (warped) brick. The geometry is defined with reference to a global $\{X, Y, Z\}$ system; see

[4] An interesting result is that the volumes of the warped and flattened bricks are identical if the $1 \times 1 \times 1$ Gauss rule is used. This comes from the fact that the Jacobian at the sample point $\xi = \eta = \zeta = 0$ is the same; a property verifiable from the transformation (32.11). On the other hand, the exact volumes furnished by the $2 \times 2 \times 2$ rule generally differs.

Figure 2(a). As noted in §2.1, nodes 1-2-3-4 define the bottom surface and 5-6-7-8 the top surface. The four edges 1-5, 2-6, 3-7 and 4-8 that connect the bottom and top surfaces collectively define the thickness direction.

§32.3.1. Global Displacements

The displacement components of an arbitrary point in the global system $\{X, Y, Z\}$ are $\{U_X, U_Y, U_Z\}$. These three functions define the displacement field of the element. For some developments they are collected into one 3-vector:

$$\vec{\mathbf{U}} = [\, U_X \quad U_Y \quad U_Z \,]^T \,. \tag{32.17}$$

The element has three translational degrees of freedom (DOFs): $\{U_{Xn}, U_{Yn}, U_{Zn}\}$ at each node $n = 1, 2 \ldots 8$. This makes a total of 24 DOFs. They are collected into the global node displacement vector in a node by node arrangement:

$$\mathbf{U}^{(e)} = [\, U_{X1} \;\; U_{Y1} \;\; U_{Z1} \;\; U_{X2} \;\; U_{Y2} \;\; U_{Z2} \;\; \ldots \;\; U_{X8} \;\; U_{Y8} \;\; U_{Z8} \,]^T \,. \tag{32.18}$$

Since the element has 6 rigid body modes, it possesses 18 deformational modes. These are allocated to mechanical response effects: membrane, bending, thickness and transverse shear, as described in §4.1.

§32.3.2. Local Displacements

The displacement components of an arbitrary point in the local system $\{x, y, z\}$ are $\{u_x, u_y, u_z\}$. These three functions define the displacement field of the element. For some developments they are collected into one 3-vector:

$$\vec{\mathbf{u}} = [\, u_x \quad u_y \quad u_z \,]^T \,. \tag{32.19}$$

The 24 DOFs are collected into the local node displacement vector in a node by node arrangement:

$$\hat{\mathbf{u}}^{(e)} = [\, u_{x1} \;\; u_{y1} \;\; u_{z1} \;\; u_{x2} \;\; u_{y2} \;\; u_{z2} \;\; \ldots \;\; u_{x8} \;\; u_{y8} \;\; u_{z8} \,]^T \,. \tag{32.20}$$

Here $\hat{\mathbf{u}}^{(e)}$ is used instead of simply $\mathbf{u}^{(e)}$ to distinguish (32.20) from the node displacements vector of the flattened brick introduced below. The local and global fields are connected by the transformation matrix $\mathbf{T}_d$ introduced in §2.3:

$$\vec{\mathbf{u}} = \mathbf{T}_d\, \vec{\mathbf{U}}, \qquad \vec{\mathbf{U}} = \mathbf{T}_d^T\, \vec{\mathbf{u}}. \tag{32.21}$$

Applying this relation to the node displacement vectors (32.18) and (32.20) gives

$$\hat{\mathbf{u}}^{(e)} = \mathbf{T}_d^{(e)}\, \mathbf{U}^{(e)}, \qquad \mathbf{U}^{(e)} = (\mathbf{T}_d^{(e)})^T\, \hat{\mathbf{u}}^{(e)}, \tag{32.22}$$

where $\mathbf{T}_d^{(e)}$ is the 24×24 block diagonal matrix formed by stacking the 3×3 matrix $\mathbf{T}_d$ eight times along its diagonal.

§32.3.3. Flattening

Flattening the brick in the local system through (32.11) in general alters the position of nodes $1, 2, \ldots 8$. These become $1^-, 2^-, \ldots 4^+$, as illustrated in Figure 3. Consequently the node displacement values change. They are collected into

$$\mathbf{u}^{(e)} = [\, u_{x1}^- \;\; u_{y1}^- \;\; u_{z1}^- \;\; u_{x2}^- \;\; u_{y2}^- \;\; u_{z2}^- \;\; \ldots \;\; u_{x4}^+ \;\; u_{y4}^+ \;\; u_{z4}^+ \,]^T \,. \tag{32.23}$$

To connect $\mathbf{u}^{(e)}$ and $\hat{\mathbf{u}}^{(e)}$ it is noted that the flattening coordinate mapping (32.11) only affects z. Assuming that the local displacement varies linearly in z (a reasonable assumption since there are only two node layers) we have the following interpolations along edges 1-5, 2-6, 3-7 and 4-8:

$$\begin{aligned} h_1 u_{x15}(z) &= u_{x5}(z - z_1) + u_{x1}(z_5 - z), \quad & h_2 u_{x26}(z) &= u_{x6}(z - z_2) + u_{x2}(z_6 - z), \\ h_3 u_{x37}(z) &= u_{x7}(z - z_3) + u_{x3}(z_7 - z), \quad & h_4 u_{x48}(z) &= u_{x8}(z - z_4) + u_{x4}(z_8 - z). \end{aligned} \tag{32.24}$$

with similar interpolations for u_y and u_z. Setting $z = \pm\frac{1}{2}h_i$ we obtain

$$\begin{aligned} h_1 u_{x1}^- &= u_{x5}(-\tfrac{1}{2}h_1 - z_1) + u_{x1}(z_5 + \tfrac{1}{2}h_1), \quad & h_2 u_{x2}^- &= u_{x6}(-\tfrac{1}{2}h_2 - z_2) + u_{x2}(z_6 + \tfrac{1}{2}h_2), \\ h_3 u_{x3}^- &= u_{x7}(-\tfrac{1}{2}h_3 - z_3) + u_{x3}(z_7 + \tfrac{1}{2}h_3), \quad & h_4 u_{x4}^- &= u_{x8}(-\tfrac{1}{2}h_4 - z_4) + u_{x4}(z_8 + \tfrac{1}{2}h_4), \\ h_1 u_{x1}^+ &= u_{x5}(\tfrac{1}{2}h_1 - z_1) + u_{x1}(z_5 - \tfrac{1}{2}h_1), \quad & h_2 u_{x2}^+ &= u_{x6}(\tfrac{1}{2}h_2 - z_2) + u_{x2}(z_6 - \tfrac{1}{2}h_2), \\ h_3 u_{x3}^+ &= u_{x7}(\tfrac{1}{2}h_3 - z_3) + u_{x3}(z_7 - \tfrac{1}{2}h_3), \quad & h_4 u_{x4}^+ &= u_{x8}(\tfrac{1}{2}h_4 - z_4) + u_{x4}(z_8 - \tfrac{1}{2}h_4), \end{aligned} \tag{32.25}$$

The u_y and u_z components are related in the same manner. From these a 24×24 transformation matrix T_h relating

$$\mathbf{u}^{(e)} = \mathbf{T}_h\, \hat{\mathbf{u}}^{(e)} \tag{32.26}$$

can be built:

$$\mathbf{T}_h = \begin{bmatrix} a_1 & 0 & 0 & 0 & 0 & 0 & 0 & 0 & 0 & 0 & b_1 & 0 & 0 & 0 & 0 & 0 & 0 & 0 & 0 & 0 \\ 0 & a_1 & 0 & 0 & 0 & 0 & 0 & 0 & 0 & 0 & 0 & b_1 & 0 & 0 & 0 & 0 & 0 & 0 & 0 & 0 \\ 0 & 0 & a_1 & 0 & 0 & 0 & 0 & 0 & 0 & 0 & 0 & 0 & b_1 & 0 & 0 & 0 & 0 & 0 & 0 & 0 \\ 0 & 0 & 0 & b_2 & 0 & 0 & 0 & 0 & 0 & 0 & 0 & 0 & 0 & b_2 & 0 & 0 & 0 & 0 & 0 & 0 \\ \cdots & & & & & & & & & & & & & & & & & & & \end{bmatrix} \tag{32.27}$$

where $a_1 = \frac{1}{2} + z_5/h_1$, $b_1 = -\frac{1}{2} - z_1/h_1$, $a_2 = \frac{1}{2} + z_6/h_2$, $b_2 = -\frac{1}{2} - z_2/h_2$ etc. This matrix has the block pattern

$$\mathbf{T}_h = \begin{bmatrix} a_1\mathbf{I}_3 & \mathbf{0} & \mathbf{0} & \mathbf{0} & b_1\mathbf{I}_3 & \mathbf{0} & \mathbf{0} & \mathbf{0} \\ \mathbf{0} & a_2\mathbf{I}_3 & \mathbf{0} & \mathbf{0} & \mathbf{0} & b_2\mathbf{I}_3 & \mathbf{0} & \mathbf{0} \\ \mathbf{0} & \mathbf{0} & a_3\mathbf{I}_3 & \mathbf{0} & \mathbf{0} & \mathbf{0} & b_3\mathbf{I}_3 & \mathbf{0} \\ \mathbf{0} & \mathbf{0} & \mathbf{0} & a_4\mathbf{I}_3 & \mathbf{0} & \mathbf{0} & \mathbf{0} & b_3\mathbf{I}_3 \\ b_5\mathbf{I}_3 & \mathbf{0} & \mathbf{0} & \mathbf{0} & a_1\mathbf{I}_3 & \mathbf{0} & \mathbf{0} & \mathbf{0} \\ \mathbf{0} & b_6\mathbf{I}_3 & \mathbf{0} & \mathbf{0} & \mathbf{0} & a_2\mathbf{I}_3 & \mathbf{0} & \mathbf{0} \\ \mathbf{0} & \mathbf{0} & b_7\mathbf{I}_3 & \mathbf{0} & \mathbf{0} & \mathbf{0} & a_3\mathbf{I}_3 & \mathbf{0} \\ \mathbf{0} & \mathbf{0} & \mathbf{0} & b_8\mathbf{I}_3 & \mathbf{0} & \mathbf{0} & \mathbf{0} & a_4\mathbf{I}_3 \end{bmatrix} \tag{32.28}$$

where $\mathbf{I}_3$ is the 3×3 identity matrix and a_i and b_i are coefficients. If the element is originally flat: $z_1 = -\frac{1}{2}h_1$, $z_5 = \frac{1}{2}h_1$, etc., all $a_i = 1$ and $b_i = 0$ and $\mathbf{T}_h$ reduces to the 24×24 identity matrix, as may be expected.

§32.4. SS8 Stiffness Matrix

This section gives an overall picture of the derivation of the stiffness matrix for the SS8 solid shell element. Figure 9 gives the schematics of the top level calculation sequence, along with the name of the *Mathematica* modules that perform them.

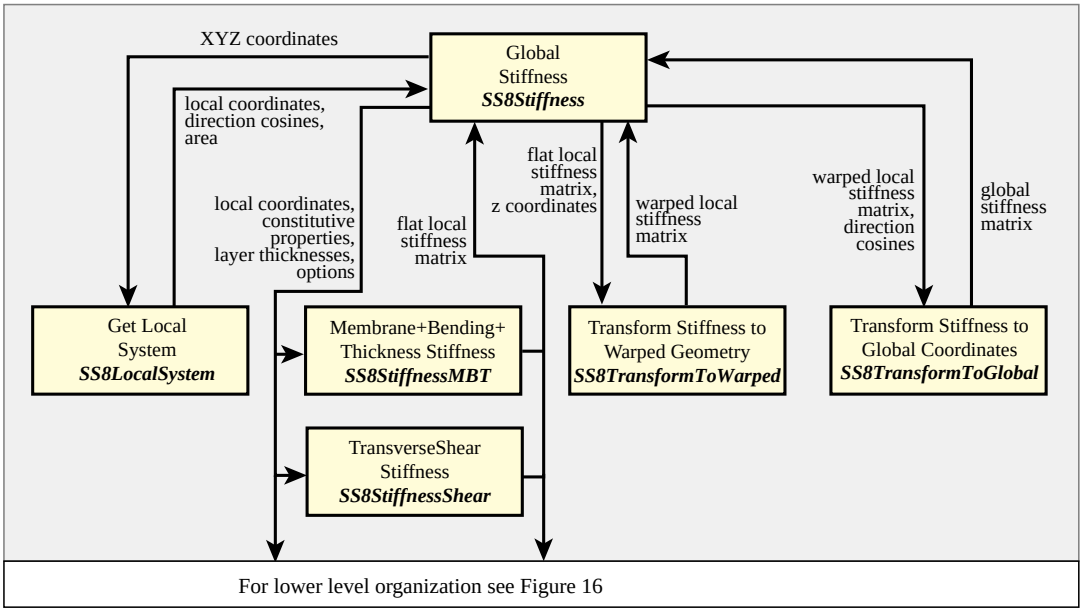

Figure 9. Organization of top-level SS8 stiffness computations.

§32.4.1. Behavioral Assumptions

The solid shell element stiffness accounts for the following mechanical actions. All of them are assumed to act in the flattened brick geometry.

Inplane response. This is controlled by strains and stresses in the $\zeta = const$ planes. These are further decoupled into *membrane* and *bending* actions. Membrane strains are constant in ζ whereas bending strains vary linearly in ζ.[5]

Thickness response. This is controlled by extensional strains and normal stresses in the ζ direction.

Transverse shear response. This is controlled by transverse shear strains and stresses, where "transverse" is to be understood in the sense of normal to the midsurface.

The fundamental assumption made in the subsequent development is:

In the flattened local geometry, transverse shear actions are decoupled from inplane and thickness actions through the constitutive equations.

Mathematically, the stress-strain constitutive equations in the flattened element local system must be of the form

$$\begin{bmatrix} \sigma^k_{xx} \\ \sigma^k_{yy} \\ \sigma^k_{xy} \\ \sigma^k_{xy} \\ \sigma^k_{yz} \\ \sigma^k_{zx} \end{bmatrix} = \begin{bmatrix} E^k_{11} & E^k_{12} & E^k_{13} & E^k_{14} & 0 & 0 \\ E^k_{12} & E^k_{22} & E^k_{23} & E^k_{24} & 0 & 0 \\ E^k_{13} & E^k_{23} & E^k_{33} & E^k_{34} & 0 & 0 \\ E^k_{14} & E^k_{24} & E^k_{34} & E^k_{44} & 0 & 0 \\ 0 & 0 & 0 & 0 & E^k_{55} & E^k_{56} \\ 0 & 0 & 0 & 0 & E^k_{56} & E^k_{66} \end{bmatrix} \begin{bmatrix} e^k_{xx} \\ e^k_{yy} \\ e^k_{zz} \\ 2e^k_{xy} \\ 2e^k_{yz} \\ 2e^k_{zx} \end{bmatrix} \tag{32.29}$$

for each k, where k is the layer index in a laminate composite construction. In other words, the material of each layer is monoclinic with z as principal material axis. If this condition is not met, this element

[5] Since the constitutive properties may vary along ζ in the case of laminate wall construction, the statement does not extend to stresses.

should not be used. A general solid element would be more appropriate. The assumption covers, however, many important cases of wall fabrication.

Note that coupling between inplane and thickness actions is permitted. In fact, even for isotropic materials such coupling exists in the form of Poisson's ratio effects.

A consequence of this assumption is that the element stiffness in the flattened geometry is the superposition of a membrane+bending+thickness stiffness (a grouping often abbreviated to MBT or mbt) and a shear stiffness:

$$\mathbf{K}^{(e)}_{mbts} = \mathbf{K}^{(e)}_{mbt} + \mathbf{K}^{(e)}_{s}. \tag{32.30}$$

As noted the element has a total of 24 degrees of freedom. Since it possesses 6 rigid body modes, it has 18 deformational modes. These are allocated to the four actions noted above: membrane, bending, thickness and transverse shear, in the numbers indicated in Table 1.

Table 1. Element Mode Count For Mechanical Actions

Action	Mode count
rigid body motions	6
membrane	5
bending	5
thickness	4
transverse shear	4
Total	24

§32.4.2. Top Level Implementation

The *Mathematica* implementation of the top level module `SS8Stiffness` is shown in Figure 10. This module is referenced as

```
Ke=SS8Stiffness[XYZcoor,{ElayerMBT,ElayerS},layers,options]
```
(32.31)

The arguments are:

`XYZcoor`	The global Cartesian coordinates of the 8 corner nodes, arranged as `{{X1,Y1,Z1},{X2,Y2,Z2}, ... {X8,Y8,Z8}}`.
`ElayerMBT`	Stress-strain constitutive matrices for MBT actions stacked in layer by layer sequence, as further described in §5.4.
`ElayerS`	Stress-strain onstitutive matrices for shear actions stacked in layer by layer sequence, as further described in §5.6.
`layers`	A list that specifies layer thicknesses, as described in §5.2ff.
`options`	Optional inputs, described later.

The module returns the 24×24 element stiffness matrix `Ke` in global coordinates.

```
SS8Stiffness[XYZcoor_,{ElayerMBT_,ElayerS_},layers_,options_]:=
  Module[{xyz,xyzcoor,xyzwh,Td,A0,Kmbt,Ks,Kmbts,Kw,Ke},
 {xyz,xyzwh,Td,A0}=SS8LocalSystem[XYZcoor];
  xyzcoor=Transpose[xyz];
  Kmbt=SS8StiffnessMBT[xyzcoor,ElayerMBT,layers,{0,0},options];
  Ks  =SS8StiffnessShear[xyzcoor,ElayerS,layers,options];
  Kmbts=Kmbt+Ks;
  Kw=SS8TransformToWarped[Kmbts,xyz[[3]] ];
  Ke=SS8TransformToGlobal[Kw,Td];
  Return[Ke]];
```

Figure 10. Top level module for calculation of global stiffness of the SS8 solid shell element.

§32.4.3. Calculation Steps

The top-level calculations steps schematized in Figure 9 are as follows.

Localization. This is done by module `SS8LocalSystem`, which was described in §2.3.

Local Stiffness Computation. Carried out by `SS8StiffnessMBT`, which returns the stiffness $\mathbf{K}_{mbt}^{(e)}$ due to membrane, bending and thickness (MBT) effects, and `SS8StiffnessShear`, which returns the stiffness $\mathbf{K}_{s}^{(e)}$ due to transverse shear effects. The two stiffnesses are added to form the local stiffness matrix as per (32.30).

Both sets of stiffness computations are carried out in the flattened brick geometry and are described in Sections 6 and 7, respectively.

Transformation to Warped Geometry. The stiffness matrix $\mathbf{K}_{mbts}^{(e)}$ of the flattened brick is transformed to the actual warped geometry by the congruential transformation

$$\mathbf{K}_{w}^{(e)} = \mathbf{T}_h^T \mathbf{K}_{mbts}^{(e)} \mathbf{T}_h, \tag{32.32}$$

where $\mathbf{T}_h$ is the transformation matrix introduced in Section 3.3.

This operation is implemented in module `SS8TransformToWarped`, which is listed in Figure 11. The implementation takes advantage of the sparse nature of matrix $\mathbf{T}_h$ to reduce the volume of operations.

The module is referenced as

`Kw=SS8TransformToWarped[Kmbts,zc]` (32.33)

where the arguments are

- `Kmbts` The flat brick stiffness matrix obtained from the addition (32.30).
- `zc` The local z coordinates $\{z_1, z_2, z_3, z_4, z_5, z_6, z_7, z_8\}$ of the warped brick corners arranged as list { `z1,z2,z3,z4,z5,z6,z7,z8` }. This list is available as third item of array `xyz` returned by `SS8LocalSystem`, as described in §2.3.

The module returns

- `Kw` The 24×24 stiffness matrix of the warped brick in local coordinates.

Transformation to Global Geometry. The stiffness matrix $\mathbf{K}_{w}^{(e)}$ produced by (32.32) is still in local coordinates. The final congruential transformation refers it to global $\{X, Y, Z\}$ coordinates:

$$\mathbf{K}^{(e)} = \mathbf{T}_d^T \mathbf{K}_{w}^{(e)} \mathbf{T}_d, \tag{32.34}$$

```
SS8TransformToWarped[Ke0_,z_]:=Module[{h1,h2,h3,h4,
  z1,z2,z3,z4,z5,z6,z7,z8,a,b,c1,c2,c3,c4,d1,d2,d3,d4,
  cc13,cc24,cc32,cd14,cd23,cd24,cd31,cd32,cd41,dd14,dd24,
  dd31,i,j,n,m,ni,nii,mj,mjj,K11,K12,K21,K22,Ke},
  {z1,z2,z3,z4,z5,z6,z7,z8}=z;
  {h1,h2,h3,h4}={z5-z1,z6-z2,z7-z3,z8-z4};
  a= 1/2+{z5/h1,z6/h2,z7/h3,z8/h4,-z1/h1,-z2/h2,-z3/h3,-z4/h4};
  b=-1/2+{z5/h1,z6/h2,z7/h3,z8/h4,-z1/h1,-z2/h2,-z3/h3,-z4/h4};
  a=Simplify[a]; b=Simplify[b]; Ke=Table[0,{24},{24}];
  For [n=1,n<=4,n++, For [m=1,m<=4,m++,
       c1=a[[n]]; c2=a[[n+4]]; c3=a[[m]]; c4=a[[m+4]];
       d1=b[[n]]; d2=b[[n+4]]; d3=b[[m]]; d4=b[[m+4]];
       cc13=c1*c3; cc24=c2*c4; cc32=c3*c2; cd14=c1*d4;
       cd24=c2*d4; cd23=c2*d3; cd31=c3*d1; cd32=c3*d2;
       cd41=c4*d1; dd14=d1*d4; dd24=d2*d4; dd31=d3*d1;
       For [i=1,i<=3,i++, ni=3*n-3+i; nii=ni+12;
           For [j=1,j<=3,j++, mj=3*m-3+j; mjj=mj+12;
               K11=Ke0[[ni,mj]];  K12=Ke0[[ni,mjj]];
               K21=Ke0[[nii,mj]]; K22=Ke0[[nii,mjj]];
               Ke[[ni,mj]]=   cc13*K11+cd14*K12+cd32*K21+dd24*K22;
               Ke[[nii,mj]]=  cd31*K11+dd14*K12+cc32*K21+cd24*K22;
               Ke[[mj,nii]]=  Ke[[nii,mj]];
               Ke[[nii,mjj]]= dd31*K11+cd41*K12+cd23*K21+cc24*K22;
      ]]]];
      Return[Ke];
  ];
```

Figure 11. Module to transform the flattened brick stiffness to the warped geometry.

```
SS8TransformToGlobal[Ke0_,Td_]:=Module[{
  st1=st2=st3=Table[0,{24}],
  t11,t12,t13,t21,t22,t23,t31,t32,t33,
  tst11,tst12,tst13,tst21,tst22,tst23,
  tst31,tst32,tst33,i,j,ib,jb, Ke=Ke0},
  {{t11,t12,t13},{t21,t22,t23},{t31,t32,t33}}=Td;
  Print[{{t11,t12,t13},{t21,t22,t23},{t31,t32,t33}}];
  For [jb=1,jb<=8,jb++, j=3*(jb-1);
      For [i=1,i<=24,i++,
          st1[[i]]=Ke[[i,j+1]]*t11+Ke[[i,j+2]]*t21+Ke[[i,j+3]]*t31;
          st2[[i]]=Ke[[i,j+1]]*t12+Ke[[i,j+2]]*t22+Ke[[i,j+3]]*t32;
          st3[[i]]=Ke[[i,j+1]]*t13+Ke[[i,j+2]]*t23+Ke[[i,j+3]]*t33];
      For [ib=1,ib<=jb,ib++, i=3*(ib-1);
          tst11=t11*st1[[i+1]]+t21*st1[[i+2]]+t31*st1[[i+3]];
          tst21=t12*st1[[i+1]]+t22*st1[[i+2]]+t32*st1[[i+3]];
          tst31=t13*st1[[i+1]]+t23*st1[[i+2]]+t33*st1[[i+3]];
          tst12=t11*st2[[i+1]]+t21*st2[[i+2]]+t31*st2[[i+3]];
          tst22=t12*st2[[i+1]]+t22*st2[[i+2]]+t32*st2[[i+3]];
          tst32=t13*st2[[i+1]]+t23*st2[[i+2]]+t33*st2[[i+3]];
          tst13=t11*st3[[i+1]]+t21*st3[[i+2]]+t31*st3[[i+3]];
          tst23=t12*st3[[i+1]]+t22*st3[[i+2]]+t32*st3[[i+3]];
          tst33=t13*st3[[i+1]]+t23*st3[[i+2]]+t33*st3[[i+3]];
          Ke[[i+1,j+1]]=tst11; Ke[[j+1,i+1]]=tst11;
          Ke[[i+1,j+2]]=tst12; Ke[[j+2,i+1]]=tst12;
          Ke[[i+1,j+3]]=tst13; Ke[[j+3,i+1]]=tst13;
          Ke[[i+2,j+1]]=tst21; Ke[[j+1,i+2]]=tst21;
          Ke[[i+2,j+2]]=tst22; Ke[[j+2,i+2]]=tst22;
          Ke[[i+2,j+3]]=tst23; Ke[[j+3,i+2]]=tst23;
          Ke[[i+3,j+1]]=tst31; Ke[[j+1,i+3]]=tst31;
          Ke[[i+3,j+2]]=tst32; Ke[[j+2,i+3]]=tst32;
          Ke[[i+3,j+3]]=tst33; Ke[[j+3,i+3]]=tst33];
          ];
      Return[Ke]];
```

Figure 12. Module to transform the warped brick stiffness to global coordinates.

where $\mathbf{T}_d^{(e)}$ is a 24×24 block diagonal matrix built from the 3×3 matrix of direction cosines as discussed

in §3.2.

This operation is implemented in module `SS8TransformToGlobal`, which is listed in Figure 12. The implementation takes advantage of the block-diagonal nature of matrix $\mathbf{T}_d^{(e)}$ to reduce the volume of operations.

The module is referenced as

```
Ke=SS8TransformToGlobal[Kw,Td]
```
(32.35)

where the arguments are

`Kw`	The warped brick stiffness matrix returned by `SS8TransformToWarped`.
`Td`	The 3×3 direction cosine matrix returned by `SS8LocalSystem`.

The module returns

`Ke`	The 24×24 stiffness matrix of the warped brick in global coordinates.

§32.5. Constitutive Properties

This section describes the method by which a layered wall configuration is treated by through-the-thickness integration. Readers not interested in these details may skip directly to Section 6.

§32.5.1. Laminate Fabrication

The SS8 element is permitted to have a laminate composite fabrication in the thickness (z or ζ) direction. If this is the case, the development of thickness-integrated constitutive equations is tricky. The complication is due to the presence of the *thickness strain*, which is an effect not present in ordinary plate and shell elements.

There are only two node layers to capture across-the-thickness deformations. It follows that only an average thickness strain $\bar{e}_{zz}$ can be sensed. But if $\bar{e}_{zz}$ is inserted in the constitutive equations of a laminated composite, the thickness stress σ_{zz} will jump between layers. This jump would grossly violate traction continuity conditions at the layer interfaces. The contradiction leads to an effect called *thickness locking*, with consequent wrong stress predictions.[6]

Note that thickness locking is not present in conventional thin plate and shell elements because for these it is assumed from the start that $\sigma_{zz} \approx 0$, which allows the use of plane stress constitutive relations in each layer.

The cure for thickness locking is in principle easy: assume a uniform thickness stress $\sigma_{zz} = \bar{\sigma}_{zz}$ instead of a uniform strain $e_{zz} = \bar{e}_{zz}$. This is in fact automatic when one derives the element by hybrid stress methods [22]. But for such elements one must assume all stress components, and one faces the opposite dilemma: the inplane stress components must be allowed to jump between layers. This is exceedingly difficult to achieve. One comes to the conclusion that the best solution is a mixture of strain and stress assumptions:

- Assume inplane strains $\{e_{xx}, e_{yy}, e_{xy}\}$ varying linearly across the thickness
- Assume a normal stress $\bar{\sigma}_{zz}$ uniform across the thickness

The two assumptions can be combined through a careful derivation of integrated stress-strain relations, as carried out below. Note that transverse shear strain effects do not come in the foregoing assumption because of the decoupling assumption made in §4.1.

[6] The effect has been called also Poisson's locking by some authors.

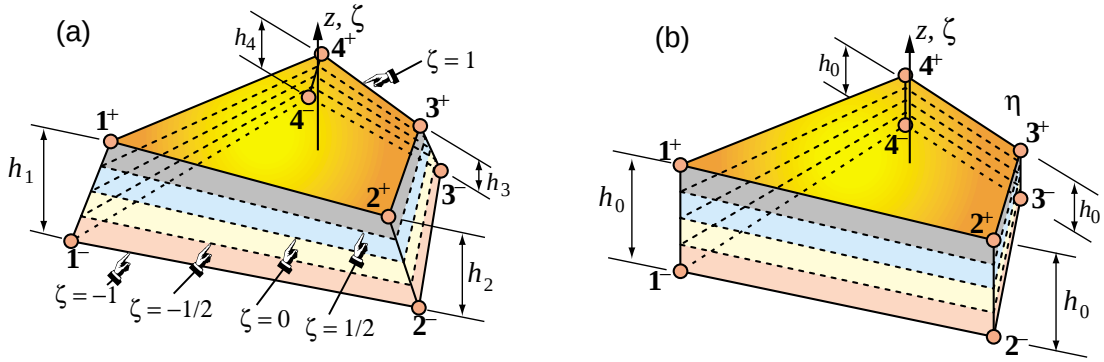

Figure 13. Wall fabrication assumption: layers are assumed to be separated by surfaces of constant ζ. Both figures illustrates the case of four equal thickness layers, separated at $\zeta = -1, -\frac{1}{2}, 0, \frac{1}{2}, 1$. If the element has variable thickness as illustrated in (a), these are not surfaces of constant z. In the case of constant thickness illustrated in (b), the separation also occurs at constant z.

§32.5.2. Wall Fabrication Assumptions

The SS8 element may have an arbitrary number of layers in the thickness direction. The properties of each layer in the inplane directions are taken to be uniform.

Layers are separated by constant-ζ lines, as illustrated in Figure 13. This assumption greatly simplifies the integration of the constitutive relations across the thickness. For variable thickness the separation assumption is not very realistic. Fortunately plates and shells fabricated as laminate composites frequently have uniform thickness because of fabrication constraints.

§32.5.3. MBT Constitutive Equations

The laminated composite has n_L layers identified by index $k = 1, \ldots n_L$. Layers are numbered from the bottom surface $\zeta = -1$ up; thus $k = 1$ is the bottom layer.

The point of departure are the transverse-shear-uncoupled stress-strain relations (32.29) for each k. From these we extract the relation for the inplane and thickness stresses and strains:

$$\begin{bmatrix} \sigma^k_{xx} \\ \sigma^k_{yy} \\ \sigma^k_{zz} \\ \sigma^k_{xy} \end{bmatrix} = \begin{bmatrix} E^k_{11} & E^k_{12} & E^k_{13} & E^k_{14} \\ E^k_{12} & E^k_{22} & E^k_{23} & E^k_{24} \\ E^k_{13} & E^k_{23} & E^k_{33} & E^k_{34} \\ E^k_{14} & E^k_{24} & E^k_{34} & E^k_{44} \end{bmatrix} \begin{bmatrix} e^k_{xx} \\ e^k_{yy} \\ e^k_{zz} \\ 2e^k_{xy} \end{bmatrix} \tag{32.36}$$

which for an isotropic material of elastic modulus E^k and Poisson's ratio ν^k reduce to

$$\begin{bmatrix} \sigma^k_{xx} \\ \sigma^k_{yy} \\ \sigma^k_{zz} \\ \sigma^k_{xy} \end{bmatrix} = \frac{E^k}{(1-2\nu^k)(1+\nu^k)} \begin{bmatrix} 1-\nu^k & \nu^k & \nu^k & 0 \\ \nu^k & 1-\nu^k & \nu^k & 0 \\ \nu^k & \nu^k & 1-\nu^k & 0 \\ 0 & 0 & 0 & \frac{1}{2}-\nu^k \end{bmatrix} \begin{bmatrix} e^k_{xx} \\ e^k_{yy} \\ e^k_{zz} \\ 2e^k_{xy} \end{bmatrix} \tag{32.37}$$

For subsequent manipulations this relation is rearranged and partitioned as follows

$$\begin{bmatrix} \boldsymbol{\sigma}^k_{\equiv} \\ \sigma^k_{zz} \end{bmatrix} = \begin{bmatrix} \sigma^k_{xx} \\ \sigma^k_{yy} \\ \sigma^k_{xy} \\ \cdots \\ \sigma^k_{zz} \end{bmatrix} = \begin{bmatrix} E^k_{11} & E^k_{12} & E^k_{14} & \vdots & E^k_{13} \\ E^k_{12} & E^k_{22} & E^k_{24} & \vdots & E^k_{23} \\ E^k_{14} & E^k_{24} & E^k_{44} & \vdots & E^k_{34} \\ \cdots & \cdots & \cdots & \cdots & \cdots \\ E^k_{13} & E^k_{23} & E^k_{34} & \vdots & E^k_{33} \end{bmatrix} \begin{bmatrix} e^k_{xx} \\ e^k_{yy} \\ 2e^k_{xy} \\ \cdots \\ e^k_{zz} \end{bmatrix} = \begin{bmatrix} \mathbf{E}^k_{\equiv} & \mathbf{E}^k_{\times} \\ (\mathbf{E}^k_{\times})^T & E^k_{zz} \end{bmatrix} \begin{bmatrix} \mathbf{e}^k_{\equiv} \\ e^k_{zz} \end{bmatrix}. \tag{32.38}$$

where subscripts $\equiv$, zz and $\times$ denote in-plane, transverse and coupled in-plane-transverse directions, respectively. The inverse relation is

$$\begin{bmatrix} \mathbf{e}^k_{\equiv} \\ e^k_{zz} \end{bmatrix} = \begin{bmatrix} \mathbf{E}^k_{\equiv} & \mathbf{E}^k_{\times} \\ (\mathbf{E}^k_{\times})^T & E^k_{zz} \end{bmatrix}^{-1} \begin{bmatrix} \boldsymbol{\sigma}^k_{\equiv} \\ \sigma^k_{zz} \end{bmatrix} = \begin{bmatrix} \mathbf{C}^k_{\equiv} & \mathbf{C}^k_{\times} \\ (\mathbf{C}^k_{\times})^T & C^k_{zz} \end{bmatrix} \begin{bmatrix} \boldsymbol{\sigma}^k_{\equiv} \\ \sigma^k_{zz} \end{bmatrix}. \tag{32.39}$$

This relation is exhibited only to establish notation since the inversion need not be done explicitly as shown later. Partial inversion yields

$$\begin{bmatrix} \boldsymbol{\sigma}^k_{\equiv} \\ e^k_{zz} \end{bmatrix} = \begin{bmatrix} (\mathbf{C}^k_{\equiv})^{-1} & -(\mathbf{C}^k_{\equiv})^{-1}\mathbf{C}^k_{\times} \\ (\mathbf{C}^k_{\times})^T(\mathbf{C}^k_{\equiv})^{-1} & C^k_{zz} - (\mathbf{C}^k_{\times})^T(\mathbf{C}^k_{\equiv})^{-1}\mathbf{C}^k_{\times} \end{bmatrix} \begin{bmatrix} e^k_{\equiv} \\ \sigma^k_{zz} \end{bmatrix} = \begin{bmatrix} \mathbf{S}^k & \mathbf{D}^k \\ -(\mathbf{D}^k)^T & R^k \end{bmatrix} \begin{bmatrix} e^k_{\equiv} \\ \sigma^k_{zz} \end{bmatrix}. \tag{32.40}$$

§32.5.4. MBT Thickness Integration

Because $\mathbf{e}_{\equiv} = \mathbf{e}_m + \zeta\,\mathbf{e}_b$ varies linearly in ζ and $\sigma_{zz} = \sigma_{zz}$ is constant along ζ, it is feasible to integrate (32.40) along ζ while taking $\mathbf{e}_m$, $\mathbf{e}_b$ and $\bar{\sigma}_{zz}$ out of the integral. Integration of $\boldsymbol{\sigma}_{\equiv}$ and $\zeta\sigma_{\equiv}$ provided by the first matrix equation gives effective membrane and bending stresses:

$$\begin{aligned} \begin{bmatrix} \bar{\boldsymbol{\sigma}}_m \\ \bar{\boldsymbol{\sigma}}_b \end{bmatrix} &= \tfrac{1}{2}\int_{-1}^{1} \begin{bmatrix} \boldsymbol{\sigma}_m \\ \zeta\boldsymbol{\sigma}_b \end{bmatrix} = \tfrac{1}{2}\int_{-1}^{1} \begin{bmatrix} \mathbf{S}^k & \mathbf{D}^k \\ \zeta\mathbf{S}^k & \zeta\mathbf{D}^k \end{bmatrix} \begin{bmatrix} \mathbf{e}_m + \zeta\,\mathbf{e}_b \\ \sigma_{zz} \end{bmatrix} d\zeta \\ &= \tfrac{1}{2}\int_{-1}^{1} \begin{bmatrix} \mathbf{S}^k & \zeta\mathbf{S}^k & \mathbf{D}^k \\ \zeta\mathbf{S}^k & \zeta^2\mathbf{S}^k & \zeta\mathbf{D}^k \end{bmatrix} d\zeta \begin{bmatrix} \mathbf{e}_m \\ \mathbf{e}_b \\ \sigma_{zz} \end{bmatrix}. \end{aligned} \tag{32.41}$$

Note that although $\bar{\boldsymbol{\sigma}}_m$ and $\bar{\boldsymbol{\sigma}}_b$ are not the stress resultants of conventional plates, they have a similar meaning. Integrating the second matrix equation one obtains the average thickness :

$$\begin{aligned} \bar{e}_z &= \tfrac{1}{2}\int_{-1}^{1} e_{zz}\,d\zeta = \tfrac{1}{2}\int_{-1}^{1} [\,-(\mathbf{D}^k)^T \;\; R^k\,] \begin{bmatrix} \mathbf{e}_p \\ \sigma_{zz} \end{bmatrix} d\zeta = \tfrac{1}{2}\int_{-1}^{1} [\,-(\mathbf{D}^k)^T \;\; R^k\,] \begin{bmatrix} \mathbf{e}_m + \zeta\,\mathbf{e}_b \\ \sigma_{zz} \end{bmatrix} d\zeta \\ &= \tfrac{1}{2}\int_{-1}^{1} [\,-(\mathbf{D}^k)^T \;\; -\zeta(\mathbf{D}^k)^T \;\; R^k\,]\, d\zeta \begin{bmatrix} \mathbf{e}_m \\ \mathbf{e}_b \\ \sigma_{zz} \end{bmatrix}. \end{aligned} \tag{32.42}$$

Introduce here the integrated constitutive matrices

$$\begin{bmatrix} \mathbf{S}_0 & \mathbf{S}_1 & \mathbf{D}_0 \\ \mathbf{S}_1 & \mathbf{S}_2 & \mathbf{D}_1 \\ -\mathbf{D}_0^T & -(\mathbf{D}_1)^T & R_0 \end{bmatrix} = \tfrac{1}{2}\int_{-1}^{1} \begin{bmatrix} \mathbf{S}^k & \zeta\mathbf{S}^k & \mathbf{D}^k \\ \zeta\mathbf{S}^k & \zeta^2\mathbf{S}^k & \mathbf{D}^k \\ -(\mathbf{D}^k)^T & -\zeta(\mathbf{D}^k)^T & R^k \end{bmatrix} d\zeta. \tag{32.43}$$

Then collecting (32.41) and (32.42) into one matrix relation and passing $\bar{e}_{zz}$ back to the right hand side gives

$$\begin{bmatrix} \bar{\boldsymbol{\sigma}}_m \\ \bar{\boldsymbol{\sigma}}_b \\ \sigma_{zz} \end{bmatrix} = \begin{bmatrix} \mathbf{S}_0 + \mathbf{D}_0\mathbf{D}_0^T/R_0 & \mathbf{S}_1 + \mathbf{D}_0\mathbf{D}_1^T/R_0 & \mathbf{D}_0/R_0 \\ \mathbf{S}_1 + \mathbf{D}_1\mathbf{D}_0^T/R_0 & \mathbf{S}_2 + \mathbf{D}_1\mathbf{D}_1^T/R_0 & \mathbf{D}_1/R_0 \\ \mathbf{D}_0^T/R_0 & \mathbf{D}_1/R_0 & 1/R_0 \end{bmatrix} \begin{bmatrix} \mathbf{e}_m \\ \mathbf{e}_b \\ \bar{e}_{zz} \end{bmatrix} = \bar{\mathbf{E}}_{mbt} \begin{bmatrix} \mathbf{e}_m \\ \mathbf{e}_b \\ \bar{e}_{zz} \end{bmatrix}, \tag{32.44}$$

The 4×4 constitutive matrix $\bar{\mathbf{E}}_{bmt}$ accounts for integrated membrane, bending and thickness effects, and can be used directly in that component of the stiffness matrix for an arbitrary layer configuration that meets the bounding assumptions of §5.2.

§32.5.5. Implementation of MBT Integration

For the computer implementation of the calculation of $\mathbf{E}_{mbt}$ the following simplification of (32.40) should be noted:

$$\begin{aligned} \mathbf{S}^k &= \begin{bmatrix} E^k_{11} - E^k_{13}E^k_{13}/E^k_{33} & E^k_{12} - E^k_{13}E^k_{23}/E^k_{33} & E^k_{14} - E^k_{13}E^k_{34}/E^k_{33} \\ E^k_{12} - E^k_{13}E^k_{23}/E^k_{33} & E^k_{22} - E^k_{23}E^k_{23}/E^k_{33} & E^k_{24} - E^k_{23}E^k_{34}/E^k_{33} \\ E^k_{14} - E^k_{13}E^k_{34}/E^k_{33} & E^k_{24} - E^k_{23}E^k_{34}/E^k_{33} & E^k_{44} - E^k_{34}E^k_{34}/E^k_{33} \end{bmatrix} \\ \mathbf{D}^k &= [\, E^k_{13} \quad E^k_{23} \quad E^k_{34} \,]/E^k_{33}, \qquad R^k = 1/E^k_{33} \end{aligned} \tag{32.45}$$

Using these simplifications the results for a one layer with

$$\mathbf{E}^1 = \begin{bmatrix} E_{11} & E_{12} & E_{13} & E_{14} \\ E_{12} & E_{22} & E_{23} & E_{24} \\ E_{13} & E_{23} & E_{33} & E_{34} \\ E_{14} & E_{24} & E_{34} & E_{44} \end{bmatrix} \tag{32.46}$$

is easily worked out to be

$$\bar{\mathbf{E}}_{bmt} = \begin{bmatrix} E_{11} & E_{12} & E_{14} & 0 & 0 & 0 & E_{13} \\ E_{12} & E_{22} & E_{24} & 0 & 0 & 0 & E_{23} \\ E_{14} & E_{24} & E_{44} & 0 & 0 & 0 & E_{34} \\ 0 & 0 & 0 & \frac{1}{3}(E_{11} - \frac{E_{13}E_{13}}{E_{33}}) & \frac{1}{3}(E_{12} - \frac{E_{13}E_{23}}{E_{33}}) & \frac{1}{3}(E_{14} - \frac{E_{13}E_{34}}{E_{33}}) & 0 \\ 0 & 0 & 0 & \frac{1}{3}(E_{12} - \frac{E_{13}E_{23}}{E_{33}}) & \frac{1}{3}(E_{22} - \frac{E_{23}E_{23}}{E_{33}}) & \frac{1}{3}(E_{24} - \frac{E_{23}E_{34}}{E_{33}}) & 0 \\ 0 & 0 & 0 & \frac{1}{3}(E_{14} - \frac{E_{13}E_{34}}{E_{33}}) & \frac{1}{3}(E_{24} - \frac{E_{23}E_{34}}{E_{33}}) & \frac{1}{3}(E_{44} - \frac{E_{34}E_{34}}{E_{33}}) & 0 \\ E_{13} & E_{23} & E_{34} & 0 & 0 & 0 & E_{33} \end{bmatrix} \tag{32.47}$$

If the one-layer wall is isotropic with modulus E and Poisson's ratio ν, (32.47) reduces to

$$\bar{\mathbf{E}}_{bmt} = \frac{E}{(1-2\nu)(1+\nu)} \begin{bmatrix} 1-\nu & \nu & 0 & 0 & 0 & 0 & \nu \\ \nu & 1-\nu & 0 & 0 & 0 & 0 & \nu \\ 0 & 0 & \frac{1}{2}-\nu & 0 & 0 & 0 & 0 \\ 0 & 0 & 0 & \frac{(1-2\nu)(1+\nu)}{3(1-\nu^2)} & \frac{\nu(1-2\nu)(1+\nu)}{3(1-\nu^2)} & \frac{\nu(1-2\nu)(1+\nu)}{3(1-\nu^2)} & 0 \\ 0 & 0 & 0 & \frac{\nu(1-2\nu)(1+\nu)}{3(1-\nu^2)} & \frac{(1-2\nu)(1+\nu)}{3(1-\nu^2)} & \frac{\nu(1-2\nu)(1+\nu)}{3(1-\nu^2)} & 0 \\ 0 & 0 & 0 & \frac{\nu(1-2\nu)(1+\nu)}{3(1-\nu^2)} & \frac{\nu(1-2\nu)(1+\nu)}{3(1-\nu^2)} & \frac{(1-2\nu)(1+\nu)}{1-\nu^2} & 0 \\ \nu & \nu & 0 & 0 & 0 & 0 & 1-\nu \end{bmatrix} \tag{32.48}$$

A *Mathematica* implementation that incorporates this simplification is shown in Figure 14. The module is referenced as

```
Embt=SS8WallIntegMBT[ElayerMBT,layers]
```
(32.49)

`ElayerMBT`	A list of 4×4 layer constitutive matrices (32.36), ordered from bottom to top.
`layers`	is a list of scaled layer thicknesses adding up to one.

The module returns the integrated constitutive matrix $\bar{\mathbf{E}}_{mbt}$ stored in `Embt`.

```
SS8ThickIntegMBT[ElayerMBT_,layers_]:=
  Module[{nlayers=Length[ElayerMBT],E11,E12,E13,E14,E22,E23,E24,
  E33,E34,E44,Ek,Sk,Dk,Rk,S0,S1,S2,D0,D1,R0,R,k,hlay,
  ζbot,ζtop,dζ,ζavg,Embt=Table[0,{7},{7}] },
   S0=S1=S2=Table[0,{3},{3}]; D0=D1=Table[0,{3}]; R=0;
   ζbot=ζtop=-1;
   For [k=1,k<=nlayers,k++,  hlay=layers[[k]];
       ζtop=ζbot+2*hlay; dζ=(ζtop-ζbot)/2; ζavg=(ζtop+ζbot)/2;
       Ek=ElayerMBT[[k]];
      {{E11,E12,E13,E14},{E12,E22,E23,E24},
       {E13,E23,E33,E34},{E14,E24,E34,E44}}=Ek;
       Sk={{E11-E13*E13/E33,E12-E13*E23/E33,E14-E13*E34/E33},
           {E12-E13*E23/E33,E22-E23*E23/E33,E24-E23*E34/E33},
           {E14-E13*E34/E33,E24-E23*E34/E33,E44-E34*E34/E33}};
       Sk=Simplify[Sk];
       Dk={E13,E23,E34}/E33; Rk=1/E33;
       S0=S0+dζ*Sk; S1=S1+dζ*ζavg*Sk;
       S2=S2+(ζtop^2+ζtop*ζbot+ζbot^2)*dζ*Sk/3;
       D0=D0+dζ*Dk; D1=D1+dζ*ζavg*Dk; R=R+dζ*Rk;
       ζbot=ζtop
       ];  {S0,S1,D0,D1,R}=Simplify[ {S0,S1,D0,D1,R}];
  S0=S0+(Transpose[{D0}].{D0})/R;
  S1=S1+(Transpose[{D0}].{D1})/R;
  S2=S2+(Transpose[{D1}].{D1})/R;
  D0=D0/R; D1=D1/R; R0=1/R;
  Embt=
{{S0[[1,1]],S0[[1,2]],S0[[1,3]],S1[[1,1]],S1[[1,2]],S1[[1,3]],D0[[1]]},
 {S0[[2,1]],S0[[2,2]],S0[[2,3]],S1[[2,1]],S1[[2,2]],S1[[2,3]],D0[[2]]},
 {S0[[3,1]],S0[[3,2]],S0[[3,3]],S1[[3,1]],S1[[3,2]],S1[[3,3]],D0[[3]]},
 {S1[[1,1]],S1[[2,1]],S1[[3,1]],S2[[1,1]],S2[[1,2]],S2[[1,3]],D1[[1]]},
 {S1[[1,2]],S1[[2,2]],S1[[3,2]],S2[[2,1]],S2[[2,2]],S2[[2,3]],D1[[2]]},
 {S1[[1,3]],S1[[2,3]],S1[[3,3]],S2[[3,1]],S2[[3,2]],S2[[3,3]],D1[[3]]},
 {D0[[1]],  D0[[2]],  D0[[3]],  D1[[1]],  D1[[2]],  D1[[3]],  R0    }};
  Return[Simplify[Embt]]];
```

Figure 14. *Mathematica* implementation of through-the-thickness integration process for the MBT constitutive equations.

To give an example, suppose that the total wall thickness is h fabricated with three layers whose thicknesses are 1/2, 1/3 and 1/6 of the total thickness, respectively. The constitutive matrices are taken to be

$$\mathbf{E}^k = \begin{bmatrix} 2k & 1 & 1 & 1 \\ 1 & 2k & 1 & 1 \\ 1 & 1 & 2k & 1 \\ 1 & 1 & 1 & k \end{bmatrix}, \quad k = 1, 2, 3. \tag{32.50}$$

[This is admittedly a contrived example, only used as benchmark.] The integrated matrix (32.44) is produced by the Mathematica statements

```
ElayerMBT1={{2,1,1,1},{1,2,1,1},{1,1,2,1},{1,1,1,1}};
ElayerMBT2={{4,1,1,1},{1,4,1,1},{1,1,4,1},{1,1,1,2}};
ElayerMBT3={{6,1,1,1},{1,6,1,1},{1,1,6,1},{1,1,1,3}};
Embt=SS8ThickIntegMBT[{ElayerMBT1,ElayerMBT2,ElayerMBT3},{1/2,1/3,1/6}];
Print["Embt=",Embt//MatrixForm];
```

```
SS8ThickIntegS[ElayerS_,layers_]:=
  Module[{nlayers=Length[ElayerS],Ek,k,ζbot,ζtop,dζ,
   Es=Table[0,{2},{2}] },
   ζbot=ζtop=-1;
   For[k=1,k<=nlayers,k++,
      ζtop=ζbot+2*layers[[k]]; dζ=(ζtop-ζbot)/2;
      Es+=dζ*ElayerS[[k]]; ζbot=ζtop;
      ];
  Return[Simplify[Es]]];
```

Figure 15. *Mathematica* implementation of through-the-thickness integration process for transverse shear constitutive equations.

The result is

$$\bar{\mathbf{E}}_{mbt} = \frac{1}{6318}\begin{bmatrix} 21060 & 6318 & 6318 & 4914 & 0 & 0 & 6318 \\ 6318 & 21060 & 6318 & 0 & 4914 & 0 & 6318 \\ 6318 & 6318 & 10530 & 0 & 0 & 2457 & 6318 \\ 4914 & 0 & 0 & 7168 & 1474 & 1474 & -1296 \\ 0 & 4914 & 0 & 1474 & 7168 & 1474 & -1296 \\ 0 & 0 & 2457 & 1474 & 1474 & 3268 & -1296 \\ 6318 & 6318 & 6318 & -1296 & -1296 & -1296 & 17496 \end{bmatrix}. \tag{32.51}$$

Note that for unsymmmetric wall fabrication, as in this example, the integrated matrix is generally full.

Two restrictions on the constitutive equations of a layer should be noted:

- If the material of the kth layer is exactly incompressible, $R^k = 0$ and division by zero will occur. In the isotropic case, this is obvious from a glance at (32.37) since the denominator vanishes if $\nu = 1/2$. Hence no layer can be incompressible.
- A "void layer", as in a sandwich construction, cannot be accomodated by setting $\mathbf{E}^k = \mathbf{0}$ since division by $E^k_{33} = 0$ will occur. To represent that case scale a nonzero $\mathbf{E}^k$ by a small number.

These two restrictions should be contrasted with conventional plates and shells, in which both incompressible and zero-stiffness layers are acceptable on account of *a priori* enforcement of plane stress conditions. The difference is that consideration of the thickness strain introduces three-dimensional effects that cannot be circumvented if two node layers are kept.

§32.5.6. Transverse Shear Constitutive Equations

The corresponding process for the transverse shear energy portion is much simpler. The transverse strains e_{xz} and e_{yz} are assumed to be uniform through the thickness, and the constitutive cross-coupling with the in-plane and thickness effects is ignored, as stated by (32.29).

Without going into the derivation details, the integrated constitutive relation to be used in the transverse shear energy is simply

$$\bar{\mathbf{E}}_s = \int_{-1}^{1} \begin{bmatrix} E^k_{55} & E^k_{56} \\ E^k_{56} & E^k_{66} \end{bmatrix} d\zeta. \tag{32.52}$$

An implementation of the integration process in *Mathematica* is shown in Figure 15.

The module is referenced as

```
Es=SS8WallIntegS[ElayerS,layers]
```
(32.53)

The arguments are

`ElayerS` A list of 2×2 layer constitutive matrices relating transverse shear stresses to transverse shear strains, as per the lower 2×2 block of (32.29).

`layers` Same as in `SS8WallIntegMBT`.

The module returns the integrated constitutive matrix $\bar{\mathbf{E}}_s$ stored in `Es` as function result.

§32.6. Membrane, Bending and Thickness (MBT) Stiffness

In this and the next section we cover the element stiffness computations that form the lower level schematized in Figure 16.

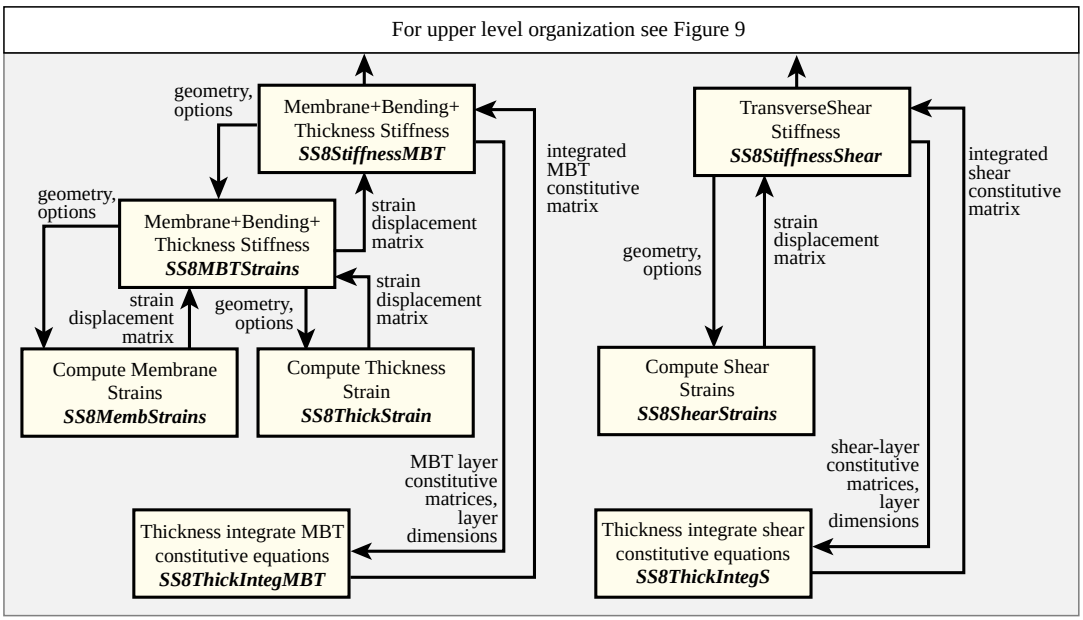

Figure 16. The lower level of the SS8 stiffness calculations.

In solid shell elements, the contributions of inplane effects: membrane and bending, are coupled to the thickness effects (deformations in the z direction) through the constitutive equations. The are collectively abbreviated to MBT effects. They are decoupled from transverse shear (TS) effects by *a priori* assumptions on the constitutive equations as discussed in §4.1. Consequently they can be separately considered and their contributions to the stiffness matrix added.

The contribution of MBT effects to the element stiffness is handled by the assumed strain method. Initial attempts to use the assumed natural strain method developed by other authors [2,8,24,25,26] led to element with high sensitivity to inplane FE distortion. A related but different method [12] was then developed over four months of experimentation with *Mathematica*. The performance of the element under distortion improved with this new field.

For flat plate elements of constant thickness, the new field can be shown to be optimal in a variational sense; that is, it cannot be improved without violating certain orthogonality and patch test satisfaction conditions. The construction of the strain field is first described with reference to a flat 4-node quadrilateral, and later transported to the SS8 element.

§32.6.1. Four-Noded Quadrilateral Geometry

We consider the quadrilateral obtained by cutting the SS8 flattened-brick geometry with the surface $\zeta = 0$, as shown in Figure 17(a). This quadrilateral is flat. Consequently it will be defined by the coordinates of the four corners: $\{x_i^Q, y_i^Q\}$, $i = 1, 2, 3, 4$. These are functions of ζ.

We shall employ the abbreviations $x_{ij}^Q = x_i^Q - x_j^Q$ and $y_{ij}^Q = y_i^Q - y_j^Q$. The coordinates of the quadrilateral center $\{\xi = 0, \eta = 0\}$, denoted by 0 in Figure x.1(a), are

$$x_0^Q = \tfrac{1}{4}(x_1^Q + x_2^Q + x_3^Q + x_4^Q), \qquad y_0^Q = \tfrac{1}{4}(y_1^Q + y_2^Q + y_3^Q + y_4^Q). \tag{32.54}$$

This point lies at the intersection of the medians. Denote by A_{ijk}^Q the signed area of the triangle spanned by the corners $\{i, j, k\}$, and A is the quadrilateral area. We have

$$\begin{aligned} &A_{123}^Q = \tfrac{1}{2}(x_{13}^Q y_{21}^Q - x_{21}^Q y_{13}^Q), \quad A_{234}^Q = \tfrac{1}{2}(x_{24}^Q y_{32}^Q - x_{32}^Q y_{24}^Q), \quad A_{341}^Q = \tfrac{1}{2}(x_{31}^Q y_{43}^Q - x_{43}^Q y_{31}^Q), \\ &A_{412}^Q = \tfrac{1}{2}(x_{42}^Q y_{14}^Q - x_{14}^Q y_{42}^Q), \quad A^Q = \tfrac{1}{2}(x_{31}^Q y_{42}^Q - x_{42}^Q y_{31}^Q) = A_{123}^Q + A_{341}^Q = A_{234}^Q + A_{412}^Q. \end{aligned} \tag{32.55}$$

The following identities are readily verified algebraically:

$$\begin{bmatrix} x_{14}^Q & x_{42}^Q & x_{34}^Q & 0 \\ x_{13}^Q & x_{32}^Q & 0 & x_{34}^Q \\ x_{12}^Q & 0 & x_{32}^Q & x_{24}^Q \\ 0 & x_{12}^Q & x_{31}^Q & x_{14}^Q \end{bmatrix} \begin{bmatrix} A_{234}^Q \\ A_{341}^Q \\ A_{412}^Q \\ A_{123}^Q \end{bmatrix} = \begin{bmatrix} 0 \\ 0 \\ 0 \\ 0 \end{bmatrix}, \quad \begin{bmatrix} y_{14}^Q & y_{42}^Q & y_{34}^Q & 0 \\ y_{13}^Q & y_{32}^Q & 0 & y_{34}^Q \\ y_{12}^Q & 0 & y_{32}^Q & y_{24}^Q \\ 0 & y_{12}^Q & y_{31}^Q & y_{14}^Q \end{bmatrix} \begin{bmatrix} A_{234}^Q \\ A_{341}^Q \\ A_{412}^Q \\ A_{123}^Q \end{bmatrix} = \begin{bmatrix} 0 \\ 0 \\ 0 \\ 0 \end{bmatrix}. \tag{32.56}$$

$$\begin{bmatrix} 1 & 1 & 1 & 1 \\ x_1^Q & x_2^Q & x_3^Q & x_4^Q \\ y_1^Q & y_2^Q & y_3^Q & y_4^Q \end{bmatrix} \begin{bmatrix} -A_{234}^Q \\ A_{341}^Q \\ -A_{412}^Q \\ A_{123}^Q \end{bmatrix} = \begin{bmatrix} 0 \\ 0 \\ 0 \\ 0 \end{bmatrix}. \tag{32.57}$$

The Jacobian determinant of the transformation between $\{x, y\}$ and $\{\xi, \eta\}$ is

$$J^Q = \left| \frac{\partial\{x, y\}}{\{\xi, \eta\}} \right| = \tfrac{1}{8}(J_0^Q + J_1^Q \xi + J_2^Q \eta). \tag{32.58}$$

where

$$J_0^Q = 2A^Q, \quad J_1^Q = x_{34}^Q y_{12}^Q - x_{12}^Q y_{34}^Q = 2\left(A_{234}^Q - A_{341}^Q\right), \quad J_2^Q = x_{23}^Q y_{14}^Q - x_{14}^Q y_{23}^Q = 2\left(A_{341}^Q - A_{412}^Q\right). \tag{32.59}$$

We note that

$$A_{123}^Q = \tfrac{1}{4}(J_0^Q + J_1^Q - J_2^Q), \; A_{234}^Q = \tfrac{1}{4}(J_0^Q + J_1^Q + J_2^Q), \; A_{412}^Q = \tfrac{1}{4}(J_0^Q - J_1^Q - J_2^Q), \; A_{341}^Q = \tfrac{1}{4}(J_0^Q - J_1^Q + J_2^Q). \tag{32.60}$$

The identities corresponding to (32.57) is $(x_{12}^Q + x_{34}^Q) J_0^Q + (x_{13}^Q + x_{24}^Q) J_1^Q + (x_{12}^Q + x_{43}^Q) J_2^Q = (x_{14}^Q + x_{32}^Q) J_0^Q + (x_{14}^Q + x_{23}^Q) J_1^Q + (x_{13}^Q + x_{42}^Q) J_2^Q = 0$ and two similar ones with y's. Let $\{\xi_C, \eta_C\}$ denote the isoparametric coordinates of the quadrilateral centroid C. (The intersection of diagonals D, shown in Figure x.1(b), is not necessary in this development.) It can be verified that

$$\xi_C = \frac{J_1^Q}{3J_0^Q}, \quad \eta_C = \frac{J_2^Q}{3J_0^Q} \tag{32.61}$$

For a rectangular or parallelogram geometry $J_1^Q = J_2^Q = 0$, and $\xi_C = \eta_C = 0$. For any other geometry C does not lie at the intersection of the medians.

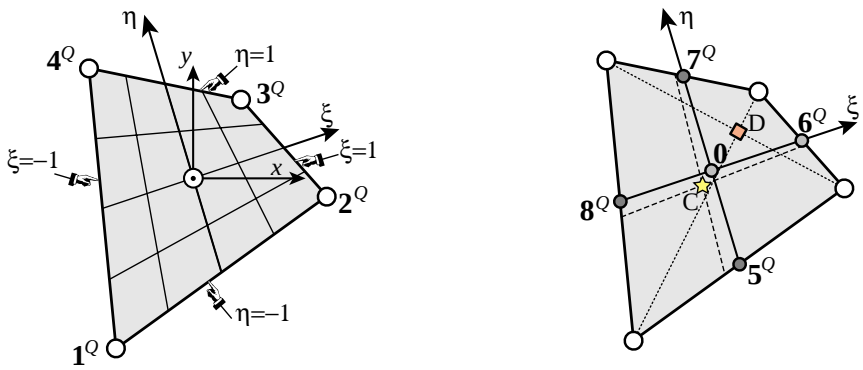

Figure 17. (a) four-node quadrilateral geometry and natural coordinates $\{\xi, \eta\}$. (b) Some special points: 5,6,7,8,0 designate midpoints and center, respectively; C is the centroid and D the intersection of diagonals.

§32.6.2. Quadrilateral Invariant Relations

Quadratic combinations of J_0^Q, J_1^Q and J_2^Q may be express rationally in terms of the squared lengths of sides and diagonals. The following formulas were found by *Mathematica* (of which only the first one is well known):

$$
\begin{aligned}
(J_0^Q)^2 &= L_{31}^2 L_{42}^2 - P^2, \\
4(J_1^Q)^2 &= 4L_{21}^2 L_{43}^2 - (L_{14}^2 - L_{31}^2 + L_{32}^2 - L_{42}^2)^2, \quad 4(J_2^Q)^2 = 4L_{14}^2 L_{32}^2 - (L_{21}^2 - L_{31}^2 - L_{42}^2 + L_{43}^2)^2, \\
4J_0^Q J_1^Q &= 2(L_{32}^2 - L_{14}^2)P + L_{31}^2 Q + L_{42}^2 R, \quad 4J_0^Q J_2^Q = 2(L_{21}^2 - L_{43}^2)P - L_{31}^2 Q + L_{42}^2 R, \\
4J_1^Q J_2^Q &= L_{14}^2 L_{21}^2 - L_{21}^2 L_{32}^2 + L_{32}^2 L_{43}^2 - L_{43}^2 L_{14}^2 + (L_{42}^2 - L_{31}^2)(S - L_{31}^2 - L_{42}^2) \\
&= \tfrac{1}{4}(R^2 - Q^2)(S - L_{31}^2 - L_{42}^2),
\end{aligned}
\tag{32.62}
$$

in which

$$
\begin{aligned}
P &= \tfrac{1}{2}(L_{21}^2 - L_{32}^2 + L_{43}^2 - L_{14}^2), \quad Q = L_{21}^2 + L_{32}^2 - L_{43}^2 - L_{14}^2, \\
R &= -L_{21}^2 + L_{32}^2 + L_{43}^2 - L_{14}^2, \quad S = L_{21}^2 + L_{32}^2 + L_{43}^2 + L_{14}^2.
\end{aligned}
\tag{32.63}
$$

The geometry of an arbitrary quadrilateral is defined by five independent quantities. It is convenient to select these to be invariants. For example, the four side lenghts and one diagonal length may be chosen, but the specification is not symmetric respect to the choice of diagonal. A more elegant specification consists of taking the three invariants J_0^Q, J_1^Q, J_2^Q plus the semisum and semidifference of the squared diagonal lengths: $K_1 = \frac{1}{2}(L_{31}^2 + L_{42}^2)$ and $K_2 = \frac{1}{2}(L_{31}^2 - L_{42}^2)$. We get

$$
\begin{aligned}
P &= -\sqrt{L_{31}L_{42} - (J_0^Q)^2} = -\sqrt{K_1^2 - K_2^2 - (J_0^Q)^2}, \\
Q &= 2\frac{(J_1^Q(K_1 - K_2 - P) - J_2^Q(K_1 - K_2 + P)}{J_0^Q}, \quad R = 2\frac{(J_1^Q(K_1 + K_2 - P) - J_2^Q(K_1 + K_2 + P)}{J_0^Q}, \\
S &= 2\frac{(J_0^Q)^2(K_1K_2 - J_1^Q J_2^Q) + (J_2^Q K_2 + J_1^Q K_1 - J_1^Q P)(J_1^Q K_2 + J_2^Q K_1 + J_2^Q P)}{(J_0^Q)^2 K_2},
\end{aligned}
\tag{32.64}
$$

The side lengths are then recovered from $L_{21}^2 = \frac{1}{4}(2P + Q - R + S)$, $L_{32}^2 = \frac{1}{4}(-2P + Q + R + S)$, $L_{43}^2 = \frac{1}{4}(2P - Q + R + S)$ and $L_{14}^2 = \frac{1}{4}(-2P - Q - R + S)$. The squared median lengths can also

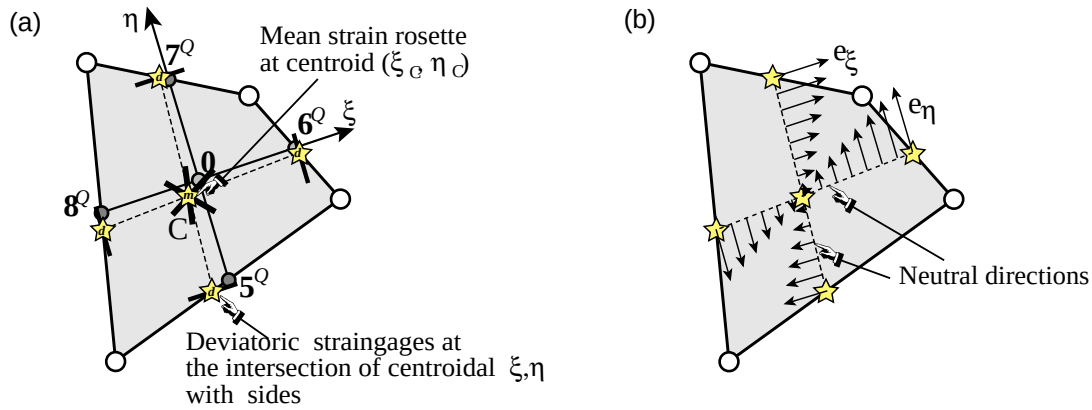

Figure 18. The strain field over the quadrilateral: (a) gages;
(b) deviatoric bending strains about the centroidal medians 9shown in dotted lines).

be expressed in terms of invariants, as discovered by *Mathematica*:

$$L_{57}^2 = \tfrac{1}{4}(L_{42}^2 + L_{31}^2 - L_{21}^2 + L_{32}^2 - L_{43}^2 + L_{14}^2) = \tfrac{1}{2}(K_1 - P)$$
$$L_{68}^2 = \tfrac{1}{4}(L_{42}^2 + L_{31}^2 + L_{21}^2 - L_{32}^2 + L_{43}^2 - L_{14}^2) = \tfrac{1}{2}(K_1 + P)$$

§32.6.3. The Assumed Strains

The assumed strain field is obtained from the gage locations shown in Figure 18(a). The strains $\mathbf{e} = \bar{\mathbf{e}} + \mathbf{e}_d$ are decomposed into a mean part $\bar{\mathbf{e}} = \mathbf{e}_C$, which is the value at the quadrilateral centroid $\{\xi_C = J_1/(3J_0, \eta_c = J_2/(3J_2\}$, and an energy-orthogonal deviatoric part that varies linearly in $\{\xi, \eta\}$.

The mean strain $\bar{\mathbf{e}}$ is obtained by putting a strain rosette at the centroid as depicted in Figure 18(a).

The deviatoric strains are assumed to consist of the response of the quadrilateral to bending about the two dotted lines sketched in Figure 18(b), which pass through the centroid. These will be called the *neutral lines*. Two appropriate choices for the neutral lines are:

1. Lines parallel to the medians 57 and 68
2. Lines of coordinates $\xi = \xi_C$, $\eta = \eta_C$, called the *centroidal medians*

The two possibilities can be subsumed in a single form by introducing a free parameter α, such that if $\alpha = 0$ or $\alpha = 1$ the neutral lines are parallel to the medians or centroidal medianms, respectively.

Both patterns consist of one-dimensional strains e_ξ and e_η where e_ξ is oriented along the axis ξ and e_η along the axis η. The latter varies linearly in $\xi - \xi_C$ and the former linearly in $\eta - \eta_C$. Four "deviatoric gages" are placed as shown to measure the amplitudes of these patterns. Note that these locations are not generally the side midpoints. Because of the assumed linear variations two of these gages are actually redundant and could be removed. For example we could keep 5 and 6 and get rid of 7 and 8. However they are retained in the configurations depicted in Figure 18 for visual symmetry.

A one dimensional strain state e_m along a direction m forming direction cosines $\{c_m, s_m\}$ with respect to $\{x, y\}$ generates the Cartesian components $e_{xx} = c_m^2 e_m$, $e_{yy} = s_m^2 e_m$ and $2e_{xy} = 2s_m c_m e_m$. Hence the foregoing strain field may be written in terms of five strain aplitudes χ_1 through χ_5 as

$$\begin{aligned} e_{xx} &= \chi_1 + c_{m\xi}^2(\xi - \xi_C)\chi_4 + c_{m\eta}^2(\eta - \eta_C)\chi_5, \\ e_{yy} &= \chi_2 + s_{m\xi}^2(\xi - \xi_C)\chi_4 + s_{m\eta}^2(\eta - \eta_C)\chi_5, \\ 2e_{xy} &= \chi_3 + 2s_{m\xi}c_{m\xi}(\xi - \xi_C)\chi_4 + 2s_{m\eta}c_{m\eta}(\eta - \eta_C)\chi_5, \end{aligned} \tag{32.65}$$

where $\{c_{m\xi}, s_{m\xi}\}$ and $\{c_{m\eta}, s_{m\eta}\}$ are the direction cosines of the neutral directions. In matrix form

$$\mathbf{e}^Q = \begin{bmatrix} e_{xx} \\ e_{yy} \\ 2e_{xy} \end{bmatrix} = \begin{bmatrix} 1 & 0 & 0 & c^2_{m\xi}(\xi-\xi_C) & c^2_{m\eta}(\eta-\eta_C) \\ 0 & 1 & 0 & s^2_{m\xi}(\xi-\xi_C) & s^2_{m\eta}(\eta-\eta_C) \\ 0 & 0 & 1 & 2s_{m\xi}c_{m\xi}(\xi-\xi_C) & 2s_{m\eta}c_{m\eta}(\eta-\eta_C) \end{bmatrix} \begin{bmatrix} \chi_1 \\ \chi_2 \\ \chi_3 \\ \chi_4 \\ \chi_5 \end{bmatrix} = \mathbf{B}^Q \boldsymbol{\chi}^Q. \tag{32.66}$$

What is the rationale behind (32.65)-(32.66)? Partly experience: for parallelograms and rectangles this distribution is known to lead to optimal elements. Partly simplicity: a linear variation in $(\xi, \eta\}$ is the simplest one. But rooting this distribution away from the center point 0 has been missed by many authors. For the displacement derived strains we take the isoparametric interpolation. Then differentiation gives

$$\begin{aligned} \mathbf{B}^Q_{iso} = \frac{J_0}{8J}\mathbf{B}_c &+ \frac{\xi}{8J}\begin{bmatrix} y^Q_{43} & 0 & y^Q_{34} & 0 & y^Q_{12} & 0 & y^Q_{21} & 0 \\ 0 & x^Q_{34} & 0 & x^Q_{43} & 0 & x^Q_{21} & 0 & x^Q_{12} \\ x^Q_{34} & y^Q_{43} & x^Q_{43} & y^Q_{34} & x^Q_{21} & y^Q_{12} & x^Q_{12} & y^Q_{21} \end{bmatrix} \\ &+ \frac{\eta}{8J}\begin{bmatrix} y^Q_{41} & 0 & y^Q_{23} & 0 & y^Q_{41} & 0 & y^Q_{23} & 0 \\ 0 & x^Q_{14} & 0 & x^Q_{32} & 0 & x^Q_{14} & 0 & x^Q_{32} \\ x^Q_{14} & y^Q_{41} & x^Q_{32} & y^Q_{23} & x^Q_{14} & y^Q_{41} & x^Q_{32} & y^Q_{23} \end{bmatrix} \end{aligned} \tag{32.67}$$

Evaluation of this matrix at the center pivot location P at $\xi^\beta_C = \beta J^Q_1/(3J^Q_0)$, $\eta^\beta_C = \beta J^Q_2/(3J^Q_0)$ yields

$$\mathbf{B}^Q_C = \frac{1}{3(J^Q_0)^2 + \beta((J^Q_1)^2 + (J^Q_2)^2)} \begin{bmatrix} B_{11} & 0 & B_{13} & 0 & B_{15} & 0 & B_{17} & 0 \\ 0 & B_{22} & 0 & B_{24} & 0 & B_{26} & 0 & B_{28} \\ B_{31} & B_{32} & B_{33} & B_{34} & B_{35} & B_{36} & B_{37} & B_{38} \end{bmatrix} \tag{32.68}$$

in which

$$\begin{aligned} B_{11} &= 3J^Q_0 y^Q_{24} + \beta(J^Q_1 y^Q_{43} + J^Q_2 y^Q_{32}), & B_{13} &= 3J^Q_0 y^Q_{31} + \beta(J^Q_1 y^Q_{34} + J^Q_2 y^Q_{14}), \\ B_{15} &= 3J^Q_0 y^Q_{42} + \beta(J^Q_1 y^Q_{12} + J^Q_2 y^Q_{41}), & B_{17} &= 3J^Q_0 y^Q_{13} + \beta(J^Q_1 y^Q_{21} + J^Q_2 y^Q_{23}), \\ B_{22} &= 3J^Q_0 x^Q_{42} + \beta(J^Q_1 x^Q_{34} + J^Q_2 x^Q_{23}), & B_{24} &= 3J^Q_0 x^Q_{13} + \beta(J^Q_1 x^Q_{43} + J^Q_2 x^Q_{41}), \\ B_{26} &= 3J^Q_0 x^Q_{24} + \beta(J^Q_1 x^Q_{21} + J^Q_2 x^Q_{14}), & B_{28} &= 3J^Q_0 x^Q_{31} + \beta(J^Q_1 x^Q_{12} + J^Q_2 x^Q_{32}), \\ B_{31} &= 3J^Q_0 x^Q_{42} + \beta(J^Q_1 x^Q_{34} + J^Q_2 x^Q_{23}), & B_{32} &= 3J^Q_0 y^Q_{24} + \beta(J^Q_1 y^Q_{43} + J^Q_2 y^Q_{32}), \\ B_{33} &= 3J^Q_0 x^Q_{13} + \beta(J^Q_1 x^Q_{43} + J^Q_2 x^Q_{41}), & B_{34} &= 3J^Q_0 y^Q_{31} + \beta(J^Q_1 y^Q_{34} + J^Q_2 y^Q_{14}), \\ B_{35} &= 3J^Q_0 x^Q_{24} + \beta(J^Q_1 x^Q_{21} + J^Q_2 x^Q_{14}), & B_{36} &= 3J^Q_0 y^Q_{42} + \beta(J^Q_1 y^Q_{12} + J^Q_2 y^Q_{41}), \\ B_{37} &= 3J^Q_0 x^Q_{31} + \beta(J^Q_1 x^Q_{12} + J^Q_2 x^Q_{32}), & B_{38} &= 3J^Q_0 y^Q_{13} + \beta(J^Q_1 y^Q_{21} + J^Q_2 y^Q_{23}), \end{aligned} \tag{32.69}$$

§32.6.4. The Fitted Strain Field

The strain fitting (SF) problem consists of constructing a matrix $\mathbf{T}^Q$ such that $\boldsymbol{\chi} = \mathbf{T}^Q\mathbf{u}^Q$ minimizes a dislocation energy functional. Details of the fitting procedure are explained in another document in preparation [12]. Only the final result is shown here:

$$\mathbf{T}^Q = \begin{bmatrix} \mathbf{B}^Q_C \\ \mathbf{W}\mathbf{H}_h \end{bmatrix} \tag{32.70}$$

where matrices $\mathbf{W}$ and $\mathbf{H}_h$ are given by

$$\mathbf{H}_h = \begin{bmatrix} H_1 & 0 & H_2 & 0 & H_3 & 0 & H_4 & 0 \\ 0 & H_1 & 0 & H_2 & 0 & H_3 & 0 & H_4 \end{bmatrix} \tag{32.71}$$

$$H_1 = \frac{J_0^Q + J_1^Q + J_2^Q}{J_0^Q},\ H_2 = \frac{-J_0^Q + J_1^Q - J_2^Q}{J_0^Q}, \quad H_3 = \frac{J_0^Q - J_1^Q + J_2^Q}{J_0^Q},\ H_4 = \frac{-J_0^Q - J_1^Q - J_2^Q}{J_0^Q}, \tag{32.72}$$

$$\begin{aligned} \mathbf{W} &= \begin{bmatrix} W_{11} & W_{12} \\ W_{21} & W_{22} \end{bmatrix}, \\ W_{11} &= \frac{(3(J_0^Q)^2 + (J_2^Q)^2\alpha)(3J_0^Q(x_{21}^Q + x_{34}^Q) + J_2^Q\alpha(x_{12}^Q + x_{34}^Q))}{18(J_0^Q)^3 L_{68C}^2} \\ W_{12} &= \frac{(3(J_0^Q)^2 + (J_2^Q)^2\alpha)(3J_0^Q(y_{21}^Q + y_{34}^Q) + J_2^Q\alpha(y_{12}^Q + y_{34}^Q))}{18(J_0^Q)^3 L_{68C}^2} \\ W_{21} &= \frac{(3(J_0^Q)^2 + (J_1^Q)^2\alpha)(3J_0^Q(x_{32}^Q + x_{41}^Q) + J_1^Q\alpha(x_{12}^Q + x_{34}^Q))}{18(J_0^Q)^3 L_{57C}^2} \\ W_{22} &= \frac{(3(J_0^Q)^2 + (J_1^Q)^2\alpha)(3J_0^Q(y_{32}^Q + y_{41}^Q) + J_1^Q\alpha(y_{12}^Q + y_{34}^Q))}{18(J_0^Q)^3 L_{57C}^2} \end{aligned} \tag{32.73}$$

If $\alpha = 0$, which means the neutral directions are parallel to the quadrilateral medians

$$W_{11} = \frac{x_{21}^Q + x_{34}^Q}{2L_{68}^2}, \quad W_{12} = \frac{y_{21}^Q + y_{34}^Q}{2L_{68}^2}, \quad W_{21} = \frac{x_{32}^Q + x_{41}^Q}{2L_{57}^2}, \quad W_{22} = \frac{y_{32}^Q + y_{41}^Q}{2L_{57}^2}. \tag{32.74}$$

The inplane Cartesian strains are then

$$\mathbf{e}^Q = \mathbf{B}_\chi^Q \mathbf{T}^Q \mathbf{u}^Q = \mathbf{B}^Q \mathbf{u}^Q. \tag{32.75}$$

It is not difficult to check that this strain field exactly represents rigid body motions and constant inplane strain states for any quadrilateral geometry. This should be expected since the derivation (not presented here) takes care of such conditions. What is surprising is that the field preserves those states also for a solid shell element of fairly general geometry, as discussed next.

§32.6.5. Extending the Quadrilateral Strains to SS8

The strain field derived in the preceding subsections for the quadrilateral will be now extended to the SS8. The two basic assumptions are:

1. The geometry is that of the flattened brick element. That is, the midsurface $\zeta = 0$ is flat, but the element may have thickness taper and variable thickness. See Figure 3.
2. The field $\mathbf{e}^Q$ evaluated for the midsurface quadrilateral is extended to any $-1 \le \zeta \le 1$ by taking a section of the flattened brick at a constant ζ.

Notice that the second assumption is relevant if the element is thickness tapered, because if so the constant-ζ section furnish different quadrilaterals.

The geometric constraints are less restrictive than those imposed for the transverse shear strains in Section 7. Why? Because it will be shown that the field $\mathbf{e}^Q$ exactly satisfies consistency conditions for the geometry (32.3) for the membrane component, and no further developments are required.[7]

[7] Exactness for a warped element would demand additional work, however, which presently seems beyond the power of computer

```
SS8MembStrains[xyzcoor_,{ξ_,η_,ζ_},Jlist_,{α_,β_},options_]:=
  Module[{x1,x2,x3,x4,x5,x6,x7,x8,y1,y2,y3,y4,y5,y6,y7,y8,
   z1,z2,z3,z4,z5,z6,z7,z8,cb,ct,
   x10,x20,x30,x40,y10,y20,y30,y40,h1,h2,h3,h4,
   x12,x13,x14,x21,x23,x24,x31,x32,x34,x41,x42,x43,
   y12,y13,y14,y21,y23,y24,y31,y32,y34,y41,y42,y43,
   Δx1,Δx2,Δx3,Δx4,Δy1,Δy2,Δy3,Δy4,numer,Jgiven,
   JQ0,JQ1,JQ2,ξC,ηC,ξ0β,η0β,dξ,dη,x5C,y5C,x6C,y6C,x7C,y7C,
   x8C,y8C,x57C,x75C,y57C,y75C,x86C,x68C,y86C,y68C,
   LL57C,LL68C,H1,H2,H3,H4,W,WH,JC,Tm,Bm},
 {{x1,y1,z1},{x2,y2,z2},{x3,y3,z3},{x4,y4,z4},
  {x5,y5,z5},{x6,y6,z6},{x7,y7,z7},{x8,y8,z8}}=xyzcoor;
   cb=(1-ζ)/2; ct=(1+ζ)/2;
  {x10,x20,x30,x40}={x5,x6,x7,x8}*ct+{x1,x2,x3,x4}*cb;
  {y10,y20,y30,y40}={y5,y6,y7,y8}*ct+{y1,y2,y3,y4}*cb;
  {Δx1,Δx2,Δx3,Δx4}={x5,x6,x7,x8}*ct-{x1,x2,x3,x4}*cb;
  {Δy1,Δy2,Δy3,Δy4}={y5,y6,y7,y8}*ct-{y1,y2,y3,y4}*cb;
  {x12,x13,x14,x21,x23,x24,x31,x32,x34,x41,x42,x43}=
    {x10-x20,x10-x30,x10-x40,x20-x10,x20-x30,x20-x40,
     x30-x10,x30-x20,x30-x40,x40-x10,x40-x20,x40-x30};
  {y12,y13,y14,y21,y23,y24,y31,y32,y34,y41,y42,y43}=
    {y10-y20,y10-y30,y10-y40,y20-y10,y20-y30,y20-y40,
     y30-y10,y30-y20,y30-y40,y40-y10,y40-y20,y40-y30};
  {numer,Jgiven}=options;
   If [Jgiven, {JQ0,JQ1,JQ2}=Jlist, JQ0=x31*y42-x42*y31;
       JQ1=x34*y12-x12*y34; JQ2=x23*y14-x14*y23];
   {ξ0,η0}={JQ1,JQ2}/(3*JQ0); {ξC,ηC}=α*{ξ0,η0}; ξ0β=β*ξ0; η0β=β*η0;
   x5C=(x1*(1-ξC)+x2*(1+ξC))/2; x6C=(x2*(1-ηC)+x3*(1+ηC))/2;
   x7C=(x3*(1+ξC)+x4*(1-ξC))/2; x8C=(x4*(1+ηC)+x1*(1-ηC))/2;
   y5C=(y1*(1-ξC)+y2*(1+ξC))/2; y6C=(y2*(1-ηC)+y3*(1+ηC))/2;
   y7C=(y3*(1+ξC)+y4*(1-ξC))/2; y8C=(y4*(1+ηC)+y1*(1-ηC))/2;
   x57C=x5C-x7C; y57C=y5C-y7C; x75C=-x57C; y75C=-y57C;
   x68C=x6C-x8C; y68C=y6C-y8C; x86C=-x68C; y86C=-y68C;
   LL57C=x57C^2+y57C^2;  LL68C=x68C^2+y68C^2;
   H1=( JQ0+JQ1+JQ2)/(2*JQ0); H2=(-JQ0+JQ1-JQ2)/(2*JQ0);
   H3=( JQ0-JQ1-JQ2)/(2*JQ0); H4=(-JQ0-JQ1+JQ2)/(2*JQ0);
   H=Simplify[{{H1,0,H2,0,H3,0,H4,0},{0,H1,0,H2,0,H3,0,H4}}];
   W={{(3*JQ0^2+JQ2^2*α)*(3*JQ0*(x21+x34)+JQ2*α*(x12+x34)),
       (3*JQ0^2+JQ2^2*α)*(3*JQ0*(y21+y34)+JQ2*α*(y12+y34))}/
        (18*JQ0^3*LL68C),
      {(3*JQ0^2+JQ1^2*α)*(3*JQ0*(x32+x41)+JQ1*α*(x12+x34)),
       (3*JQ0^2+JQ1^2*α)*(3*JQ0*(y32+y41)+JQ1*α*(y12+y34))}/
        (18*JQ0^3*LL57C)};
   WH=Simplify[W.H]; JC=3*JQ0^2+β*(JQ1^2+JQ2^2);
   Tm={{3*JQ0*y24+β*(JQ1*y43+JQ2*y32),0,
        3*JQ0*y31+β*(JQ1*y34+JQ2*y14),0,
        3*JQ0*y42+β*(JQ1*y12+JQ2*y41),0,
        3*JQ0*y13+β*(JQ1*y21+JQ2*y23),0}/JC,
       {0,3*JQ0*x42+β*(JQ1*x34+JQ2*x23),
        0,3*JQ0*x13+β*(JQ1*x43+JQ2*x41),
        0,3*JQ0*x24+β*(JQ1*x21+JQ2*x14),
        0,3*JQ0*x31+β*(JQ1*x12+JQ2*x32)}/JC,
       {3*JQ0*x42+β*(JQ1*x34+JQ2*x23),3*JQ0*y24+β*(JQ1*y43+JQ2*y32),
        3*JQ0*x13+β*(JQ1*x43+JQ2*x41),3*JQ0*y31+β*(JQ1*y34+JQ2*y14),
        3*JQ0*x24+β*(JQ1*x21+JQ2*x14),3*JQ0*y42+β*(JQ1*y12+JQ2*y41),
        3*JQ0*x31+β*(JQ1*x12+JQ2*x32),3*JQ0*y13+β*(JQ1*y21+JQ2*y23)}/JC,
                    WH[[1]],WH[[2]]};
   dη=η-η0β;   dξ=ξ-ξ0β;
   Bm={{1,0,0,     (x68C^2/LL68C)*dη,     (x75C^2/LL57C)*dξ},
       {0,1,0,     (y68C^2/LL68C)*dη,     (y75C^2/LL57C)*dξ},
       {0,0,1,2*(x68C*y68C/LL68C)*dη,2*(x75C*y75C/LL57C)*dξ}};
   If [numer,Return[N[{Bm,Tm}]]]; Return[{Bm,Tm}] ];
```

Figure 19. *Mathematica* implementation of the fitted strain field over a quadrilateral

§32.6.6. Membrane Strain Implementation

A *Mathematica* implementation of the foregoing assumptions for computing the matrix components

algebra systems.

$\mathbf{T}^Q$ and $\mathbf{B}^Q_\chi$ is listed in Figure 19.

The module is referenced as

```
{TQ,BQ}=SS8MembStrains[xyzcoor, {ξ,η ζ}, Jlist, {α,β}, options]
```
(32.76)

where

`xyzcoor`	The local coordinates of the flattened brick, arranged as `{{x1,x2,...x8},{y1,y2,...y8},{z1,z2,...z8}}` Here `z1=-h1/2`, `z2=-h2/2`, etc.
$\{\xi, \eta, \zeta\}$	ξ and η are quadrilateral coordinates, while ζ specifies the cutting surface that produces the quadrilateral. The ability to evaluate strains at the bottom surface $\zeta = -1$ and top surface $\zeta = 1$ will be found important in the treatment of the bending response.
`Jlist`	If logical flag `Jgiven` in `options` is `True`, a list `{J0,J1,J2}` of Jacobians to be used instead of internally calculated from the corner coordinates. Primarily used in element development and testing.
$\{\alpha, \beta\}$	Free parameters α and β. The second one is far more important as regard element performance. In the present SS8 implementation both parameters are set to zero by the higher levels, because optimal values are not precisely known yet. They are left as arguments for future developments.
`options`	Logical flags `{numer,Jgiven}`

The module returns the matrix list `{Bm,Tm}`. The first one is the 3×5 matrix $\mathbf{B}^Q$ that transforms $\boldsymbol{\chi}^Q = \mathbf{T}^Q\mathbf{u}^{(e)}$ to Cartesian components as per (32.66). The second one is the 5×8 strain-amplitude-displacement matrix $\mathbf{T}^Q$.

§32.6.7. Thickness Interpolation

To find a strain interpolation along ζ, relation (32.75) is manipulated as follows. First, $\mathbf{u}_Q$ at a fixed ζ is expanded to include all degrees of freedom of the SS8 element:

$$\begin{aligned}
\mathbf{u}^Q(\zeta) &= [\,u^Q_{x1}(\zeta) \quad u^Q_{y1}(\zeta) \quad u^Q_{x2}(\zeta) \quad \ldots \quad u^Q_{x4}(\zeta)\,]^T = \tfrac{1}{2}(1-\zeta)\mathbf{u}^{Q-} + \tfrac{1}{2}(1+\zeta)\mathbf{u}^{Q+} \\
\mathbf{u}^{Q-} &= [\,u^-_{x1} \quad u^-_{y1} \quad u^-_{x2} \quad u^-_{y2} \quad u^-_{x3} \quad u^-_{y3} \quad u^-_{x4} \quad u^-_{y4}\,]^T \\
\mathbf{u}^{Q+} &= [\,u^+_{x1} \quad u^+_{y1} \quad u^+_{x2} \quad u^+_{y2} \quad u^+_{x3} \quad u^+_{y3} \quad u^+_{x4} \quad u^+_{y4}\,]^T
\end{aligned} \tag{32.77}$$

In turn $\mathbf{u}^{Q-} = \mathbf{L}^-\mathbf{u}^{(e)}$, $\mathbf{u}^{Q+} = \mathbf{L}^+\mathbf{u}^{(e)}$ where $\mathbf{L}^-$ and $\mathbf{L}^+$ are 8×24 localization matrices that extract the freedoms in $\mathbf{u}^{Q-}$ and $\mathbf{u}^{Q+}$ from the 24 freedoms of the full node displacement vector:

$$
\mathbf{L}^- = \begin{bmatrix}
1&0&0&0&0&0&0&0&0&0&0&0&0&0&0&0&0&0&0&0&0&0&0&0\\
0&1&0&0&0&0&0&0&0&0&0&0&0&0&0&0&0&0&0&0&0&0&0&0\\
0&0&0&1&0&0&0&0&0&0&0&0&0&0&0&0&0&0&0&0&0&0&0&0\\
0&0&0&0&1&0&0&0&0&0&0&0&0&0&0&0&0&0&0&0&0&0&0&0\\
0&0&0&0&0&0&1&0&0&0&0&0&0&0&0&0&0&0&0&0&0&0&0&0\\
0&0&0&0&0&0&0&1&0&0&0&0&0&0&0&0&0&0&0&0&0&0&0&0\\
0&0&0&0&0&0&0&0&0&1&0&0&0&0&0&0&0&0&0&0&0&0&0&0\\
0&0&0&0&0&0&0&0&0&0&1&0&0&0&0&0&0&0&0&0&0&0&0&0
\end{bmatrix}
$$

$$
\mathbf{L}^+ = \begin{bmatrix}
0&0&0&0&0&0&0&0&0&0&0&0&1&0&0&0&0&0&0&0&0&0&0&0\\
0&0&0&0&0&0&0&0&0&0&0&0&0&1&0&0&0&0&0&0&0&0&0&0\\
0&0&0&0&0&0&0&0&0&0&0&0&0&0&0&1&0&0&0&0&0&0&0&0\\
0&0&0&0&0&0&0&0&0&0&0&0&0&0&0&0&1&0&0&0&0&0&0&0\\
0&0&0&0&0&0&0&0&0&0&0&0&0&0&0&0&0&0&1&0&0&0&0&0\\
0&0&0&0&0&0&0&0&0&0&0&0&0&0&0&0&0&0&0&1&0&0&0&0\\
0&0&0&0&0&0&0&0&0&0&0&0&0&0&0&0&0&0&0&0&0&1&0&0\\
0&0&0&0&0&0&0&0&0&0&0&0&0&0&0&0&0&0&0&0&0&0&1&0
\end{bmatrix}
\tag{32.78}
$$

Substitution into the first of (32.77) yields

$$
\mathbf{u}^Q = \tfrac{1}{2}(\mathbf{L}^+ + \mathbf{L}^-)\mathbf{u}^{(e)} + \tfrac{1}{2}(\mathbf{L}^+ - \mathbf{L}^-)\zeta\,\mathbf{u}^{(e)} \tag{32.79}
$$

As can be seen the strain $\mathbf{e}^Q = \mathbf{T}^Q\mathbf{u}^Q$ splits naturally into a membrane and a bending part, each containing 3 strain components:

$$
\mathbf{e}^Q = \mathbf{e}_m + \mathbf{e}_b = \mathbf{T}^Q\,\tfrac{1}{2}(\mathbf{L}^+ + \mathbf{L}^-)\mathbf{u}^{(e)} + \mathbf{T}^Q\,\tfrac{1}{2}(\mathbf{L}^+ - \mathbf{L}^-)\mathbf{u}^{(e)}) = \mathbf{B}_m\mathbf{u}^{(e)} + \mathbf{B}_b\mathbf{u}^{(e)} \tag{32.80}
$$

The thickness strain $e_{zz} = \mathbf{B}_t\mathbf{u}^{(e)}$ is adjoined to the components of $\mathbf{e}_m$ and $\mathbf{e}_b$ to complete a 7-vector:

$$
\mathbf{e}_{mbt} = \begin{bmatrix}\mathbf{e}_m\\ \mathbf{e}_b\\ \mathbf{e}_t\end{bmatrix} = \begin{bmatrix}\mathbf{B}_m\\ \mathbf{B}_b\\ \mathbf{B}_t\end{bmatrix}\mathbf{u}^{(e)} \tag{32.81}
$$

The expression of $\mathbf{B}_t$ is developed in §6.9.

§32.6.8. Strain Field Consistency Checks

Consider the 12×24 basic-states matrix of the Free Formulation [4,5,6]:

$$
\mathbf{G}_{rc}^T = \begin{bmatrix}
1&0&0&1&0&0&1&0&0&1&0&0&\ldots&1&0&0\\
0&1&0&0&1&0&0&1&0&0&1&0&\ldots&0&1&0\\
0&0&1&0&0&1&0&0&1&0&0&1&\ldots&0&0&1\\
y_1&-x_1&0&y_2&-x_2&0&y_3&-x_3&0&y_4&-x_4&0&\ldots&y_8&-x_8&0\\
0&z_1&-y_1&0&z_2&-y_2&0&z_3&-y_3&0&z_4&-y_4&\ldots&0&z_8&-y_8\\
-z_1&0&x_1&-z_2&0&x_2&-z_3&0&x_3&-z_4&0&x_4&\ldots&-z_8&0&x_8\\
x_1&0&0&x_2&0&0&x_3&0&0&x_4&0&0&\ldots&x_8&0&0\\
0&y_1&0&0&y_2&0&0&y_3&0&0&y_4&0&\ldots&0&y_8&0\\
0&0&z_1&0&0&z_2&0&0&z_3&0&0&z_4&\ldots&0&0&z_8\\
y_1&x_1&0&y_2&x_2&0&y_3&x_3&0&y_4&x_4&0&\ldots&y_8&x_8&0\\
0&z_1&y_1&0&z_2&y_2&0&z_3&y_3&0&z_4&y_4&\ldots&0&z_8&y_8\\
z_1&0&x_1&z_2&0&x_2&z_3&0&x_3&z_4&0&x_4&\ldots&z_8&0&x_8
\end{bmatrix}. \tag{32.82}
$$

The first six columns of $\mathbf{G}_{rc}$ specify the six rigid body modes of three-dimensional space. The next six columns specify uniform strain states $e_{xx} = 1$, $e_{yy} = 1$, $e_{zz} = 1$, $2e_{xy} = 2$, $2e_{yz} = 2$ and $2e_{zx} = 2$, in that order.

Insert in (32.82) the coordinates (32.4) of an arbitrary flattened brick in symbolic form. Perform the multiplication $\mathbf{e}^Q(\zeta) = \mathbf{T}^Q[(\mathbf{L}^+ + \mathbf{L}^-) + (\mathbf{L}^+ - \mathbf{L}^-)]\mathbf{G}_{rc}$. The result should be

$$\begin{bmatrix} e^Q_{xx} \\ e^Q_{yy} \\ 2e^Q_{xy} \end{bmatrix} = \begin{bmatrix} 0 & 0 & 0 & 0 & 0 & 0 & 1 & 0 & 0 & 0 & 0 & 0 \\ 0 & 0 & 0 & 0 & 0 & 0 & 0 & 1 & 0 & 0 & 0 & 0 \\ 0 & 0 & 0 & 0 & 0 & 0 & 0 & 0 & 0 & 2 & 0 & 0 \end{bmatrix} \tag{32.83}$$

And indeed a symbolic computation verifies (32.83) exactly for any combination of coordinates in (32.5) and arbitrary ζ. Note that this verification takes care of the membrane strains at any ζ. A similar check for the bending strains $\mathbf{e}_b$ gave the following result: uniform bending strain states are exactly reproduced if the element has constant thickness $h_1 = h_2 = h_4 = h_4 = h_0$, even if it is thickness tapered. If the thickness varies, uniform bending states are not exactly preserved.[8]

§32.6.9. The Thickness Strain

The thickness strain is the average extensional strain $\bar{e}_{zz}$ in the z direction normal to the midplane. Note that this is only and average value because an element with only two node layers in the z direction cannot resolve more. If this average strain is taken as the actual strain e_{zz} stress-jump contradictions arise in laminate wall constructions; these are resolved as explained in Section 5.

To get $\bar{e}_{zz}$ from the nodal displacements the most effective method is the use of the conventional isoparametric interpolation, differentiated and evaluate it at $\zeta = 0$. The derivation ofers no surprises and only the final result is given here.

$$\bar{e}_{zz} = \bar{e}_{zz1}N^Q_1(\xi,\eta) + \bar{e}_{zz2}N^Q_2(\xi,\eta) + \bar{e}_{zz3}N^Q_3(\xi,\eta) + \bar{e}_{zz4}N^Q_4(\xi,\eta) = \mathbf{B}_{zz}\mathbf{u}^{(e)}. \tag{32.84}$$

whwre N^Q_i are the bilinear quadrilateral shape functions, and $\bar{e}_{zzi}$ are the average thickness strains at the corners $i = 1, 2, 3, 4$. These are given by the relations

$$\bar{e}_{zz1} = \mathbf{B}_{zz1}\mathbf{u}^{(e)}, \quad \bar{e}_{zz2} = \mathbf{B}_{zz2}\mathbf{u}^{(e)}, \quad e_{zz3} = \mathbf{B}_{zz3}\mathbf{u}^{(e)}, \quad e_{zz4} = \mathbf{B}_{zz4}\mathbf{u}^{(e)}. \tag{32.85}$$

The $\mathbf{B}_{zzi}$ are the 1×24 strain-displacement matrices

$$\begin{aligned}
\mathbf{B}_{t1} &= \big[\,0 \quad 0 \quad B_{z11} - \frac{1}{h_1} \quad 0 \quad 0 \quad B_{z12} \quad 0 \quad 0 \quad 0 \quad 0 \quad 0 \quad B_{z14} \\
&\qquad 0 \quad 0 \quad B_{z11} + \frac{1}{h_1} \quad 0 \quad 0 \quad B_{z12} \quad 0 \quad 0 \quad 0 \quad 0 \quad 0 \quad B_{z14}\,\big] \\
\mathbf{B}_{t2} &= \big[\,0 \quad 0 \quad B_{z21} \quad 0 \quad 0 \quad B_{z22} - \frac{1}{h_2} \quad 0 \quad 0 \quad B_{z23} \quad 0 \quad 0 \quad 0 \\
&\qquad 0 \quad 0 \quad B_{z21} \quad 0 \quad 0 \quad B_{z22} + \frac{1}{h_2} \quad 0 \quad 0 \quad B_{z23} \quad 0 \quad 0 \quad 0\,\big] \\
\mathbf{B}_{t3} &= \big[\,0 \quad 0 \quad 0 \quad 0 \quad 0 \quad B_{z32} \quad 0 \quad 0 \quad B_{z33} - \frac{1}{h_3} \quad 0 \quad 0 \quad B_{z34} \\
&\qquad 0 \quad 0 \quad 0 \quad 0 \quad 0 \quad B_{z32} \quad 0 \quad 0 \quad B_{z33} + \frac{1}{h_3} \quad 0 \quad 0 \quad B_{z34}\,\big] \\
\mathbf{B}_{t4} &= \big[\,0 \quad 0 \quad B_{z41} \quad 0 \quad 0 \quad 0 \quad 0 \quad 0 \quad B_{z43} \quad 0 \quad 0 \quad B_{z44} - \frac{1}{h_4} \\
&\qquad 0 \quad 0 \quad B_{z41} \quad 0 \quad 0 \quad 0 \quad 0 \quad 0 \quad B_{z43} \quad 0 \quad 0 \quad B_{z44} + \frac{1}{h_4}\,\big]
\end{aligned} \tag{32.86}$$

[8] It is not presently know if the strain field definition can be adjusted to extend bending strain exactness to variable thickness configurations. An attempt in that direction failed because the symbolic computations "exploded" in intermediate stages and expressions could not be simplified over a reasonable amount of time.

where

$$
\begin{aligned}
B_{z11} &= (\Delta y_1\bar{x}_{24} + \Delta x_1\bar{y}_{42})/(8J_{c1}), \quad & B_{z12} &= (\Delta y_1\bar{x}_{41} + \Delta x_1\bar{y}_{14})/(8J_{c1}) \\
B_{z14} &= (\Delta y_1\bar{x}_{12} + \Delta x_1\bar{y}_{21})/(8J_{c1}), \quad & B_{z21} &= (\Delta y_2\bar{x}_{23} + \Delta x_2\bar{y}_{32})/(8J_{c2}) \\
B_{z22} &= (\Delta y_2\bar{x}_{31} + \Delta x_2\bar{y}_{13})/(8J_{c2}), \quad & B_{z23} &= (\Delta y_2\bar{x}_{12} + \Delta x_2\bar{y}_{21})/(8J_{c2}) \\
B_{z32} &= (\Delta y_3\bar{x}_{34} + \Delta x_3\bar{y}_{43})/(8J_{c3}), \quad & B_{z33} &= (\Delta y_3\bar{x}_{42} + \Delta x_3\bar{y}_{24})/(8J_{c3}) \\
B_{z34} &= (\Delta y_3\bar{x}_{23} + \Delta x_3\bar{y}_{32})/(8J_{c3}), \quad & B_{z41} &= (\Delta y_4\bar{x}_{34} + \Delta x_4\bar{y}_{43})/(8J_{c4}) \\
B_{z43} &= (\Delta y_4\bar{x}_{41} + \Delta x_4\bar{y}_{14})/(8J_{c4}), \quad & B_{z44} &= (\Delta y_4\bar{x}_{13} + \Delta x_4\bar{y}_{31})/(8J_{c4}), \\
J_{c1} &= (J_0^Q - J_1^Q - J_2^Q)h_1, \qquad & J_{c1} &= (J_0^Q + J_1^Q - J_2^Q)h_2, \\
J_{c3} &= (J_0^Q + J_1^Q + J_2^Q)h_3, \qquad & J_{c4} &= (J_0^Q - J_1^Q + J_2^Q)h_4.
\end{aligned}
\tag{32.87}
$$

in which J_0^Q, J_1^Q and J_2^Q are the Jacobian coefficients of the quadrilateral at $\zeta = 0$. Obviously

$$
\mathbf{B}_{zz} = \mathbf{B}_{zz1}N_1^Q + \mathbf{B}_{zz2}N_2^Q + \mathbf{B}_{zz3}N_3^Q + \mathbf{B}_{zz4}N_4^Q. \tag{32.88}
$$

This 1×4 matrix is a function of $\{\xi, \eta\}$ only through the N_i^Q's. Postmultiplying $\mathbf{B}_{zz}$ by $\mathbf{G}_{rc}$ gives

$$
\mathbf{B}_{zz}\mathbf{G}_{rc} = [\,0 \quad 0 \quad 0 \quad 0 \quad 0 \quad 0 \quad 0 \quad 0 \quad 1 \quad 0 \quad 0 \quad 0\,] \tag{32.89}
$$

for any combination of coordinates. Hence the strain-displacement relation satisfies conservation of basic states.

It should be noted that if one attempts to use the tensorial thickness strains to get $\bar{e}_{zz}$ as done by several authors, the resulting strains are generally incorrect unless the element is thickness prismatic: $\Delta x_1 = \Delta x_2 = \Delta x_3 = \Delta x_4 = \Delta y_1 = \Delta y_2 = \Delta y_3 = \Delta y_4 = 0$.

§32.6.10. Thickness Strain Implementation

The *Mathematica* module `SS8ThickStrain` listed in Figure 20 implements the computation of $\mathbf{B}_{zz}$. The module is referenced as

```
Bz = SS8ThickStrain[xyzcoor, {ξ, η}, options]
```
(32.90)

where

`xyzcoor`	The local coordinates of the flattened brick, arranged as `{{x1,x2,...x8},{y1,y2,...y8},{z1,z2,...z8}}` Here `z1=-h1/2`, `z2=-h2/2`, etc.
$\{\xi, \eta\}$	Quadrilateral coordinates of point at which $\mathbf{B}_{zz}$ will be evaluated.
`options`	Logical flag `{numer}`. If `True`, compute $\mathbf{B}_{zz}$ using floating point arithmetic.

The module returns `Bz`, which is the 1×24 matrix $\mathbf{B}_{zz}$ defined in (32.88).

As an example, consider the element with the node coordinates shown in Figure 21. From this

$$
\begin{aligned}
x_1^0 &= -1/3, \quad x_2^0 = 12/5, \quad x_3^0 = 5/3, \quad x_4^0 = 2/5, \\
y_1^0 &= 1/5, \quad y_2^0 = -3/7, \quad y_3^0 = 7/3, \quad y_4^0 = 9/5, \\
\Delta x_1 &= 1/12, \quad \Delta x_2 = -2/7, \quad \Delta x_3 = 1/9, \quad \Delta x_4 = 1/7, \\
\Delta y_1 &= -2/15, \quad \Delta y_2 = -1/9, \quad \Delta y_3 = -1/11, \quad \Delta y_4 = -1/3, \\
h_1 &= 6/5, \quad h_2 = 8/7, \quad h_3 = 4/5, \quad h_4 = 3/5,
\end{aligned}
\tag{32.91}
$$

```
SS8ThickStrain[xyzcoor_,{ξ_,η_},options_]:=Module[
  {x1,x2,x3,x4,x5,x6,x7,x8,y1,y2,y3,y4,y5,y6,y7,y8,
   z1,z2,z3,z4,z5,z6,z7,z8,
   x10,x20,x30,x40,y10,y20,y30,y40,h1,h2,h3,h4,
   x12,x13,x14,x21,x23,x24,x31,x32,x34,x41,x42,x43,
   y12,y13,y14,y21,y23,y24,y31,y32,y34,y41,y42,y43,
   Δx1,Δx2,Δx3,Δx4,Δy1,Δy2,Δy3,Δy4,JQ0,JQ1,JQ2,numer,
   NQ1,NQ2,NQ3,NQ4,Jc1,Jc2,Jc3,Jc4,Bz11,Bz12,Bz14,Bz21,Bz22,
   Bz23,Bz32,Bz33,Bz34,Bz41,Bz42,Bz43,Bz44,Bz},
 {{x1,y1,z1},{x2,y2,z2},{x3,y3,z3},{x4,y4,z4},
  {x5,y5,z5},{x6,y6,z6},{x7,y7,z7},{x8,y8,z8}}=xyzcoor;
  {x10,x20,x30,x40}={x5+x1,x6+x2,x7+x3,x8+x4}/2;
  {y10,y20,y30,y40}={y5+y1,y6+y2,y7+y3,y8+y4}/2;
  {Δx1,Δx2,Δx3,Δx4}={x5-x1,x6-x2,x7-x3,x8-x4}/2;
  {Δy1,Δy2,Δy3,Δy4}={y5-y1,y6-y2,y7-y3,y8-y4}/2;
  {h1,h2,h3,h4}={z5-z1,z6-z2,z7-z3,z8-z4};
  {x12,x13,x14,x21,x23,x24,x31,x32,x34,x41,x42,x43}=
     {x10-x20,x10-x30,x10-x40,x20-x10,x20-x30,x20-x40,
      x30-x10,x30-x20,x30-x40,x40-x10,x40-x20,x40-x30};
  {y12,y13,y14,y21,y23,y24,y31,y32,y34,y41,y42,y43}=
    {y10-y20,y10-y30,y10-y40,y20-y10,y20-y30,y20-y40,
     y30-y10,y30-y20,y30-y40,y40-y10,y40-y20,y40-y30};
  JQ0=x31*y42-x42*y31; JQ1=x34*y12-x12*y34; JQ2=x23*y14-x14*y23;
  Jc1=(JQ0-JQ1-JQ2)*h1/2; Jc2=(JQ0+JQ1-JQ2)*h2/2;
  Jc3=(JQ0+JQ1+JQ2)*h3/2; Jc4=(JQ0-JQ1+JQ2)*h4/2;
  Bz11=(Δy1*x24+Δx1*y42)/Jc1; Bz12=(Δy1*x41+Δx1*y14)/Jc1;
  Bz14=(Δy1*x12+Δx1*y21)/Jc1; Bz21=(Δy2*x23+Δx2*y32)/Jc2;
  Bz22=(Δy2*x31+Δx2*y13)/Jc2; Bz23=(Δy2*x12+Δx2*y21)/Jc2;
  Bz32=(Δy3*x34+Δx3*y43)/Jc3; Bz33=(Δy3*x42+Δx3*y24)/Jc3;
  Bz34=(Δy3*x23+Δx3*y32)/Jc3; Bz41=(Δy4*x34+Δx4*y43)/Jc4;
  Bz43=(Δy4*x41+Δx4*y14)/Jc4; Bz44=(Δy4*x13+Δx4*y31)/Jc4;
  NQ1=(1-ξ)*(1-η)/4; NQ2=(1+ξ)*(1-η)/4; NQ3=(1+ξ)*(1+η)/4;
  NQ4=(1-ξ)*(1+η)/4;  numer=options[[1]];
  Bz=  {0,0,Bz11-1/h1, 0,0,Bz12, 0,0,0, 0,0,Bz14,
        0,0,Bz11+1/h1, 0,0,Bz12, 0,0,0, 0,0,Bz14}*NQ1+
       {0,0,Bz21, 0,0,Bz22-1/h2, 0,0,Bz23, 0,0,0,
        0,0,Bz21, 0,0,Bz22+1/h2, 0,0,Bz23, 0,0,0}*NQ2+
       {0,0,0, 0,0,Bz32, 0,0,Bz33-1/h3, 0,0,Bz34,
        0,0,0, 0,0,Bz32, 0,0,Bz33+1/h3, 0,0,Bz34}*NQ3+
       {0,0,Bz41, 0,0,0, 0,0,Bz43, 0,0,Bz44-1/h4,
        0,0,Bz41, 0,0,0, 0,0,Bz43, 0,0,Bz44+1/h4}*NQ4;
  If [numer,Return[N[Bz]]]; Return[Bz] ];
```

Figure 20. *Mathematica* implementation of thickness strain-displacement matrix.

Running the *Mathematica* code for this geometry and evaluating at the corners gives

$$
\begin{aligned}
\mathbf{B}_{zz1} &= [\,0\;\;0\;\;-\tfrac{51185}{60912}\;\;0\;\;0\;\;-\tfrac{455}{22842}\;\;0\;\;0\;\;0\;\;0\;\;0\;\;\tfrac{4915}{182736}\;\;0\;\;0\;\;\tfrac{50335}{60912}\;\;0\;\;0\;\;-\tfrac{455}{22842}\;\;0\;\;0\;\;0\;\;0\;\;0\;\;\tfrac{4915}{182736}\,] \\
&= [\,0\;\;0\;\;-0.8403\;\;0\;\;0\;\;-0.0199\;\;0\;\;0\;\;0\;\;0\;\;0\;\;0.0269\;\;0\;\;0\;\;0.8264\;\;0\;\;0\;\;-0.01992\;\;0\;\;0\;\;0\;\;0\;\;0\;\;0.0269\,] \\
\mathbf{B}_{zz2} &= [\,0\;\;0\;\;-\tfrac{28795}{535872}\;\;0\;\;0\;\;-\tfrac{76013}{89312}\;\;0\;\;0\;\;\tfrac{15985}{535872}\;\;0\;\;0\;\;0\;\;0\;\;0\;\;-\tfrac{28795}{535872}\;\;0\;\;0\;\;\tfrac{80283}{89312}\;\;0\;\;0\;\;\tfrac{15985}{535872}\;\;0\;\;0\;\;0\,] \\
&= [\,0\;\;0\;\;-0.05373\;\;0\;\;0\;\;-0.8511\;\;0\;\;0\;\;0.02983\;\;0\;\;0\;\;0\;\;0\;\;0\;\;-0.05373\;\;0\;\;0\;\;0.8989\;\;0\;\;0\;\;0.02983\;\;0\;\;0\;\;0\,] \\
\mathbf{B}_{zz3} &= [\,0\;\;0\;\;0\;\;0\;\;0\;\;-\tfrac{45325}{1617264}\;\;0\;\;0\;\;-\tfrac{28315}{22462}\;\;0\;\;0\;\;\tfrac{5675}{147024}\;\;0\;\;0\;\;0\;\;0\;\;0\;\;-\tfrac{45325}{1617264}\;\;0\;\;0\;\;\tfrac{13920}{11231}\;\;0\;\;0\;\;\tfrac{5675}{147024}\,] \\
&= [\,0\;\;0\;\;0\;\;0\;\;0\;\;-0.02803\;\;0\;\;0\;\;-1.261\;\;0\;\;0\;\;0.03860\;\;0\;\;0\;\;0\;\;0\;\;0\;\;-0.02803\;\;0\;\;0\;\;1.239\;\;0\;\;0\;\;0.0386\,] \\
\mathbf{B}_{zz4} &= [\,0\;\;0\;\;-\tfrac{3925}{15456}\;\;0\;\;0\;\;0\;\;0\;\;0\;\;-\tfrac{3725}{15456}\;\;0\;\;0\;\;-\tfrac{9055}{7728}\;\;0\;\;0\;\;-\tfrac{3925}{15456}\;\;0\;\;0\;\;0\;\;0\;\;0\;\;-\tfrac{3725}{15456}\;\;0\;\;0\;\;\tfrac{16705}{7728}\,] \\
&= [\,0\;\;0\;\;-0.2539\;\;0\;\;0\;\;0\;\;0\;\;0\;\;-0.2410\;\;0\;\;0\;\;-1.172\;\;0\;\;0\;\;-0.2539\;\;0\;\;0\;\;0\;\;0\;\;0\;\;-0.2410\;\;0\;\;0\;\;2.162\,]
\end{aligned}
\tag{32.92}
$$

§32.6.11. MBT Strain Implementation

$x_1^- = -\frac{3}{8}$	$x_2^- = \frac{89}{35}$	$x_3^- = \frac{29}{18}$	$x_4^- = \frac{23}{70}$	$x_1^+ = -\frac{7}{24}$	$x_2^+ = \frac{79}{35}$	$x_3^+ = \frac{31}{18}$	$x_4^+ = \frac{33}{70}$
$y_1^- = \frac{4}{15}$	$y_2^- = -\frac{47}{126}$	$y_3^- = \frac{157}{66}$	$y_4^- = \frac{59}{30}$	$y_1^+ = \frac{2}{15}$	$y_2^+ = -\frac{61}{126}$	$y_3^+ = \frac{151}{66}$	$y_4^+ = \frac{49}{30}$
$z_1^- = -\frac{3}{5}$	$z_2^- = -\frac{4}{7}$	$z_3^- = -\frac{2}{5}$	$z_4^- = -\frac{3}{10}$	$z_1^+ = \frac{3}{5}$	$z_2^+ = \frac{4}{7}$	$z_3^+ = \frac{2}{5}$	$z_4^+ = \frac{3}{10}$

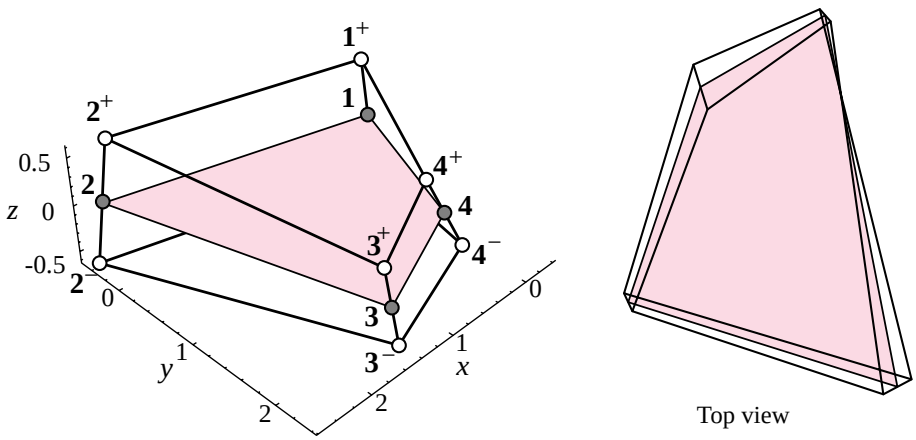

Figure 21. Example of thickness strain calculations for a thickness tapered element of variable thickness.

```
SS8MBTStrains[xyzcoor_,{ξ_,η_},{α_,β_},{numer_}]:=Module[
{Bm,Tm,Bz,B,NQ1,NQ2,NQ3,NQ4,i,j,n,c0,c1,c2,Bmbt,Grc,Gh},
{Bm1,Tm1}=SS8MembStrains[xyzcoor,{ξ,η,-1},{},{α,β},{numer,False}];
{Bm2,Tm2}=SS8MembStrains[xyzcoor,{ξ,η, 1},{},{α,β},{numer,False}];
{Bm0,Tm0}=SS8MembStrains[xyzcoor,{ξ,η, 0},{},{α,β},{numer,False}];
 Bz=SS8ThickStrain[xyzcoor,{ξ,η},{numer}];
 B1=Simplify[Bm1.Tm1]; B2=Simplify[Bm2.Tm2];
 B0=Simplify[Bm0.Tm0];
 {B1,B2,B0}=Simplify[{B1,B2,B0}];
 Bmbt=Table[0,{7},{24}];
 For [n=1,n<=8,n++, j={1,2,4,5,7,8,10,11}[[n]];
     For [i=1,i<=3,i++,
          c1=B1[[i,n]]/2; c2=B2[[i,n]]/2; c0=B0[[i,n]]/2;
          Bmbt[[i,j]]=c0; Bmbt[[i,j+12]]=c0;
          Bmbt[[i+3,j]]=-c1; Bmbt[[i+3,j+12]]=c2 ];
     Bmbt[[7,3*n]]= Bz[[3*n]] ];
 If [numer,Return[N[Bmbt]]]; Return[Bmbt] ];
```

Figure 22. *Mathematica* module for evaluating $\mathbf{B}_{mbt}$.

The *Mathematica* module listed in Figure 22 merges the strain-displacement matrices produced by `SS8MembStrains` and `SS8MBTStrains` to form the 7×24 matrix $\mathbf{B}_{mbt}$ defined by (32.81).

The module is referenced as

$$\texttt{Bmbt = SS8MBTStrains[xyzcoor, } \{\xi, \eta\}\texttt{, } \{\alpha, \beta\}\texttt{, options]} \tag{32.93}$$

where

`xyzcoor`	The local coordinates of the flattened brick, arranged as `{{x1,x2,...x8},{y1,y2,...y8},{z1,z2,...z8}}` Here `z1=-h1/2`, `z2=-h2/2`, etc.
$\{\xi, \eta\}$	Quadrilateral coordinates of midsurface point at which $\mathbf{B}_{mbt}$ will be evaluated.
$\{\alpha, \beta\}$	Parameters passed to `SS8MembStrains`.

```
SS8StiffnessMBT[xyzcoor_,ElayerMBT_,layers_,{α_,β_},options_]:=Module[
   {x1,x2,x3,x4,x5,x6,x7,x8,y1,y2,y3,y4,y5,y6,y7,y8,
   z1,z2,z3,z4,z5,z6,z7,z8,h1,h2,h3,h4,h0,h,
   x10,x20,x30,x40,y10,y20,y30,y40,
   Δx1,Δx2,Δx3,Δx4,Δy1,Δy2,Δy3,Δy4,numer,Jconst,
   JQ0,JQ1,JQ2,J,ξ,η,g1=1/Sqrt[3],gp1,gp2,gp3,gp4,
   Jg1,Jg2,Jg3,Jg4,Bg1,Bg2,Bg3,Bg4,Bmbt,Kmbt},
  {{x1,y1,z1},{x2,y2,z2},{x3,y3,z3},{x4,y4,z4},
   {x5,y5,z5},{x6,y6,z6},{x7,y7,z7},{x8,y8,z8}}=xyzcoor;
   {x10,x20,x30,x40}={x5+x1,x6+x2,x7+x3,x8+x4}/2;
   {y10,y20,y30,y40}={y5+y1,y6+y2,y7+y3,y8+y4}/2;
   {h1,h2,h3,h4}={z5-z1,z6-z2,z7-z3,z8-z4};
    NQ1=(1-ξ)*(1-η)/4; NQ2=(1+ξ)*(1-η)/4;
    NQ3=(1+ξ)*(1+η)/4; NQ4=(1-ξ)*(1+η)/4;
    h=Simplify[h1*NQ1+h2*NQ2+h3*NQ3+h4*NQ4];
    JQ0=(x30-x10)*(y40-y20)-(x40-x20)*(y30-y10);
    JQ1=(x30-x40)*(y10-y20)-(x10-x20)*(y30-y40);
    JQ2=(x20-x30)*(y10-y40)-(x10-x40)*(y20-y30);
    {numer,Jconst}=options;
    h0=(h1+h2+h3+h4)/4; If [Jconst, JQ1=JQ2=0; h=h0];
    Embt=SS8ThickIntegMBT[ElayerMBT,layers];
    Bmbt=SS8MBTStrains[xyzcoor,{ξ,η},{α,β},{numer}];
    J=h*(JQ0+JQ1*ξ+JQ2*η)/8; J=Simplify[J];
    gp1={ξ->-g1,η->-g1}; gp2={ξ-> g1,η->-g1};
    gp3={ξ-> g1,η-> g1}; gp4={ξ->-g1,η-> g1};
    Jg1=J/.gp1; Jg2=J/.gp2; Jg3=J/.gp3; Jg4=J/.gp4;
   {Jg1,Jg2,Jg3,Jg4}=Simplify[{Jg1,Jg2,Jg3,Jg4}];
    Bg1=(Bmbt/.gp1); Bg2=(Bmbt/.gp2);
    Bg3=(Bmbt/.gp3); Bg4=(Bmbt/.gp4);
     Kmbt= Transpose[Bg1].Embt.Bg1*Jg1+
           Transpose[Bg2].Embt.Bg2*Jg2+
           Transpose[Bg3].Embt.Bg3*Jg3+
           Transpose[Bg4].Embt.Bg4*Jg4;
     Return[Kmbt]];
```

Figure 23. *Mathematica* module for evaluating $\mathbf{K}_{mbt}$.

`options` Logical flag { `numer` }. If `True`, compute $\mathbf{B}_{mbt}$ using floating point arithmetic.

The module returns `Bmbt`, which is the 7×24 matrix $\mathbf{B}_{mbt}$ defined in (32.82).

§32.6.12. The MBT Stiffness Matrix

The hard work has been to obtain the strain-displacement matrix $\mathbf{B}_{mbt}$. The rest is easier. The MBT stiffness matrix is

$$\mathbf{K}_{mbt} = \int_{V^{(e)}} \mathbf{B}_{mbt}^T \, \bar{\mathbf{E}}_{mbt} \, \mathbf{B}_{mbt} \, dV \tag{32.94}$$

where $V^{(e)}$ is the volume of the flattened brick and $\bar{\mathbf{E}}_{mbt}$ the thickness-integrated MBT constitutive relation derived in §5.4.

The stiffness may be evaluated by a 2×2 two-dimensional Gauss rule since the volume Jacobian splits as $J^Q \, h$, in whcih $h(\xi, \eta) = h_1 N_1^Q + h_2 N_2 + h_3 N_3^Q + h_4 N_4^Q$ is the interpolated thickness:

$$\mathbf{K}_{mbt} = \sum_{i=1}^{2} \sum_{j=1}^{2} \mathbf{B}_{mbt}^T(\xi_i, \eta_j) \, \bar{\mathbf{E}}_{mbt} \, \mathbf{B}_{mbt}(\xi_i, \eta_j) \; J^Q(\xi_i, \eta_j) \, h(\xi_i \eta_j) \, w_{ij}. \tag{32.95}$$

Here the weights $w_{ij} = 1$ for the 2×2 rule can be omitted.

A *Mathematica* implementation is listed in Figure 23. The module is referenced as

`Kmbt = SS8StiffnessMBT[xyzcoor,ElayerMBT,layers, {α, β},options]` (32.96)

where

`xyzcoor` The local coordinates of the flattened brick, arranged as
`{{x1,x2,...x8},{y1,y2,...y8},{z1,z2,...z8}}`
Here `z1=-h1/2`, `z2=-h2/2`, etc.

`ElayerMBT` MBT constitutive inputs. See Section 5 for details.

`layers` Layer extent list; see Section 5 for details.

$\{\alpha, \beta\}$ Parameters passed to `SS8MembStrains`.

`options` Logical flag {`numer`}. If `True`, compute $\mathbf{B}_{mbt}$ using floating point arithmetic.

The module returns `Kmbt`, which is the 24×24 matrix $\mathbf{K}_{mbt}$ defined in (32.85).

§32.7. Transverse Shear Stiffness

The contribution of the transverse shear to the element stiffness is handled by the assumed natural strain method. To make the construction of the strain field practical a number of simplifying assumptions will be made.

§32.7.1. Assumptions and Requirements

The construction of the assumed strains proceeds under the following constraints.

Geometric restriction. The flattened brick may be of variable thickness but it must be thickness prismatic. The Jacobian at a point $\{\xi, \eta\}$ is

$$J = \tfrac{1}{32}(x_{2134}y_{3241} - x_{3241}y_{2134})\, h = J^Q\, h. \tag{32.97}$$

where J^Q is the Jacobian determinant of the flat midsurface quadrilateral, with $x_{2134} = x_{21}(1-\eta) + x_{34}(1+\eta)$, $y_{2134} = y_{21}(1-\eta) + y_{34}(1+\eta)$, $x_{3241} = x_{32}(1+\xi) + x_{41}(1-\xi)$ and $y_{3241} = y_{32}(1+\xi) + y_{41}(1-\xi)$.

Natural strain interpolation. The natural transverse shear strains

$$\gamma_{\zeta\xi} = e_{\xi\zeta} + e_{\zeta\xi}, \quad \gamma_{\zeta\eta} = e_{\eta\zeta} + e_{\zeta\eta} \tag{32.98}$$

are uniform across the thickness; that is, they do not depend on ζ. (Note that generally $e_{\xi\zeta} \neq e_{\zeta\xi}$ and $e_{\xi\zeta} \neq e_{\zeta\xi}$, thus the sum in (32.98) cannot be replaced by duplication.) The dependence on ξ and η is defined by the midpoint interpolations

$$\begin{aligned}
\gamma_{\zeta\xi} &= \gamma_{\xi\zeta}(\xi,\eta) = \tfrac{1}{2}\gamma_{\xi,\zeta|5}(1-\eta) + \tfrac{1}{2}\gamma_{\xi,\zeta|7}(1+\eta),\\
\gamma_{\zeta\eta} &= \gamma_{\eta\zeta}(\xi,\eta) = \tfrac{1}{2}\gamma_{\eta,\zeta|8}(1-\xi) + \tfrac{1}{2}\gamma_{\eta,\zeta|6}(1+\xi)\\
\gamma_{\zeta\xi|5} &= \gamma_{\zeta\xi}\big|_{\xi=0,\eta=-1,\zeta=0}, \gamma_{\zeta\xi|7} = \gamma_{\zeta\xi}\big|_{\xi=0,\eta=1,\zeta=0},\\
\gamma_{\zeta\eta|8} &= \gamma_{\zeta\eta}\big|_{\xi=-1,\eta=0,\zeta=0}, \gamma_{\zeta\eta|6} = \gamma_{\zeta\eta}\big|_{\xi=1,\eta=0,\zeta=0}.
\end{aligned} \tag{32.99}$$

Cartesian shear strain recovery. The Cartesian transverse shear strains are recovered by the following transformation

$$\boldsymbol{\gamma}_z = \begin{bmatrix}\gamma_{yz}\\ \gamma_{zx}\end{bmatrix} = \begin{bmatrix}2e_{yz}\\ 2e_{zx}\end{bmatrix} = \begin{bmatrix}Y_{11} & Y_{12}\\ Y_{21} & Y_{22}\end{bmatrix}\begin{bmatrix}\gamma_{\zeta\eta}\\ \gamma_{\zeta\xi}\end{bmatrix} = \mathbf{Y}\boldsymbol{\gamma}_\zeta. \tag{32.100}$$

Matrix $\mathbf{Y}$ must preserve exactness of the two constant transverse shear states

$$\begin{aligned}
u_y = Cz, \quad u_z = Cy, \quad &\rightarrow \quad \text{evaluate at nodes} \quad \rightarrow \quad \gamma_{yz} = 2C,\\
u_x = Cz, \quad u_z = Cx, \quad &\rightarrow \quad \text{evaluate at nodes} \quad \rightarrow \quad \gamma_{zx} = 2C,
\end{aligned} \tag{32.101}$$

for arbitrary quadrilateral planforms and corner thicknesses, but within the constraint of no thickness taper.

§32.7.2. Comment on the Foregoing Assumptions

The geometric restriction is a concession to the limited time available to develop this component of the puzzle. If the element is allowed to be thickness tapered, symbolic computations with *Mathematica* to meet (32.101) became far too complicated to be finalized within reasonable time. Fulfillment of that condition in fact requires consideration of additional natural strain components at the midpoints, not just two. It is possible that such condition be eventually fulfilled by the simplification noted in §10.3.

The natural strain interpolation (32.99) was discovered to be optimal for C^0 flat plate elements by researchers in the mid 1980s [2] so it may be taken as a given. True, optimality has not been proven for solid shell configurations, and several benchmarks discussed in §9 show this to be far from optimal for thickness tapered elements. Nonetheless the particular choice of interpolation in $\{\xi, \eta\}$ turns out to be unimportant. Any deviations from it are compensated by the far stricter condition (32.101).

A new advance is the exact recovery of constant transverse shear states for varying thickness. While (32.99) has been well studied, the backtransformation process (32.100) available in the literature only works correctly for constant thickness $h_1 = h_2 = h_3 = h_4$. Several weeks of computations with *Mathematica* eventually produced, after harrowing simplifications, a relatively manageable yet exact form for the matrix Y_{ij}. This brings hope that an equally simple form could be eventually be discovered for thickness-tapered geometries.

§32.7.3. Strain Computation

Getting to (32.99) is the easy part. The natural strains are obtained as follows. Recall the definition of the 8-node isoparametric brick

$$\begin{aligned} x = \mathbf{N}_{iso}\mathbf{x}, \quad y = \mathbf{N}_{iso}\mathbf{y}, \quad z = \mathbf{N}_{iso}\mathbf{z}, \\ u_x = \mathbf{N}_{iso}\mathbf{u}_x, \quad u_y = \mathbf{N}_{iso}\mathbf{u}_y, \quad u_z = \mathbf{N}_{iso}\mathbf{u}_z, \end{aligned} \tag{32.102}$$

with

$$\begin{aligned} \mathbf{x} &= [\, x_1 \quad x_2 \quad x_3 \quad x_4 \quad x_5 \quad x_6 \quad x_7 \quad x_8 \,] \\ \mathbf{y} &= [\, y_1 \quad y_2 \quad y_3 \quad y_4 \quad y_5 \quad y_6 \quad y_7 \quad y_8 \,] \\ \mathbf{z} &= [\, z_1 \quad z_2 \quad z_3 \quad z_4 \quad z_5 \quad z_6 \quad z_7 \quad z_8 \,] \\ \mathbf{N}_{iso} &= [\, N_1 \;\; N_2 \;\; N_3 \;\; N_4 \;\; N_5 \;\; N_6 \;\; N_7 \;\; N_8 \,] \\ N_1 &= \tfrac{1}{8}(1-\xi)(1-\eta)(1-\zeta), \quad N_2 = \tfrac{1}{8}(1+\xi)(1-\eta)(1-\zeta), \\ N_3 &= \tfrac{1}{8}(1+\xi)(1+\eta)(1-\zeta), \quad N_4 = \tfrac{1}{8}(1-\xi)(1+\eta)(1-\zeta), \\ N_5 &= \tfrac{1}{8}(1-\xi)(1-\eta)(1+\zeta), \quad N_6 = \tfrac{1}{8}(1+\xi)(1-\eta)(1+\zeta), \\ N_7 &= \tfrac{1}{8}(1+\xi)(1+\eta)(1+\zeta), \quad N_8 = \tfrac{1}{8}(1-\xi)(1+\eta)(1+\zeta). \end{aligned} \tag{32.103}$$

Let $\mathbf{X} = [\, x \quad y \quad z \,]^T$ and $\mathbf{U} = [\, u_x \quad u_y \quad u_z \,]^T$. The natural transverse shear strains are defined as

$$\gamma_{\zeta\xi} = \frac{\partial \mathbf{X}}{\partial \zeta}^T \frac{\partial \mathbf{U}}{\partial \xi} + \frac{\partial \mathbf{X}}{\partial \xi}^T \frac{\partial \mathbf{U}}{\partial \zeta}, \qquad \gamma_{\zeta\eta} = \frac{\partial \mathbf{X}}{\partial \zeta}^T \frac{\partial \mathbf{U}}{\partial \eta} + \frac{\partial \mathbf{X}}{\partial \eta}^T \frac{\partial \mathbf{U}}{\partial \zeta}, \tag{32.104}$$

According to geometric restriction stated in §7.1, the geometry of the brick is specialized to

$$\begin{aligned} \mathbf{x} &= [\, x_1^0 \quad x_2^0 \quad x_3^0 \quad x_4^0 \quad x_1^0 \quad x_2^0 \quad x_3^0 \quad x_4^0 \,] \\ \mathbf{y} &= [\, y_1^0 \quad y_2^0 \quad y_3^0 \quad y_4^0 \quad y_1^0 \quad y_2^0 \quad y_3^0 \quad y_4^0 \,] \\ \mathbf{z} &= [\, -\tfrac{1}{2}h_1 \quad -\tfrac{1}{2}h_2 \quad -\tfrac{1}{2}h_3 \quad -\tfrac{1}{2}h_4 \quad \tfrac{1}{2}h_1 \quad \tfrac{1}{2}h_2 \quad \tfrac{1}{2}h_3 \quad \tfrac{1}{2}h_4 \,] \end{aligned} \tag{32.105}$$

```
SS8ShearStrains[xyzcoor_,{ξ_,η_},numer_]:=  Module[
  {x1,x2,x3,x4,x5,x6,x7,x8,y1,y2,y3,y4,y5,y6,y7,y8,
   z1,z2,z3,z4,z5,z6,z7,z8,x10,x20,x30,x40,y10,y20,y30,y40,
   h1,h2,h3,h4,h,h12m,h23m,h34m,h41m,
   x12,x13,x14,x21,x23,x24,x31,x32,x34,x41,x42,x43,
   y12,y13,y14,y21,y23,y24,y31,y32,y34,y41,y42,y43,
   ξm,ξp,ηm,ηp,hx1243,hx2314,hy1243,hy2314,Bγu,Y,Bs},
 {{x1,y1,z1},{x2,y2,z2},{x3,y3,z3},{x4,y4,z4},
  {x5,y5,z5},{x6,y6,z6},{x7,y7,z7},{x8,y8,z8}}=xyzcoor;
  {x10,x20,x30,x40}=({x5,x6,x7,x8}+{x1,x2,x3,x4})/2;
  {y10,y20,y30,y40}=({y5,y6,y7,y8}+{y1,y2,y3,y4})/2;
  {h1,h2,h3,h4}={z5-z1,z6-z2,z7-z3,z8-z4};
  {x12,x13,x14,x21,x23,x24,x31,x32,x34,x41,x42,x43}=
    {x10-x20,x10-x30,x10-x40,x20-x10,x20-x30,x20-x40,
     x30-x10,x30-x20,x30-x40,x40-x10,x40-x20,x40-x30};
  {y12,y13,y14,y21,y23,y24,y31,y32,y34,y41,y42,y43}=
    {y10-y20,y10-y30,y10-y40,y20-y10,y20-y30,y20-y40,
     y30-y10,y30-y20,y30-y40,y40-y10,y40-y20,y40-y30};
    h12m=(h1+h2)/2; h23m=(h2+h3)/2; h34m=(h3+h4)/2;
    h41m=(h1+h4)/2; ξm=1-ξ; ξp=1+ξ; ηm=1-η; ηp=1+η;
    Bγu=(1/16)*
   {{x14*ξm, y14*ξm,-h41m*ξm, x23*ξp, y23*ξp,-h23m*ξp,
     x23*ξp, y23*ξp, h23m*ξp, x14*ξm, y14*ξm, h41m*ξm,
    -x14*ξm,-y14*ξm,-h41m*ξm, x32*ξp, y32*ξp,-h23m*ξp,
     x32*ξp, y32*ξp, h23m*ξp,-x14*ξm,-y14*ξm, h41m*ξm},
    {x12*ηm, y12*ηm,-h12m*ηm, x12*ηm, y12*ηm, h12m*ηm,
     x43*ηp, y43*ηp, h34m*ηp, x43*ηp, y43*ηp,-h34m*ηp,
    -x12*ηm,-y12*ηm,-h12m*ηm,-x12*ηm,-y12*ηm, h12m*ηm,
     x34*ηp, y34*ηp, h34m*ηp, x34*ηp, y34*ηp,-h34m*ηp}};
    x2134=x21*ηm+x34*ηp; y2134=y21*ηm+y34*ηp;
    x3241=x32*ξp+x41*ξm; y3241=y32*ξp+y41*ξm;
    hx1243= h12m*x12*ηm+h34m*x43*ηp;
    hx2314= h23m*x23*ξp+h41m*x14*ξm;
    hy1243= h12m*y12*ηm+h34m*y43*ηp;
    hy2314= h23m*y23*ξp+h41m*y14*ξm;
    Y=8*{{hx1243,-hx2314},{-hy1243,hy2314}}/
         (hx2314*hy1243-hx1243*hy2314);
    If [numer, Bγu=N[Bγu]; Y=N[Y]]; Bs=Simplify[Y.Bγu];
    Return[Bs]];
```

Figure 24. *Mathematica* module for evaluating the shear-strain-displacement matrix $\mathbf{B}_s$.

Insertion of (32.102), (32.103) and (32.105) into (32.104) yields a natural strain field that contains up to cubic terms such as $\xi^2\eta$. This is filtered by evaluating at the midpoints 5, 6, 7 and 8 to yield

$$\begin{bmatrix} \gamma_{\zeta\eta} \\ \gamma_{\zeta\xi} \end{bmatrix} = \mathbf{B}_{\gamma u}\mathbf{u}^{(e)}. \tag{32.106}$$

Here $\mathbf{u}^{(e)}$ are the solid shell node displacements arranged as per (32.23), and

$$\begin{aligned}\mathbf{B}_{\gamma u} = \tfrac{1}{16}\Bigg[& x_{14}(1-\xi) \;\; y_{14}(1-\xi) \;\; -\bar{h}_{41}(1-\xi) \;\; x_{23}(1+\xi) \;\; y_{23}(1+\xi) \;\; -\bar{h}_{23}(1+\xi) \\ & x_{12}(1-\eta) \;\; y_{12}(1-\eta) \;\; -\bar{h}_{12}(1-\eta) \;\; x_{12}(1-\eta) \;\; y_{12}(1-\eta) \;\; \bar{h}_{12}(1-\eta) \\ & x_{23}(1+\xi) \;\; y_{23}(1+\xi) \;\; \bar{h}_{23}(1+\xi) \;\; x_{14}(1-\xi) \;\; y_{14}(1-\xi) \;\; \bar{h}_{41}(1-\xi) \\ & x_{43}(1+\eta) \;\; y_{43}(1+\eta) \;\; \bar{h}_{34}(1+\eta) \;\; x_{43}(1+\eta) \;\; y_{43}(1+\eta) \;\; -\bar{h}_{34}(1+\eta) \\ & x_{41}(1-\xi) \;\; y_{41}(1-\xi) \;\; -\bar{h}_{41}(1-\xi) \;\; x_{32}(1+\xi) \;\; y_{32}(1+\xi) \;\; -\bar{h}_{23}(1+\xi) \\ & x_{21}(1-\eta) \;\; y_{21}(1-\eta) \;\; -\bar{h}_{12}(1-\eta) \;\; x_{21}(1-\eta) \;\; y_{21}(1-\eta) \;\; \bar{h}_{12}(1-\eta) \\ & x_{32}(1+\xi) \;\; y_{32}(1+\xi) \;\; \bar{h}_{23}(1+\xi) \;\; x_{41}(1-\xi) \;\; y_{41}(1-\xi) \;\; \bar{h}_{41}(1-\xi) \\ & x_{34}(1+\eta) \;\; y_{34}(1+\eta) \;\; \bar{h}_{34}(1+\eta) \;\; x_{34}(1+\eta) \;\; y_{34}(1+\eta) \;\; -\bar{h}_{34}(1+\eta) \Bigg]\end{aligned} \tag{32.107}$$

in which $\bar{h}_{12} = \frac{1}{2}(h_1 + h_2)$, $\bar{h}_{23} = \frac{1}{2}(h_2 + h_3)$, $\bar{h}_{34} = \frac{1}{2}(h_3 + h_4)$ and $\bar{h}_{41} = \frac{1}{2}(h_1 + h_4)$.

The next step is more difficult and only possible with the help of a computer algebra package. Consider the basic-states matrix $\mathbf{G}_{rc}$ of the Free Formulation, given by (32.82). The first 6 columns pertain to

rigid body modes, and the last 6 to constant strain states ordered e_{xx}, e_{yy}, e_{zz}, $2e_{xy}$, $2e_{yz}$ and $2e_{zx}$. Replace the coordinates (32.105) into (32.107) and require that

$$\gamma_z = \mathbf{Y}\mathbf{B}_{\gamma u}\mathbf{G}_{rc} = \mathbf{B}_s\mathbf{G}_{rc} = \begin{bmatrix} 0 & 0 & 0 & 0 & 0 & 0 & 0 & 0 & 0 & 0 & 2 & 0 \\ 0 & 0 & 0 & 0 & 0 & 0 & 0 & 0 & 0 & 0 & 0 & 2 \end{bmatrix} \tag{32.108}$$

identically for any $\{\xi, \eta\}$ and any combination of coordinates and thicknesses. The meaning of (32.108) is: rigid body motions and constant strain states should produce zero transverse shear strains, except for the two uniform strain states (32.101), which for $C = 1$ are represented by the last two columns of $\mathbf{G}_{rc}$. This requirement provides a unique $\mathbf{Y}$, which turns out to be

$$\mathbf{Y} = \frac{8}{x^h_{2314}y^h_{1243} - x^h_{1243}y^h_{2314}} \begin{bmatrix} x^h_{1243} & -x^h_{2314} \\ -y^h_{1243} & y^h_{2314} \end{bmatrix} \tag{32.109}$$

in which

$$\begin{aligned} x^h_{1243} &= h^m_{12}x_{12}(1-\eta) + h^m_{34}x_{43}(1+\eta), \quad & x^h_{2314} &= h^m_{23}x_{23}(1+\xi) + h^m_{41}x_{14}(1-\xi), \\ y^h_{1243} &= h^m_{12}y_{12}(1-\eta) + h^m_{34}y_{43}(1+\eta), \quad & y^h_{2314} &= h^m_{23}y_{23}(1+\xi) + h^m_{41}y_{14}(1-\xi). \end{aligned} \tag{32.110}$$

§32.7.4. Transverse Shear Strain Implementation

The *Mathematica* module listed in Figure 24 implements the computation of the shear-strain-displacement matrix. The module is referenced as

```
Bs = SS8ShearStrains[xyzcoor, {ξ, η}, numer]
```
(32.111)

where

`xyzcoor`	The local coordinates of the flattened brick, arranged as `{{x1,x2,...x8},{y1,y2,...y8},{z1,z2,...z8}}` Here `z1=-h1/2`, `z2=-h2/2`, etc.
$\{\xi, \eta\}$	Quadrilateral coordinates of midsurface point at which $\mathbf{B}_s$ will be evaluated.
`numer`	Logical flag. If `True`, compute $\mathbf{B}_s$ using floating point arithmetic.

The module returns `Bs`, which is the 2×24 matrix $\mathbf{B}_s = \mathbf{Y}\mathbf{B}_{\gamma u}$.

§32.7.5. Shear Stiffness Matrix Implementation

The contribution of the transverse shear to the SS8 element stiffness is given by

$$\mathbf{K}_s = \int_{V^{(e)}} \mathbf{B}_s^T \bar{\mathbf{E}}_s \mathbf{B}_s \; dV = \int_{-1}^{1}\int_{-1}^{1} \mathbf{B}_s^T \bar{\mathbf{E}}_s \mathbf{B}_s \; J^Q h \, d\xi \, d\eta. \tag{32.112}$$

where $\bar{\mathbf{E}}_s$ is the thickness-integrated shear constitutive matrix defined in §5.4. This evaluation is done by a 2×2 Gauss integration rule:

$$\mathbf{K}_s = \sum_{i=1}^{2}\sum_{j=1}^{2} \mathbf{B}_g(\xi_i, \eta_j)\, \bar{\mathbf{E}}_s\, \mathbf{B}_g(\xi_i, \eta_j)\; J^Q(\xi_i, \eta_j)\, h(\xi_i, \eta_j) w_{ij}. \tag{32.113}$$

in which $\{\xi_i, \eta_j\}$ are abcissas $\pm\sqrt{1/3}$ of the sample points of the 2×2 Gauss rule, which has unit weights $w_{ij} = 1$.

```
SS8StiffnessShear[xyzcoor_,ElayerS_,layers_,options_]:=
  Module[{x1,x2,x3,x4,x5,x6,x7,x8,y1,y2,y3,y4,
   y5,y6,y7,y8,z1,z2,z3,z4,z5,z6,z7,z8,
   x10,x20,x30,x40,y10,y20,y30,y40,h1,h2,h3,h4,h,
   x12,x13,x14,x21,x23,x24,x31,x32,x34,x41,x42,x43,
   y12,y13,y14,y21,y23,y24,y31,y32,y34,y41,y42,y43,
   numer,Jconst,ξ,η,ξm,ξp,ηm,ηp,NQ1,NQ2,NQ3,NQ4,
   x2134,y3241,x3241,y2134,R,WR,Rcorr,
   Eshr,J,Jg1,Jg2,Jg3,Jg4,Bg1,Bg2,Bg3,Bg4,
   g1=1/Sqrt[3],gp1,gp2,gp3,gp4,Ks},  Rcorr=False;
  {{x1,y1,z1},{x2,y2,z2},{x3,y3,z3},{x4,y4,z4},
  {x5,y5,z5},{x6,y6,z6},{x7,y7,z7},{x8,y8,z8}}=xyzcoor;
  {x10,x20,x30,x40}=({x5,x6,x7,x8}+{x1,x2,x3,x4})/2;
  {y10,y20,y30,y40}=({y5,y6,y7,y8}+{y1,y2,y3,y4})/2;
  {h1,h2,h3,h4}={z5-z1,z6-z2,z7-z3,z8-z4};
  {x12,x13,x14,x21,x23,x24,x31,x32,x34,x41,x42,x43}=
    {x10-x20,x10-x30,x10-x40,x20-x10,x20-x30,x20-x40,
     x30-x10,x30-x20,x30-x40,x40-x10,x40-x20,x40-x30};
  {y12,y13,y14,y21,y23,y24,y31,y32,y34,y41,y42,y43}=
    {y10-y20,y10-y30,y10-y40,y20-y10,y20-y30,y20-y40,
     y30-y10,y30-y20,y30-y40,y40-y10,y40-y20,y40-y30};
    gp1={ξ->-g1,η->-g1}; gp2={ξ-> g1,η->-g1};
    gp3={ξ-> g1,η-> g1}; gp4={ξ->-g1,η-> g1};
    {numer,Jconst}=options;
    Eshr=SS8ThickIntegS[ElayerS,layers];
    Bg1=SS8ShearStrains[xyzcoor,{-g1,-g1},numer];
    Bg2=SS8ShearStrains[xyzcoor,{ g1,-g1},numer];
    Bg3=SS8ShearStrains[xyzcoor,{ g1, g1},numer];
    Bg4=SS8ShearStrains[xyzcoor,{-g1, g1},numer];
    If [Rcorr,
       R=Transpose[
       {{1,0,0,1,0,0,1,0,0,1,0,0,1,0,0,1,0,0,1,0,0,1,0,0},
        {0,1,0,0,1,0,0,1,0,0,1,0,0,1,0,0,1,0,0,1,0,0,1,0},
        {0,0,1,0,0,1,0,0,1,0,0,1,0,0,1,0,0,1,0,0,1,0,0,1},
        {y1,-x1,0,y2,-x2,0,y3,-x3,0,y4,-x4,0,
         y5,-x5,0,y6,-x6,0,y7,-x7,0,y8,-x8,0},
        {0,z1,-y1,0,z2,-y2,0,z3,-y3,0,z4,-y4,
         0,z5,-y5,0,z6,-y6,0,z7,-y7,0,z8,-y8},
        {-z1,0,x1,-z2,0,x2,-z3,0,x3,-z4,0,x4,
         -z5,0,x5,-z6,0,x6,-z7,0,x7,-z8,0,x8}}];
       If [numer,R=N[R]]; W=Simplify[Transpose[R].R];
       WR=Inverse[W].Transpose[R];
       Bg1=Bg1-(Bg1.R).WR; Bg2=Bg2-(Bg2.R).WR;
       Bg3=Bg3-(Bg3.R).WR; Bg4=Bg4-(Bg4.R).WR];
    ξm=1-ξ; ξp=1+ξ; ηm=1-η; ηp=1+η;
    NQ1=ξm*ηm/4; NQ2=ξp*ηm/4; NQ3=ξp*ηp/4; NQ4=ξm*ηp/4;
    h=Simplify[h1*NQ1+h2*NQ2+h3*NQ3+h4*NQ4];
    x2134=x21*ηm+x34*ηp; y2134=y21*ηm+y34*ηp;
    x3241=x32*ξp+x41*ξm; y3241=y32*ξp+y41*ξm;
    J=Simplify[h*(x2134*y3241-x3241*y2134)/16];
    h0=(h1+h2+h3+h4)/4;
    Jg1=J/.gp1; Jg2=J/.gp2; Jg3=J/.gp3; Jg4=J/.gp4;
    If [Jconst, Jg1=Jg2=Jg3=Jg4=J/.{ξ->0,η->0}; h=h0];
   {Jg1,Jg2,Jg3,Jg4}=Simplify[{Jg1,Jg2,Jg3,Jg4}];
    Ks= Transpose[Bg1].Eshr.Bg1*Jg1+Transpose[Bg2].Eshr.Bg2*Jg2+
        Transpose[Bg3].Eshr.Bg3*Jg3+Transpose[Bg4].Eshr.Bg4*Jg4;
    If [numer, Return[Ks], Return[Simplify[Ks]] ] ];
```

Figure 25. Mathematica implementation of transverse shear stiffness computations.

The *Mathematica* module `SS8ShearStiffness` listed in Figure 25 implements the calculation of $\mathbf{K}_s$. The module is called by

```
Ks=SS8ShearStiffness[xyhcoor,ElayerS,layers,options]
```
(32.114)

The arguments are:

`xyzcoor`	The local coordinates of the flattened brick, arranged as `{{x1,x2,...x8},{y1,y2,...y8},{z1,z2,...z8}}` Here `z1=-h1/2`, `z2=-h2/2`, etc.

`ElayerS`	List of transverse-shear layer constitutive matrices. See section 5.
`layers`	Extents of layer thicknesses. See Section 5.
`options`	A list of two logical flags: { `numer`, `Jconst` } `numer` If `True` carry calculations in floating point arithmetic `Jconst` If `True` use a constant Jacobian $J^Q = J_0^Q = J^Q\big\vert_{\xi=0,\eta=0}$ and average thickness $h_0 = (h_1 + h_2 + h_3 + h_4)/4$ in the Gauss integration rule (32.113).

As an example, suppose the element is unit square with unit thickness and fabricated of a single layer of isotropic material with $G = 48$. The *Mathematica* statements

```
a=b=1; {x1,x2,x3,x4}={-a,a,a,-a}/2; {y1,y2,y3,y4}={-b,-b,b,b}/2;
h0=1;  {h1,h2,h3,h4}={h0,h0,h0,h0};
xyhcoor={{x1,y1,h1},{x2,y2,h2},{x3,y3,h3},{x4,y4,h4}}; Eshr={{48,0},{0,48}};
Ks=SS8ShearStiffness[xyhcoor,{Eshr},{1},{False,True}];
Print["Ks=",Ks//InputForm];
```

are run producing

$$\mathbf{K}_s = 2\begin{bmatrix}
2 & 0 & 2 & 2 & 0 & -2 & 1 & 0 & -1 & 1 & 0 & 1 & -2 & 0 & 2 & -2 & 0 & -2 & -1 & 0 & -1 & -1 & 0 & 1 \\
0 & 2 & 2 & 0 & 1 & 1 & 0 & 1 & -1 & 0 & 2 & -2 & 0 & -2 & 2 & 0 & -1 & 1 & 0 & -1 & -1 & 0 & -2 & -2 \\
2 & 2 & 4 & 2 & 1 & -1 & 1 & 1 & -2 & 1 & 2 & -1 & -2 & -2 & 4 & -2 & -1 & -1 & -1 & -1 & -2 & -1 & -2 & -1 \\
2 & 0 & 2 & 2 & 0 & -2 & 1 & 0 & -1 & 1 & 0 & 1 & -2 & 0 & 2 & -2 & 0 & -2 & -1 & 0 & -1 & -1 & 0 & 1 \\
0 & 1 & 1 & 0 & 2 & 2 & 0 & 2 & -2 & 0 & 1 & -1 & 0 & -1 & 1 & 0 & -2 & 2 & 0 & -2 & -2 & 0 & -1 & -1 \\
-2 & 1 & -1 & -2 & 2 & 4 & -1 & 2 & -1 & -1 & 1 & -2 & 2 & -1 & -1 & 2 & -2 & 4 & 1 & -2 & -1 & 1 & -1 & -2 \\
1 & 0 & 1 & 1 & 0 & -1 & 2 & 0 & -2 & 2 & 0 & 2 & -1 & 0 & 1 & -1 & 0 & -1 & -2 & 0 & -2 & -2 & 0 & 2 \\
0 & 1 & 1 & 0 & 2 & 2 & 0 & 2 & -2 & 0 & 1 & -1 & 0 & -1 & 1 & 0 & -2 & 2 & 0 & -2 & -2 & 0 & -1 & -1 \\
-1 & -1 & -2 & -1 & -2 & -1 & -2 & -2 & 4 & -2 & -1 & -1 & 1 & 1 & -2 & 1 & 2 & -1 & 2 & 2 & 4 & 2 & 1 & -1 \\
1 & 0 & 1 & 1 & 0 & -1 & 2 & 0 & -2 & 2 & 0 & 2 & -1 & 0 & 1 & -1 & 0 & -1 & -2 & 0 & -2 & -2 & 0 & 2 \\
0 & 2 & 2 & 0 & 1 & 1 & 0 & 1 & -1 & 0 & 2 & -2 & 0 & -2 & 2 & 0 & -1 & 1 & 0 & -1 & -1 & 0 & -2 & -2 \\
1 & -2 & -1 & 1 & -1 & -2 & 2 & -1 & -1 & 2 & -2 & 4 & -1 & 2 & -1 & -1 & 1 & -2 & -2 & 1 & -1 & -2 & 2 & 4 \\
-2 & 0 & -2 & -2 & 0 & 2 & -1 & 0 & 1 & -1 & 0 & -1 & 2 & 0 & -2 & 2 & 0 & 2 & 1 & 0 & 1 & 1 & 0 & -1 \\
0 & -2 & -2 & 0 & -1 & -1 & 0 & -1 & 1 & 0 & -2 & 2 & 0 & 2 & -2 & 0 & 1 & -1 & 0 & 1 & 1 & 0 & 2 & 2 \\
2 & 2 & 4 & 2 & 1 & -1 & 1 & 1 & -2 & 1 & 2 & -1 & -2 & -2 & 4 & -2 & -1 & -1 & -1 & -1 & -2 & -1 & -2 & -1 \\
-2 & 0 & -2 & -2 & 0 & 2 & -1 & 0 & 1 & -1 & 0 & -1 & 2 & 0 & -2 & 2 & 0 & 2 & 1 & 0 & 1 & 1 & 0 & -1 \\
0 & -1 & -1 & 0 & -2 & -2 & 0 & -2 & 2 & 0 & -1 & 1 & 0 & 1 & -1 & 0 & 2 & -2 & 0 & 2 & 2 & 0 & 1 & 1 \\
-2 & 1 & -1 & -2 & 2 & 4 & -1 & 2 & -1 & -1 & 1 & -2 & 2 & -1 & -1 & 2 & -2 & 4 & 1 & -2 & -1 & 1 & -1 & -2 \\
-1 & 0 & -1 & -1 & 0 & 1 & -2 & 0 & 2 & -2 & 0 & -2 & 1 & 0 & -1 & 1 & 0 & 1 & 2 & 0 & 2 & 2 & 0 & -2 \\
0 & -1 & -1 & 0 & -2 & -2 & 0 & -2 & 2 & 0 & -1 & 1 & 0 & 1 & -1 & 0 & 2 & -2 & 0 & 2 & 2 & 0 & 1 & 1 \\
-1 & -1 & -2 & -1 & -2 & -1 & -2 & -2 & 4 & -2 & -1 & -1 & 1 & 1 & -2 & 1 & 2 & -1 & 2 & 2 & 4 & 2 & 1 & -1 \\
-1 & 0 & -1 & -1 & 0 & 1 & -2 & 0 & 2 & -2 & 0 & -2 & 1 & 0 & -1 & 1 & 0 & 1 & 2 & 0 & 2 & 2 & 0 & -2 \\
0 & -2 & -2 & 0 & -1 & -1 & 0 & -1 & 1 & 0 & -2 & 2 & 0 & 2 & -2 & 0 & 1 & -1 & 0 & 1 & 1 & 0 & 2 & 2 \\
1 & -2 & -1 & 1 & -1 & -2 & 2 & -1 & -1 & 2 & -2 & 4 & -1 & 2 & -1 & -1 & 1 & -2 & -2 & 1 & -1 & -2 & 2 & 4
\end{bmatrix} \tag{32.115}$$

This matrix has rank four, with nonzero eigenvalues 12, 24, 48, 48.

§32.7.6. RBM Cleanup

If the foregoing shear stiffness matrix is used for a thickness tapered element, two defects are detected upon transforming to global coordinates:

1. $\mathbf{K}_s$ becomes "polluted" with respect to rigid body modes (RBMs). Mathematically, let $\mathbf{R}$ denote the 24×6 RBM matrix for the original 8-node hexahedron geometry. $\mathbf{R}$ is constructed by taking the first 6 columns of (32.82) and replacing the global node coordinates. It is found that $\mathbf{K}_s\mathbf{R} \neq \mathbf{0}$. Physically: a RBM motion produces nonzero shear strains and hence nonzero node forces.

2. The shear and inplane strains interlock to stiffen the element in inextensional bending modes.

The first defect is cured by the projection method described in [10]. Let

$$\mathbf{P} = \mathbf{I} - \mathbf{R}(\mathbf{R}\mathbf{R})^{-1}\mathbf{R}^T = \mathbf{P}^T, \tag{32.116}$$

be the projector that filters out rigid body motions, in which $\mathbf{I}$ is the identity matrix of order 24. Then $\mathbf{P}\mathbf{K}_s\mathbf{P}$ is RBM clean. In the implementation of Figure 25 the projector is not applied to $\mathbf{K}_s$ but to $\mathbf{B}_s$: $\mathbf{B}_s\mathbf{P}$ is used in the numerical integration process that produces $\mathbf{K}_s$. The cure for the second defect: inextensional bending locking, is discussed in §10.3.

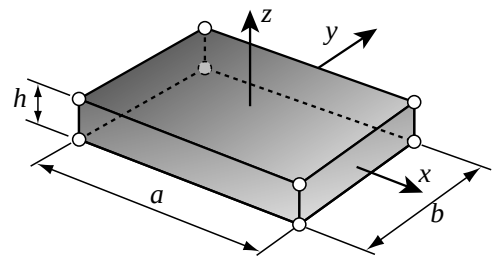

Figure 26. Rectangular parallelepiped element dimensioned $a \times b \times h$.

§32.8. A Special Geometry

§32.8.1. Stiffness of an Isotropic Rectangular-Prismatic Element

Consider the element of rectangular-prismatic geometry of inplane dimensions $a \times b$, constant thickness h and one layer of isotropic material with elastic modulus E and Poisson's ratio ν, as shown in Figure 26. The element stiffness matrix in local coordinates was computed in closed symbolic form by *Mathematica*.

This closed form is useful for spot checks of new implementations, as well as for investigations such as the torsional stiffness analyis reported in the next subsection. The stiffness entries were generated and compared symbolically for duplication; then *Mathematica* generated the necessary TEX expressions listed below.

$$
\begin{aligned}
&K^{(e)}_{1,1} = K^{(e)}_{4,4} = K^{(e)}_{7,7} = K^{(e)}_{10,10} = K^{(e)}_{13,13} = K^{(e)}_{16,16} = K^{(e)}_{19,19} = K^{(e)}_{22,22} = \\
&\qquad 2E(3a^2(b^2+h^2)(1-3\nu+2\nu^2) + 2b^2h^2(4-8\nu+3\nu^2))/K_{fac}, \\
&K^{(e)}_{1,2} = K^{(e)}_{4,11} = K^{(e)}_{5,10} = K^{(e)}_{7,8} = K^{(e)}_{13,14} = K^{(e)}_{16,23} = K^{(e)}_{17,22} = K^{(e)}_{19,20} = \\
&\qquad -3aEbh^2(-2+2\nu+\nu^2)/K_{fac}, \\
&K^{(e)}_{1,3} = K^{(e)}_{4,15} = K^{(e)}_{6,13} = K^{(e)}_{7,24} = K^{(e)}_{9,22} = K^{(e)}_{10,12} = K^{(e)}_{16,18} = K^{(e)}_{19,21} = \\
&\qquad -6aEb^2h(-1+\nu)/K_{fac}, \\
&K^{(e)}_{1,4} = K^{(e)}_{7,10} = K^{(e)}_{13,16} = K^{(e)}_{19,22} = \\
&\qquad 2E(3a^2(b^2+h^2)(1-3\nu+2\nu^2) - 2b^2h^2(4-8\nu+3\nu^2))/K_{fac}, \\
&K^{(e)}_{1,5} = K^{(e)}_{2,10} = K^{(e)}_{4,8} = K^{(e)}_{7,11} = K^{(e)}_{13,17} = K^{(e)}_{14,22} = K^{(e)}_{16,20} = K^{(e)}_{19,23} = \\
&\qquad -3aEbh^2(2-10\nu+9\nu^2)/K_{fac}, \\
&K^{(e)}_{1,6} = K^{(e)}_{3,13} = K^{(e)}_{4,18} = K^{(e)}_{7,21} = K^{(e)}_{9,10} = K^{(e)}_{12,22} = K^{(e)}_{15,16} = K^{(e)}_{19,24} = \\
&\qquad -6aEb^2h(1-\nu)(1-4\nu)/K_{fac}, \\
&K^{(e)}_{1,7} = K^{(e)}_{4,10} = K^{(e)}_{13,19} = K^{(e)}_{16,22} = \\
&\qquad E(3a^2(b^2-2h^2)(1-3\nu+2\nu^2) - 2b^2h^2(4-8\nu+3\nu^2))/K_{fac}, \\
&K^{(e)}_{1,8} = K^{(e)}_{2,7} = K^{(e)}_{4,5} = K^{(e)}_{10,11} = K^{(e)}_{13,20} = K^{(e)}_{14,19} = K^{(e)}_{16,17} = K^{(e)}_{22,23} = \\
&\qquad 3aEbh^2(-2+2\nu+\nu^2)/K_{fac}, \\
&K^{(e)}_{1,9} = K^{(e)}_{3,22} = K^{(e)}_{4,21} = K^{(e)}_{6,10} = K^{(e)}_{7,18} = K^{(e)}_{12,13} = K^{(e)}_{15,19} = K^{(e)}_{16,24} = \\
&\qquad -3aEb^2h(1-\nu)(1-4\nu)/K_{fac}, \\
&K^{(e)}_{1,10} = K^{(e)}_{4,7} = K^{(e)}_{13,22} = K^{(e)}_{16,19} = \\
&\qquad E(3a^2(b^2-2h^2)(1-3\nu+2\nu^2) + 2b^2h^2(4-8\nu+3\nu^2))/K_{fac},
\end{aligned}
\tag{32.117}
$$

$$
\begin{aligned}
&K^{(e)}_{1,11} = K^{(e)}_{2,4} = K^{(e)}_{5,7} = K^{(e)}_{8,10} = K^{(e)}_{13,23} = K^{(e)}_{14,16} = K^{(e)}_{17,19} = K^{(e)}_{20,22} = \\
&\qquad 3aEbh^2(2-10\nu+9\nu^2)/K_{fac}, \\
&K^{(e)}_{1,12} = K^{(e)}_{3,10} = K^{(e)}_{4,24} = K^{(e)}_{6,22} = K^{(e)}_{7,15} = K^{(e)}_{9,13} = K^{(e)}_{16,21} = K^{(e)}_{18,19} = \\
&\qquad -3aEb^2h(-1+\nu)/K_{fac}, \\
&K^{(e)}_{1,13} = K^{(e)}_{4,16} = K^{(e)}_{7,19} = K^{(e)}_{10,22} = \\
&\qquad E(-3a^2(2b^2-h^2)(1-3\nu+2\nu^2)+4b^2h^2(2-4\nu+3\nu^2))/K_{fac}, \\
&K^{(e)}_{1,14} = K^{(e)}_{2,13} = K^{(e)}_{4,23} = K^{(e)}_{5,22} = K^{(e)}_{7,20} = K^{(e)}_{8,19} = K^{(e)}_{10,17} = K^{(e)}_{11,16} = \\
&\qquad 3aEbh^2(1-\nu+\nu^2)/K_{fac}, \\
&K^{(e)}_{1,15} = K^{(e)}_{3,4} = K^{(e)}_{6,16} = K^{(e)}_{7,12} = K^{(e)}_{9,19} = K^{(e)}_{10,24} = K^{(e)}_{13,18} = K^{(e)}_{21,22} = \\
&\qquad 6aEb^2h(1-\nu)(1-4\nu)/K_{fac}, \\
&K^{(e)}_{1,16} = K^{(e)}_{4,13} = K^{(e)}_{7,22} = K^{(e)}_{10,19} = \\
&\qquad -(E(3a^2(2b^2-h^2)(1-3\nu+2\nu^2)+4b^2h^2(2-4\nu+3\nu^2)))/K_{fac}, \\
&K^{(e)}_{1,17} = K^{(e)}_{2,22} = K^{(e)}_{4,20} = K^{(e)}_{5,13} = K^{(e)}_{7,23} = K^{(e)}_{8,16} = K^{(e)}_{10,14} = K^{(e)}_{11,19} = \\
&\qquad -3aEbh^2(1-5\nu+3\nu^2)/K_{fac}, \\
&K^{(e)}_{1,18} = K^{(e)}_{3,16} = K^{(e)}_{4,6} = K^{(e)}_{7,9} = K^{(e)}_{10,21} = K^{(e)}_{12,19} = K^{(e)}_{13,15} = K^{(e)}_{22,24} = \\
&\qquad 6aEb^2h(-1+\nu)/K_{fac}, \\
&K^{(e)}_{1,19} = K^{(e)}_{4,22} = K^{(e)}_{7,13} = K^{(e)}_{10,16} = \\
&\qquad -(E(3a^2(b^2+h^2)(1-3\nu+2\nu^2)+2b^2h^2(2-4\nu+3\nu^2)))/K_{fac}, \\
&K^{(e)}_{1,20} = K^{(e)}_{2,19} = K^{(e)}_{4,17} = K^{(e)}_{5,16} = K^{(e)}_{7,14} = K^{(e)}_{8,13} = K^{(e)}_{10,23} = K^{(e)}_{11,22} = \\
&\qquad -3aEbh^2(1-\nu+\nu^2)/K_{fac}, \\
&K^{(e)}_{1,21} = K^{(e)}_{3,19} = K^{(e)}_{4,9} = K^{(e)}_{6,7} = K^{(e)}_{10,18} = K^{(e)}_{12,16} = K^{(e)}_{13,24} = K^{(e)}_{15,22} = \\
&\qquad 3aEb^2h(-1+\nu)/K_{fac}, \\
&K^{(e)}_{1,22} = K^{(e)}_{4,19} = K^{(e)}_{7,16} = K^{(e)}_{10,13} = \\
&\qquad E(-3a^2(b^2+h^2)(1-3\nu+2\nu^2)+2b^2h^2(2-4\nu+3\nu^2))/K_{fac}, \\
&K^{(e)}_{1,23} = K^{(e)}_{2,16} = K^{(e)}_{4,14} = K^{(e)}_{5,19} = K^{(e)}_{7,17} = K^{(e)}_{8,22} = K^{(e)}_{10,20} = K^{(e)}_{11,13} = \\
&\qquad 3aEbh^2(1-5\nu+3\nu^2)/K_{fac}, \\
&K^{(e)}_{1,24} = K^{(e)}_{3,7} = K^{(e)}_{4,12} = K^{(e)}_{6,19} = K^{(e)}_{9,16} = K^{(e)}_{10,15} = K^{(e)}_{13,21} = K^{(e)}_{18,22} = \\
&\qquad 3aEb^2h(1-\nu)(1-4\nu)/K_{fac}. \\
&K^{(e)}_{2,2} = K^{(e)}_{5,5} = K^{(e)}_{8,8} = K^{(e)}_{11,11} = K^{(e)}_{14,14} = K^{(e)}_{17,17} = K^{(e)}_{20,20} = K^{(e)}_{23,23} = \\
&\qquad 2E(3b^2h^2(1-3\nu+2\nu^2)+a^2(2h^2(4-8\nu+3\nu^2)+b^2(3-9\nu+6\nu^2)))/K_{fac}, \\
&K^{(e)}_{2,3} = K^{(e)}_{5,6} = K^{(e)}_{8,18} = K^{(e)}_{9,17} = K^{(e)}_{11,15} = K^{(e)}_{12,14} = K^{(e)}_{20,21} = K^{(e)}_{23,24} = \\
&\qquad -6a^2Ebh(-1+\nu)/K_{fac}, \\
&K^{(e)}_{2,5} = K^{(e)}_{8,11} = K^{(e)}_{14,17} = K^{(e)}_{20,23} = \\
&\qquad E(-6b^2h^2(1-3\nu+2\nu^2)+a^2(2h^2(4-8\nu+3\nu^2)+b^2(3-9\nu+6\nu^2)))/K_{fac}, \\
&K^{(e)}_{2,6} = K^{(e)}_{3,5} = K^{(e)}_{8,15} = K^{(e)}_{9,14} = K^{(e)}_{11,18} = K^{(e)}_{12,17} = K^{(e)}_{20,24} = K^{(e)}_{21,23} = \\
&\qquad -3a^2Ebh(-1+\nu)/K_{fac}, \\
&K^{(e)}_{2,8} = K^{(e)}_{5,11} = K^{(e)}_{14,20} = K^{(e)}_{17,23} = \\
&\qquad E(-6b^2h^2(1-3\nu+2\nu^2)+a^2(-2h^2(4-8\nu+3\nu^2)+b^2(3-9\nu+6\nu^2)))/K_{fac}, \\
&K^{(e)}_{2,9} = K^{(e)}_{3,17} = K^{(e)}_{5,12} = K^{(e)}_{6,14} = K^{(e)}_{8,24} = K^{(e)}_{11,21} = K^{(e)}_{15,20} = K^{(e)}_{18,23} = \\
&\qquad -3a^2Ebh(1-\nu)(1-4\nu)/K_{fac},
\end{aligned}
\tag{32.118}
$$

$$
\begin{aligned}
&K^{(e)}_{2,11} = K^{(e)}_{5,8} = K^{(e)}_{14,23} = K^{(e)}_{17,20} = \\
&\qquad 2E(3b^2h^2(1-3\nu+2\nu^2) + a^2(-2h^2(4-8\nu+3\nu^2) + b^2(3-9\nu+6\nu^2)))/K_{fac}, \\
&K^{(e)}_{2,12} = K^{(e)}_{3,14} = K^{(e)}_{5,9} = K^{(e)}_{6,17} = K^{(e)}_{8,21} = K^{(e)}_{11,24} = K^{(e)}_{15,23} = K^{(e)}_{18,20} = \\
&\qquad -6a^2Ebh(1-\nu)(1-4\nu)/K_{fac}, \\
&K^{(e)}_{2,14} = K^{(e)}_{5,17} = K^{(e)}_{8,20} = K^{(e)}_{11,23} = \\
&\qquad E(3b^2h^2(1-3\nu+2\nu^2) - 2a^2(-2h^2(2-4\nu+3\nu^2) + b^2(3-9\nu+6\nu^2)))/K_{fac}, \\
&K^{(e)}_{2,15} = K^{(e)}_{3,11} = K^{(e)}_{5,18} = K^{(e)}_{6,8} = K^{(e)}_{9,20} = K^{(e)}_{12,23} = K^{(e)}_{14,24} = K^{(e)}_{17,21} = \\
&\qquad 6a^2Ebh(1-\nu)(1-4\nu)/K_{fac}, \\
&K^{(e)}_{2,17} = K^{(e)}_{5,14} = K^{(e)}_{8,23} = K^{(e)}_{11,20} = \\
&\qquad E(-3b^2h^2(1-3\nu+2\nu^2) + a^2(b^2(-3+9\nu-6\nu^2) + 2h^2(2-4\nu+3\nu^2)))/K_{fac}, \\
&K^{(e)}_{2,18} = K^{(e)}_{3,8} = K^{(e)}_{5,15} = K^{(e)}_{6,11} = K^{(e)}_{9,23} = K^{(e)}_{12,20} = K^{(e)}_{14,21} = K^{(e)}_{17,24} = \\
&\qquad 3a^2Ebh(1-\nu)(1-4\nu)/K_{fac}, \\
&K^{(e)}_{2,20} = K^{(e)}_{5,23} = K^{(e)}_{8,14} = K^{(e)}_{11,17} = \\
&\qquad -(E(3b^2h^2(1-3\nu+2\nu^2) + a^2(2h^2(2-4\nu+3\nu^2) + b^2(3-9\nu+6\nu^2))))/K_{fac}, \\
&K^{(e)}_{2,21} = K^{(e)}_{3,20} = K^{(e)}_{5,24} = K^{(e)}_{6,23} = K^{(e)}_{8,12} = K^{(e)}_{9,11} = K^{(e)}_{14,18} = K^{(e)}_{15,17} = \\
&\qquad 3a^2Ebh(-1+\nu)/K_{fac}, \\
&K^{(e)}_{2,23} = K^{(e)}_{5,20} = K^{(e)}_{8,17} = K^{(e)}_{11,14} = \\
&\qquad E(3b^2h^2(1-3\nu+2\nu^2) - 2a^2(2h^2(2-4\nu+3\nu^2) + b^2(3-9\nu+6\nu^2)))/K_{fac}, \\
&K^{(e)}_{2,24} = K^{(e)}_{3,23} = K^{(e)}_{5,21} = K^{(e)}_{6,20} = K^{(e)}_{8,9} = K^{(e)}_{11,12} = K^{(e)}_{14,15} = K^{(e)}_{17,18} = \\
&\qquad 6a^2Ebh(-1+\nu)/K_{fac}, \\
&K^{(e)}_{3,3} = K^{(e)}_{6,6} = K^{(e)}_{9,9} = K^{(e)}_{12,12} = K^{(e)}_{15,15} = K^{(e)}_{18,18} = K^{(e)}_{21,21} = K^{(e)}_{24,24} = \\
&\qquad -2E(1-\nu)(3b^2h^2(-1+2\nu) + a^2(8b^2(-1+\nu) + 3h^2(-1+2\nu)))/K_{fac}, \\
&K^{(e)}_{3,6} = K^{(e)}_{9,12} = K^{(e)}_{15,18} = K^{(e)}_{21,24} = \\
&\qquad -E(1-\nu)(6b^2h^2(1-2\nu) + a^2(8b^2(-1+\nu) + 3h^2(-1+2\nu)))/K_{fac}, \\
&K^{(e)}_{3,9} = K^{(e)}_{6,12} = K^{(e)}_{15,21} = K^{(e)}_{18,24} = \\
&\qquad E(a^2(3h^2(1-2\nu) + 4b^2(-1+\nu)) + 3b^2h^2(1-2\nu))(-1+\nu)/K_{fac}, \\
&K^{(e)}_{3,12} = K^{(e)}_{6,9} = K^{(e)}_{15,24} = K^{(e)}_{18,21} = \\
&\qquad -E(1-\nu)(2a^2(3h^2(1-2\nu) + 4b^2(-1+\nu)) + 3b^2h^2(-1+2\nu))/K_{fac}, \\
&K^{(e)}_{3,15} = K^{(e)}_{6,18} = K^{(e)}_{9,21} = K^{(e)}_{12,24} = \\
&\qquad -2E(1-\nu)(3b^2h^2(-1+2\nu) + a^2(-8b^2(-1+\nu) + 3h^2(-1+2\nu)))/K_{fac}, \\
&K^{(e)}_{3,18} = K^{(e)}_{6,15} = K^{(e)}_{9,24} = K^{(e)}_{12,21} = \\
&\qquad -E(1-\nu)(6b^2h^2(1-2\nu) + a^2(-8b^2(-1+\nu) + 3h^2(-1+2\nu)))/K_{fac}, \\
&K^{(e)}_{3,21} = K^{(e)}_{6,24} = K^{(e)}_{9,15} = K^{(e)}_{12,18} = \\
&\qquad E(a^2(3h^2(1-2\nu) - 4b^2(-1+\nu)) + 3b^2h^2(1-2\nu))(-1+\nu)/K_{fac}, \\
&K^{(e)}_{3,24} = K^{(e)}_{6,21} = K^{(e)}_{9,18} = K^{(e)}_{12,15} = \\
&\qquad -E(1-\nu)(a^2(6h^2(1-2\nu) - 8b^2(-1+\nu)) + 3b^2h^2(-1+2\nu))/K_{fac},
\end{aligned}
\tag{32.119}
$$

The common denominator is $K_{fac} = 144abh(1-\nu^2)(1-2\nu)$. Only 48 entries (of the $24 \times 25/2 = 300$ entries of the upper triangle) are different.

For this geometry the α and β parameters of the membrane strain field introduced in §6.3 do not have any influence on the stiffness.

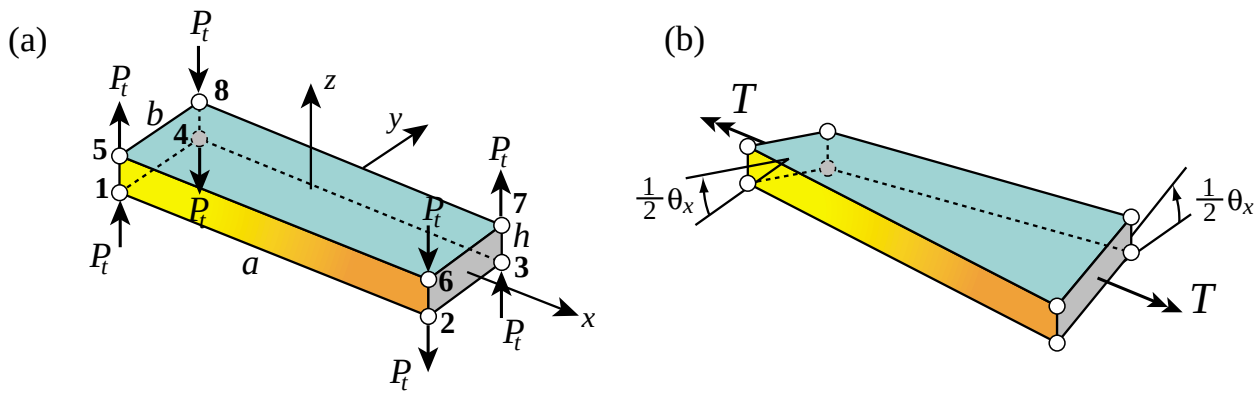

Figure 27. SS8 torsion response test.

Using the foregoing analytical form it is easily to verify symbolically that a single element of this (rectangular prismatic) geometry and homogeneous-isotropic wall construction is exact for any $\{a, b, h, E\}$ for the following actions:

(i) Uniform in-plane stretching (any ν)

(ii) Pure in-plane bending (if $\nu = 0$)

(iii) Pure out-of-plane bending (if $\nu = 0$)

(iv) Pure transverse shear (any ν)

Response exactness for (ii) and (iii) is not achievable with the standard 8-node brick element. This should not come as a surprise since the SS8 element was designed explicitly to be exact under those conditions, which are important for thin and thick shells. But the behavior under torsion was not explicitly considered in the element design. It remains to be checked *a posteriori*. This is done below.

§32.8.2. Torsion Response of Individual Element

To check torsion consider an element as in Figure 27, torqued about the local x axis. Apply the twist force system $\mathbf{f}_t$ shown in Figure 27(a). The eight P_z loads are equivalent to a torque $T = 4P_z(b/2) = 2P_z b$ about the x axis. Solve $\mathbf{K}^{(e)}\mathbf{u}_t = \mathbf{f}_t$ for $\mathbf{u}_t$ using the free-free flexibility to project out the rigid body motions [9,10]. The computed node displacements form the pattern

$$\begin{aligned}\mathbf{u}_t^T = [\,&-u_x\ \ -u_y\ \ u_z\ \ -u_x\ \ u_y\ \ -u_z\ \ u_x\ \ u_y\ \ u_z\ \ u_x\ \ -u_y\ \ -u_z\\ &u_x\ \ u_y\ \ u_z\ \ u_x\ \ -u_y\ \ -u_z\ \ -u_x\ \ -u_y\ \ u_z\ \ -u_x\ \ u_y\ \ -u_z\,]\end{aligned} \tag{32.120}$$

where

$$u_z = \frac{3}{2}\frac{a^2(b^2+h^2)+b^2h^2}{Gabh^3}P_z,\quad u_x = \frac{a^2(b^2-h^2)+b^2h^2}{a^3(b^2+h^2)+ab^2h^2}hu_z,\quad u_y = \frac{a^2(b^2+h^2)-b^2h^2}{a^2b(b^2+h^2)+b^3h^2}hu_z. \tag{32.121}$$

The twist angle is $\theta_x = u_z/b$; whence the twist in terms of T and the effective torsional rigidity are given by

$$\theta_x = \frac{3(b^2h^2+a^2(b^2+h^2)T}{Gab^3h^3} \stackrel{\text{def}}{=} \frac{Ta}{GJ_t},\quad \rightarrow\quad J_t = \tfrac{1}{3}\frac{a^2b^3h^3}{a^2(b^2+h^2)+b^2h^2}. \tag{32.122}$$

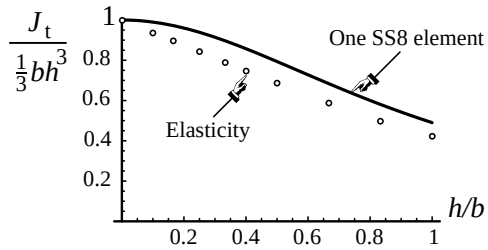

Figure 28. Effective J_t component of torsional rigidity GJ_t (normalized to $J_{thin} = \frac{1}{3}bh^3$) of individual SS8 element versus Saint-Venant's elasticity theory.

As $h \to 0$ while keeping a and b fixed, $J_t - > J_{thin} = \frac{1}{3}bh^3$, which is correct for a torqued thin rectangle. Consequently the SS8 element of this special geometry is torsion exact in the thin plate limit. For finite h/b the ratio J_t/J_{thin} is plotted in Figure 28, and compared to the J_t/J_{thin} given by the Saint-Venant's elasticity thory as tabulated in Timoshenko and Goodier [28].

The agreement is surprisingly good for two reasons: the element is very low order as regards shear stress representation, and no special tuning was done for the torsional response.[9]

[9] Torsion tuning for this particular element is actually impossible because the transverse shear strain field, which dominates the torsional response, has no free parameters.

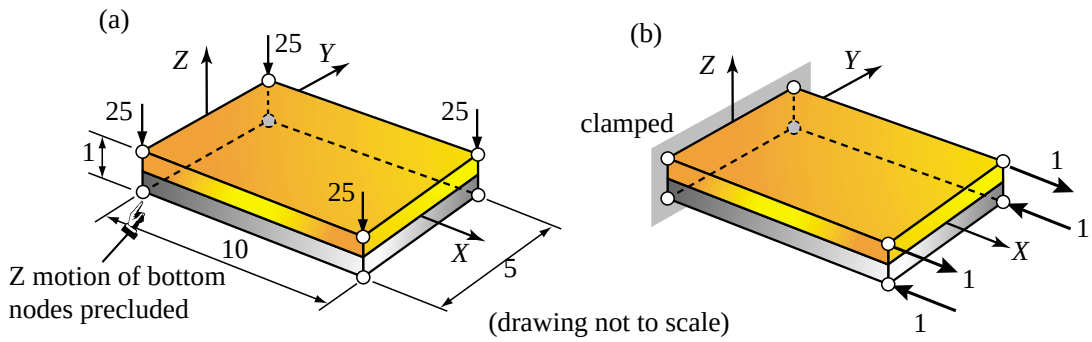

Figure 29. Two ply rectangular plate modeled by one element:
(a) transverse compression tests, (b) pure bending test.

§32.9. Numerical Tests

§32.9.1. Patch Tests

The SS8 element passes all rigid-body motion and constant strain mode patch tests exactly if it is thickness prismatic and of constant thickness. It passes rigid body motion tests for arbitrary geometries. It passes some higher order patch tests for rectangular planforms of constant thickness.

For bending patch tests in tapered thickness geometries see Sections 6 and 7. For the torsion test, which may be viewed as a special high order patch test, see §8.2.

§32.9.2. Invariance

The element is invariant with respect to global node numbering. This was a concern in the initial development, since for expediency the inplane stiffness component was treated with a selective-reduced integration scheme [18], which turned out to depend on node numbering.[10] This problem was eliminated later when the development of the membrane field discussed in Section 7 permitted use of a standard 2×2 Gauss integration on the midsurface.

§32.9.3. Two-Ply Rectangular Plate

This test has been proposed by Sze, Yao and Cheung [27], and is used with some modifications, notably use of symbolic computation. The rectangular-prismatic 2-ply laminated plate shown in Figure 29, which is dimensioned $10 \times 5 \times 1$, is modeled with one SS8 element. Both layers are isotropic but have different properties: E_1 and ν_1 for the bottom layer, and E_2 and ν_2 for the top layer. Two types of tests are performed.

With the bottom surface restrained in the Z direction, but able to move inplane, the rectangular block is subjected to a pressure $p_z = 2$ on the top surface. This is lumped to four $f_{zi} = 25$ node forces as shown in Figure 29(a). The displacement results are exact for any combination $\{E_1, \nu_1, E_2, \nu_2\}$.

The $X = 0$ face is clamped and the plate is subjected to a pure bending load as shown in Figure 29(b). The mean tip deflection agrees closely with composite beam theory, and is exact if $\nu_1 = \nu_2 = 0$ because the clamped condition precludes lateral root expansion for nonzero Poisson's ratios.[11]

[10] Because the choice of local axes $\{x, y\}$ depends on which corner is numbered first. Selective integration relies on picking up a shear strain component to be 1-point integrated. This necessarily brings directional anisotropy, which can be highly disturbing for anisotropic laminate construction.

[11] This test would be more convincing for arbitrary ν_1 and ν_2 if carried out on a free-free element, as done for the torsion test in

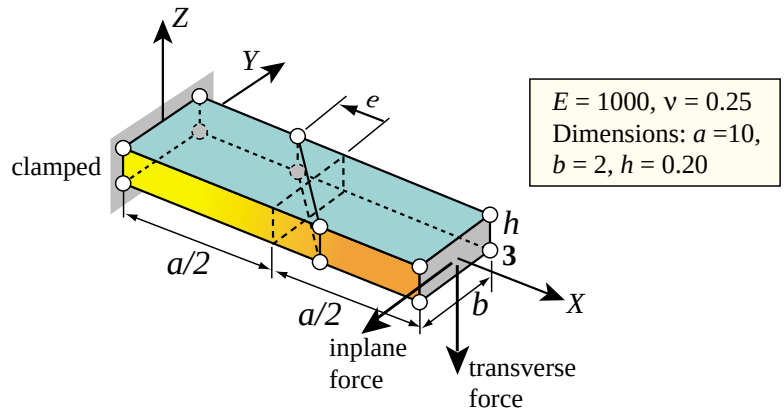

Figure 30. Two-element distortion sensitivity tests for inplane (membrane) and out of plane (bending) loading.

§32.9.4. Inplane Distortion Sensitivity

Figure 30 shows a cantilever plate modeled by two elements whose inplane distortions are characterized by the eccentricity e. Inplane and out-of-plane end shear forces are applied. After normalized by the analytical solutions, the mean tip deflections for the two loading cases are reported in Table 2. They are compared agaisnt a solid-shell element developed by Sze, Yao and Cheung [27], labeled SYC therein.[12]

As can be observed the SS8 element has lower distortion sensitivity for in-plane bending. The distortion sensitivity for out-of-plane bending is similar for both elements.[13]

Table 2. Results for Distortion Sensitivity Test

Element	In-plane loading norm. deflection				Out-of-plane loading norm. deflection			
Model	$e = 0$	$e = 1$	$e = 2$	$e = 3$	$e = 0$	$e = 1$	$e = 2$	$e = 3$
SS8	0.8993	0.6029	0.5598	0.5878	0.9337	0.9319	0.9091	0.8696
SYC	0.8993	0.3480	0.2474	0.1812	0.9345	0.9285	0.9021	0.8526

§8.2, using free-free flexibility methods. It was not done that way since the symbolic computations became messy and could not be completed on time.

[12] Actually [27] tests more solid shell elements. The one compared to here is that reported to be their best.

[13] These results were obtained with $\alpha = \beta = 0$ for the free parameters of the membrane strain field, as preset by `SS8Stiff`. If one sets $\beta = -1.5$, which is suspected (but not proven) of being close to the optimal value, the in-plane loading result for $e = 2$ rises to 0.7080, almost 3 times that of SYC.

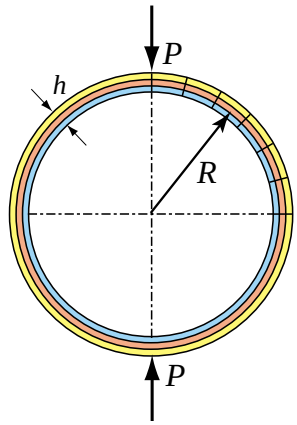

Figure 31. Pinched composite ring shell modeled with N_e elements over one quadrant; figure shows $N_e = 6$.

§32.9.5. Homogeneous and Laminated Pinched Ring

The problem is defined in Figure 31. The ring is pinched by two diametrically opposed loads P. The deflection response is strongly dominated by inextensional circumferential bending, particularly for high R/h ratios.

One quarter of the ring is modeled with N_e elements. Two isotropic materials with properties $E_1 = 10$, $\nu_1 = 0.30$ and $E_2 = 1$, $\nu_2 = 0.20$, respectively, are considered. The homogeneous ring is made up of material 1. Two and three ply laminations of equal thickness are also considered. The two ply lamination is unsymmetric and consists of materials 1 and 2 whereas the three-ply lamination is symetric and consists of materials 1, 2 and 1. Two radius-to-thickness R/h ratios are examined. The vertical deflections under the line force are computed and normalized by curved Bernoulli-Euler beam solutions, which ignore the effects of membrane and shear.

Results for one and two plies are shown in Table 3. Results for the symmetric 3-ply laminate were similar to the one-play case and are not shown. Once N_e exceeds 16 convergence is satisfactory. However, the response is too stiff for coarse meshes, especially for high R/h. This overstiffness was traced to transverse shear-membrane coupling that hinders inextensional bending response when the element is thickness tapered, as in the case here in the circumferential direction.

Table 3. Normalized Deflections for the Pinched Composite Ring

Wall:	One ply: $E = 10, \nu = .3$		Two plies: $E = 10, 1; \nu = .3, .2$	
N_e	$R/h = 20$	$R/h = 100$	$R/h = 20$	$R/h = 100$
2	0.0190	0.0008	0.0172	0.0009
4	0.5746	0.0062	0.5421	0.0072
6	0.8993	0.4322	0.8640	0.4158
8	0.9582	0.7813	0.9320	0.7502
16	0.9896	0.9659	0.9759	0.9480
32	0.9955	0.9753	0.9916	0.9691

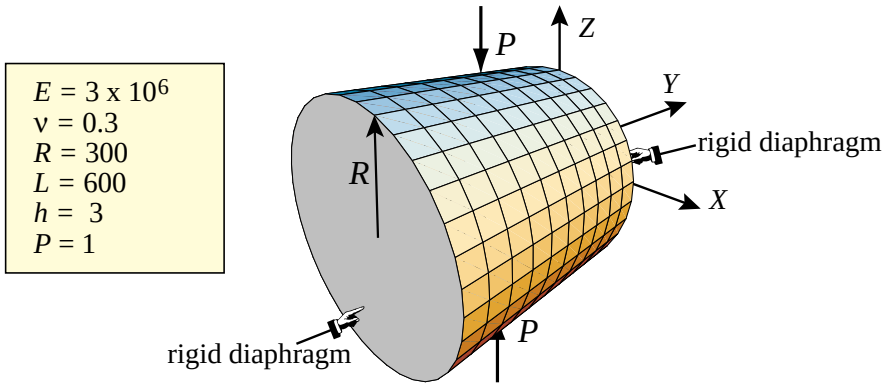

Figure 32. Pinched cylindrical shell benchmark.

§32.9.6. Pinched Cylindrical Shell

A test in the MacNeal-Harder benchmark suite [16,17]. The cylinder is pinched by two diametrically opposite point loads as shown in Figure 32. As in the previous case, the deflection under the load is dominated by inextensional bending response, which now is bidirectional.

Owing to symmetry, only one eight of the shell needs is considered. Over the rigid diaphragms the boundary conditions are $U_X^- = U_Y^- = U_Z^- = 0$. The deflection of the node under the point force is computed and normalized against the reference solution 0.18248×10^{-4} given by Belytschko, Wong and Stolarki [3]. The results are too stiff and the convergence unsatisfactory. As in the case of the pinched ring, this is caused by shear-mermbrane locking for thickness tapered elements. The effect is exacerbated here because the localization in the vicinity of the load is more pronounced.

Table 4. Normalized Deflections for the Pinched Cylinder Benchmark

Mesh	4×4	8×8	16×16	32×32
SS8	0.0762	0.2809	0.5366	0.8029

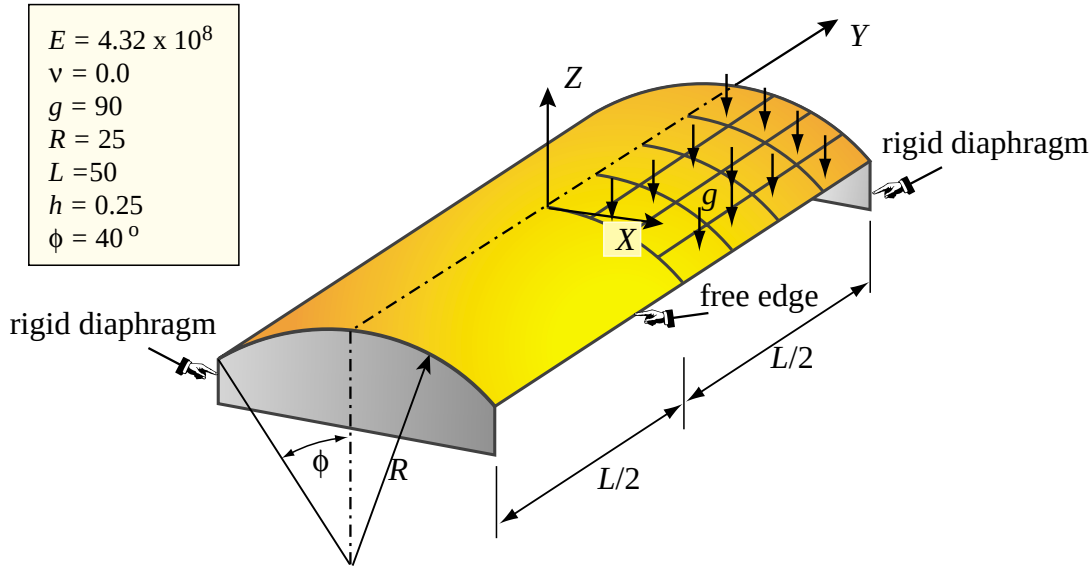

Figure 33. The Scordelis-Lo Roof Benchmark.

§32.9.7. Scordelis-Lo Roof

This widely used benchmark is defined in Figure 33. The roof is mounted on two rigid diaphragms and loaded under its own weight specified as g per unit of midsurface area. The boundary conditions at the diaphragms are $U_X^- = U_Y^- = U_Z^- = 0$. Only a quarter of the roof is analyzed due to symmetry. The vertical deflections at the midspan point of thre free edge are normalized by the reference solution 0.3086 given by MacNeal and Harder[17].

The results for the SS8 element are shown in Table 5. The convergence is satisfactory and occurs from above. Good results are expected because in this problem the free edge deflection is dominated by longitudinal membrane-bending extensional coupling, and the elements are not tapered in the longitudinal (Y) direction.

It should be noted that the results appear to converge to the deep-shell analytical solution of 0.3012. This is about 3% lower than the MacNeal-Harder value of 0.3086 quoted above, which is based on a different shell theory.

Table 5. Normalized Deflections for the Scordelis-Lo Roof Benchmark

Mesh	2×2	4×4	8×8	16×16
SS8	1.2928	1.0069	0.9844	0.9772

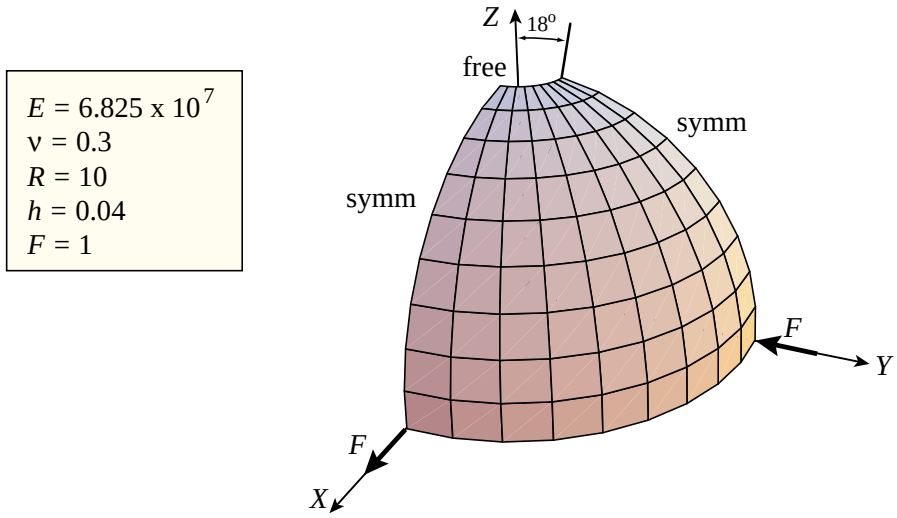

Figure 34. Pinched hemispherical shell with a 18° polar cutout.
Only the FEM-modeled quadrant is shown.

§32.9.8. Pinched Hemisphere

This is another widely used benchmark which is part of the test suite of MacNeal and Harder [17]. A quarter of a closed spherical shell is shown in Figure 34. The shell is acted upon by two pairs of orthogonal point loads. The reference solution is 0.0940 [17].

The normalized displacement of the nodes subjected to the point forces are listed in Table 6. The convergence is partly affected by inextensional bending overstiffness. The results of Key, Gunerud and Koteras [15], who use a stress-resultant-based, homogeneous solid shell element are listed for a 10×10 mesh and three different values of their hourglass control parameter s_{HG}

Table 6. Normalized Deflections for the Pinched Hemisphere

Mesh	2×2	4×4	8×8	10×10
SS8	0.6541	0.9219	0.9853	
Key et al, $s_{HG} = 0.000$				1.0191
Key et al, $s_{HG} = 0.015$				0.9979
Key et al, $s_{HG} = 0.030$				0.9766

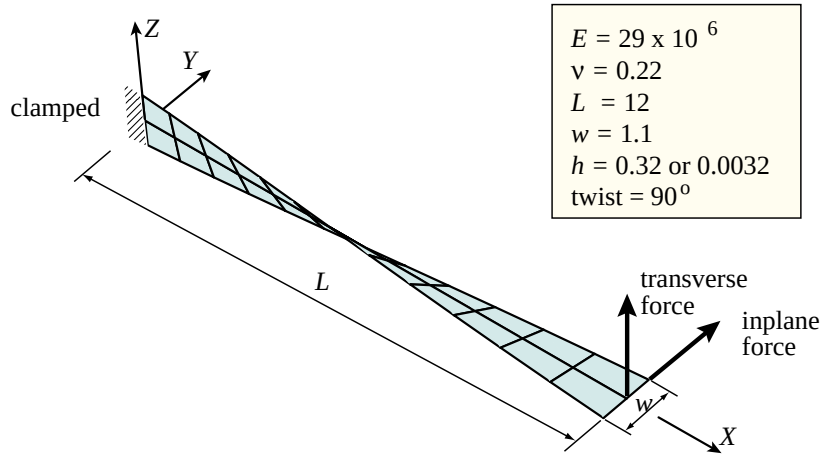

Figure 35. Pretwisted beam modeled by a 2×12 mesh.

§32.9.9. Pretwisted Beam

In this problem, defined in Figure 35, the elements warp. For the beam thickness equal to 0.32 the forces acting are 1 unit. The deflections along the loading direction are 5.424×10^{-3} and 1.754×10^{-3} for the inplane and out of plane loadings, respectively. For the thickness of 0.0032, the applied force is 10^{-6} units. The deflections along the loading directions are are 5.256×10^{-3} and 1.294×10^{-3} for the inplane and out of plane loadings, respectively [3,17].

The results for two coarse meshes run with $h = 0.32$ are listed in Table 7. Running $h = 0.0032$ caused the *Mathematica* equation solver to complain about a very high condition number (approximately 10^{14}) with consequent loss of solution accuracy.

Table 7. Normalized Deflections for the Pretwisted Beam Problem with $h = 0.32$

Mesh	In-plane loading	Out of plane loading
1×6	1.0257	0.9778
2×12	1.0041	0.9930

§32.10. Conclusions

Solid shells fill a modeling void in the grey area between thin shell and 3D solid elements. Such models are particularly useful for laminate wall constructions that do not need to be treated with high accuracy, and hence do not merit making each layer a separate element. One SS8 element can take arbitrary number of layers across the thickness while keeping the same node and freedom configuration.

Following is a summary of the strengths and weaknesses of this new element as assessed from benchmarks conducted as of this writing.

§32.10.1. General Strengths

Efficiency. SS8 does not need condensation of internal degrees of freedom, as required in most stress-hybrid and incompatible-mode elements. Consequently processing is highly efficient. Formation time in the local system is not much higher than that of the 8-node isoparametric brick element. This time is barely affected by the number of layers defined across the thickness. The transformations to the warped and global systems increase the local formation time by a mild factor.

Laminate Wall Construction. Through-the-thickness behavior of laminate wall construction is rendered physically correct by assuming an uniform normal transverse stress. This is corroborated by benchmarks.

§32.10.2. Special Strengths

Membrane Response. The assumed membrane strain field, obtained by a new energy fitting method discovered this fall [12] is believed to the the best to date as regards reduction of inplane distorsion sensitivity. For thickness-prismatic elements the bending field is also insensitive to inplane distortion.

Consistency. The element has the correct rank of 18. It passes the patch test for flat thickness-prismatic configurations. The rectangular-prismatic element also verifies exactly some high order patch tests, as summarized in §8.1.

Torsion Response. The torsion behavior of an individual TP element of rectangular planform is surprisingly good, and becomes exact in the thin plate limit.

§32.10.3. Weaknesses and Question Marks

Inextensional Bending. Thickness-tapered elements do not capture inextensional bending well. This was evident from the pinched-ring and pinched-cylindrical-shell tests. In fact the element exhibits severe bending-shear lock if the taper exceeds a few degrees.

To cure this problem the transverse shear strain field will have to be corrected by coupling it to the membrane strain field as a function of taper, with the correction vanishing if the element is thickness prismatic. Initial attempts were made to find the correction by symbolic computations but expressions were forbiddingly complex for arbitrary geometries. Approximate corrections might be achieved by considering median transverse sections $\xi = 0$ and $\eta = 0$, but this scheme has not been tried.

Warping. The effect of severe midsurface warping on element performance is unknown. All benchmarks but one (the pretwisted beam) have dealt with flat-midsurface elements. The flat-to-warped displacement transformation geometry described in §3.3 remains a question mark, since it has not been proposed by any other author. Pending further validation the SS8 should be used only for slightly warped geometries bounded by $\Psi < 0.01$, where the warping measure Ψ is defined in §2.5.

§32.11. Acknowledgements

The present work has been supported by Sandia National Laboratory under a Summer Faculty Research Award and the Finite Elements for Salinas contract, monitored by Garth M. Reese of Computational Solid Mechanics and Structural Dynamics group, Engineering Science Center of SNL.

§32.12. References

[1] M. F. Ausserer and S. W. Lee, An eighteen node solid element for thin shell analysis, *Int. J. Numer. Meth. Engrg.*, **26**, 1345–1364, 1988.

[2] K.J. Bathe and E. N. Dvorkin, A formulation of general shell elements — the use of mixed interpolation of tensorial components, *Int. J. Numer. Meth. Engrg.*, **22**, 697-722, 1986.

[3] T. Belytschko, B. K. Wong and H. Stolarski, Assumed strain stabilization procedure for the 9-node Lagrange shell element, *Int. J. Numer. Meth. Engrg.*, **28**, 385–414, 1989.

[4] P. G. Bergan, Finite elements based on energy orthogonal functions, *International Journal of Numerical Methods in Engineering*, **15**, 1141–1555, 1980.

[5] P. G. Bergan and M. K. Nygård, Finite elements with increased freedom in choosing shape functions, *International Journal of Numerical Methods in Engineering*, **20**, 643–664, 1984.

[6] P. G. Bergan and C. A. Felippa, A triangular membrane element with rotational degrees of freedom, *Comp. Meths. Appl. Mech. Engrg.*, **50**, 25–69, 1985

[7] P. Betch and E. Stein, An assumed strain approach avoiding artificial thickness straining for a nonlinear 4-node shell element, *Comp. Meths. Appl. Mech. Engrg.*, **11**, 899–909, 1997.

[8] M. Bischoff and E. Ramm, Shear deformable shell elements for large strains and rotations, *Int. J. Numer. Meth. Engrg.*, **40**, 445–452, 1997.

[9] C. A. Felippa, K. C. Park and M. R. Justino F., The construction of free-free flexibility matrices as generalized stiffness inverses, *Computers & Structures*, **68**, 411–418, 1998.

[10] C. A. Felippa, K. C. Park, The construction of free-free flexibility matrices for multilevel structural analysis, *Comp. Meths. Appl. Mech. Engrg.*, **191**, 2111–2140, 2002.

[11] C. A. Felippa, The SS8 solid shell element: a Fortran implementation, Center for Aerospace Structures Report CU-CAS-02-04, University of Colorado at Boulder, March 2002.

[12] C. A. Felippa, Fitting displacements and strain fields by mimimizing a dislocation functional, in preparation.

[13] D. J. Haas and S. W. Lee, A nine-node assumed-strain finite element for composite plates and shells, *Computers & Structures*, **26**, 445–452, 1987.

[14] R. Hauptmann and K. Schweizerhof, A systematic development of solid-shell element formulations for linear and nonlinear analysis employing only displacement degrees of freedom, *Int. J. Numer. Meth. Engrg.*, **42**, 49–69, 1988.

[15] S. W. Key, A. S. Gunerud, and J. R. Koteras, A low-order, hexahedral finite element for modeling shells, Sandia National Laboratory preprint.

[16] R. H. MacNeal, Toward a defect free four-noded membrane element, *Finite Elem. Anal. Des.*, **5**, 31–37, 1989.

[17] R. H. MacNeal anf R. L. Harder, A proposed standard set of problems to test finite element accuracy, *Finite Elem. Anal. Des.*, **1**, 3–20, 1985.

[18] D. S. Malkus and T. J. R. Hughes, Mixed finite element methods — reduced and selective integration techniques: a unification of concepts, *Comp. Meths. Appl. Mech. Engrg.*, **15**, 63–81, 1978.

[19] H. Parish, A continuum-based shell theory for nonlinear application, *Int. J. Numer. Meth. Engrg.*, **38**, 1855–1883, 1995.

[20] H. C. Park, C. Cho and S. W. Lee, An efficient assumed strain element model with six dof per node for geometrically nonlinear shells, *Int. J. Numer. Meth. Engrg.*, **38**, 4101-4122, 1995.

[21] K. C. Park and G. M. Stanley, A curved C^0 shell element based on assumed natural coordinate strains, *J. Appl. Mech.*, **53**, 278–290, 1986.

[22] T. H. H. Pian, Finite elements based on consistently assumed stresses and displacements, *Finite Elem. Anal. Des.*, **1**, 131–140, 1985.

[23] J. C. Simo and M. S. Rifai, A class of mixed assumed strain methods and the method of incompatible modes, *Int. J. Numer. Meth. Engrg.*, **29**, 1595–1638, 1990.

[24] K. Y. Sze and A. Ghali, A hexahedral element for plates, shells and beam by selective scaling, *Int. J. Numer. Meth. Engrg.*, **36**, 1519–1540, 1993.

[25] K. Y. Sze, S. Yi and M. H. Tay, An explicit hybrid-stabilized eighteen node solid element for thin shell analysis, *Int. J. Numer. Meth. Engrg.*, **40**, 1839–1856, 1997.

[26] K. Y. Sze, D. Zhu, An quadratic assumed natural strain curved triangular shell element, *Comp. Meths. Appl. Mech. Engrg.*, **174**, 57–71, 1999.

[27] K. Y. Sze, L.-Q. Yao and Y. K. Cheung, A hybrid stabilized solid shell element with particular reference to laminated structures, Proc ECCOMAS 2000, Barcelona, Spain, Sep 2000.

[28] S. Timoshenko and J. N. Goodier, *Theory of Elasticity*, McGraw-Hill, New York, 3rd ed., 1970.